

# Functionalization of hyaluronic acid with a chondroprotective molecule and preparation of sulfonated HA-based materials

PhD in Chemical Sciences, XXXIII Cycle

Faculty of Mathematical, Physical and Natural Sciences

Department of Chemistry

Sapienza University of Rome, 2020

Doctoral thesis by

Elisa Sturabotti

Supervisors

Prof. Andrea Martinelli

Prof. Francesca Leonelli

PhD coordinator

Prof. Osvaldo Lanzalunga

# INDEX

<b>1. INTRODUCTION AND AIM OF THE THESIS .....</b>	<b>5</b>
<b>1.1 Hyaluronic acid: general properties .....</b>	<b>9</b>
<b>1.2 Chemical modification of hyaluronic acid .....</b>	<b>10</b>
<b>1.3 General applications of HA .....</b>	<b>12</b>
1.3.1 Viscosupplementation.....	12
1.3.2 HA as Drug delivery system for viscosupplementation .....	13
1.3.3 HA-based hydrogels preparation for chondrocytes .....	14
<b>1.4 Sulfonated materials.....</b>	<b>16</b>
<b>1.5 Sulfonation of hyaluronic acid: state of the art and aim of the thesis .....</b>	<b>17</b>
<b>1.6 References.....</b>	<b>21</b>
<b>2. SYNTHESIS OF HA-NAPA BIOCONJUGATE.....</b>	<b>30</b>
<b>2.1 Synthesis of NAPA.....</b>	<b>32</b>
2.1.1 Synthesis of compound <b>III</b> : direct preparation of NAPA .....	32
2.1.2 Synthesis of compound <b>III</b> : preparation of precursor <b>IV</b> .....	34
2.1.3 Racemization of N-Acetyl-L-phenylalanine.....	39
2.1.4 Coupling of N-Acetyl-L-phenylalanine using TBTU.....	41
2.1.5 Coupling of N-(Carbobenzyloxy)-L-phenylalanine using TBTU .....	49
2.1.6 T3P for the coupling of N-Acetyl and N- Carbobenzyloxy amino acids .....	50
2.1.7 Synthesis of compound <b>III</b> : deacetylation of <b>IV</b> .....	52
<b>2.2 Regioselective Esterification of NAPA.....</b>	<b>53</b>
2.2.1 Esterification with 4-bromobutyric acid .....	54
2.2.2 Esterification with acyl chlorides .....	55
<b>2.3 Esterification of hyaluronic acid with a NAPA derivative .....</b>	<b>60</b>
<b>2.4 Materials and methods .....</b>	<b>63</b>
2.4.1 Strategy 1 .....	63
2.4.2 Strategy 2 .....	63
2.4.3 Strategy 3 .....	64
2.4.4 Strategy 4 .....	70
2.4.5 Strategy 5 .....	70
2.4.6 Synthesis of HA-NAPA bioconjugates 5,6 .....	71
<b>3. BIOLOGICAL ANALYSES .....</b>	<b>72</b>
<b>3.1 Materials and methods.....</b>	<b>72</b>
3.1.1 Cell culture.....	72
3.1.2 Cell viability .....	73
3.1.3 Cells treatment and RNA extraction.....	74
3.1.4 Reverse transcription .....	74
3.1.5 Quantitative Real-Time-PCR (q-RT-PCR).....	75
3.1.6 Immunofluorescence.....	75
3.1.7 Micromasses .....	76

<b>3.2 HA-NAPA derivative: biological evaluation .....</b>	<b>77</b>
3.2.1 Cells viability .....	77
3.2.2 Effect of molecules on cytokines expression in HPCs .....	79
3.2.3 Effect of HA-NAPA 20% on Collagen II production: an immunofluorescence analysis.....	81
3.2.4 Effect of HA, NAPA and HA-NAPA 20% on Collagen II production: a 3D model .....	83
<b>3.3 Conclusion .....</b>	<b>86</b>
<b>3.4 References.....</b>	<b>88</b>
<b>4. SULFONATION OF HYALURONIC ACID: AMIDATION WITH TAURINE .....</b>	<b>93</b>
<b>4.1 Materials and methods.....</b>	<b>93</b>
4.1.1 General procedure for amidation of HA: coupling with EDC HCl and DMTMM .....	94
4.1.2 <sup>1</sup> H-NMR Measurements .....	97
4.1.3 Infrared spectroscopy (FTIR) .....	97
4.1.4 Thermo gravimetric measurements (TGA) .....	97
4.1.5 Cell viability investigations .....	97
<b>4.2 Results.....</b>	<b>98</b>
4.2.1 Coupling with EDC: mechanism and NMR analysis .....	98
4.2.2 Coupling with DMTMM: mechanism and NMR analysis .....	105
4.2.3 Infrared and thermal characterization of HA-Tau derivatives.....	108
4.2.4 Cytotoxicity of samples .....	114
<b>4.3 Conclusion .....</b>	<b>115</b>
<b>4.4 References.....</b>	<b>116</b>
<b>5. SULFONATION OF HYALURONIC ACID: PREPARATION OF HA-BASED SULFONATED HYDROGEL .....</b>	<b>118</b>
<b>5.1 Materials and methods.....</b>	<b>122</b>
5.1.1 General procedure for hyaluronic acid coupling .....	122
5.1.2 Infrared spectroscopy (FTIR) .....	125
5.1.3 Swelling studies .....	125
5.1.4 Thermal analysis .....	125
5.1.5 Mechanical measurements.....	127
5.1.6 Bulk structure analyses (SEM) .....	127
5.1.7 <i>In vitro</i> degradation.....	127
<b>5.2 Results.....</b>	<b>129</b>
5.2.1 FTIR analysis .....	131
5.2.2 Swelling studies .....	133
5.2.3 Thermal and mechanical characterization .....	136
5.2.4 Bulk structure analyses .....	141
5.2.5 <i>In vitro</i> degradation.....	143
<b>5.3 Conclusion .....</b>	<b>145</b>

<b>5.4 References.....</b>	<b>146</b>
<b>6. GENERAL CONCLUSION.....</b>	<b>149</b>
<b>List of Abbreviations .....</b>	<b>150</b>
Chapter 2.....	150
Chapter 4 and 5 .....	151

# 1. INTRODUCTION AND AIM OF THE THESIS

A normal/healthy joint allows nearly frictionless and pain-free movement because it can support efficiently stresses of everyday life. However, diseases and articular trauma can lead to the degeneration of soft tissues such as tendons, ligaments and cartilages. Nowadays arthritic disorders, such as osteoarthritis (OA) and rheumatoid arthritis, are the most common disease that afflict many patients all around the world. OA is a degenerative and chronic joints disease which causes articular alterations and consequent local inflammations and joint effusions. Disorders provoked by OA mostly depends on the activity of cells that synthesized the cartilage tissue, the chondrocytes. Those cells are immersed in the extracellular matrix (ECM) which is high hydrated and mainly composed by collagen, glycosaminoglycans (GAG) and proteoglycans. Alteration of growth, differentiation and degradation mechanisms (apoptosis) that rule the activity of the chondrocytes represents the principal cause of OA arise. The joints most commonly affected are those of knees, elbows, shoulders, hips, fingers and toes. More than 25% of the over 50 year old suffer from OA and more than 80% of those over 65 suffer from some form of degenerative joint disease.<sup>1</sup>

Therapeutic treatments in the late stages of the disease require necessarily surgery which includes the implantation of new cartilage tissues or, in the most serious cases, joint prosthesis. On the other hand, in the early stages of the disease, rehabilitative therapy, analgesics or anti-inflammatory drugs are administered. Another popular medical treatment is represented by the administration of hyaluronic acid (HA),<sup>2</sup> a polymer of natural origin synthesized by the human body, through intra-articular injections into the affected joints, with a procedure known as viscosupplementation. Hyaluronic acid is a linear glycosaminoglycan presents mainly in the extracellular matrix of connective tissues, in synovial fluids, in the vitreous humor of the eye and in the skin. In viscosupplementation procedures, the use of HA, characterized by high molecular weight and proper viscoelasticity properties, allows joints lubrications, inflammation and pain reduction and the restoring of the synovial fluids properties. Some studies suggest that the action of hyaluronic acid in viscosupplementation is caused by the ability of the biopolymer to promote the synthesis of new HA from synovial cells, stimulate the proliferation of chondrocytes and inhibit the degradation of cartilage and thus, improving quantitatively and qualitatively the joint tissues.<sup>3,4</sup> HA finds many

applications in the biomedical industry thanks to its biocompatibility, biodegradability and its viscoelastic properties. It is largely used for the production of eye drops, in wound healing, in tissue engineering, in the treatment of many pathologies and in the cosmetic field, being one of the main constituents of products for topical use.<sup>5</sup>

One of the most recent pharmacological approach in the treatment of OA involves the use of chondroprotective drugs which can prevent the occurrence of degenerative disease. The chondroprotectors are also able to stimulate the production of new cartilage acting on the growth mechanisms of the chondrocytes. Glucosamine hydrochloride (GlcN, figure 1.1), alone or in addition with chondroitin sulfate, is commonly used for the oral treatment of OA disorders.<sup>6,7</sup> Furthermore, the administration effects of D-glucosamine sulfate<sup>8,9</sup> and N-acetyl-glucosamine<sup>10</sup> are widely studied on animal models.

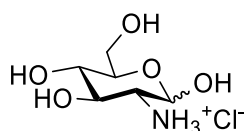


**Fig. 1.1:** Chemical structure of D-Glucosamine hydrochloride (GlcN).

D-glucosamine seems to have a fundamental role in the synthesis of glycosaminoglycans, which are one of the main constituents of cartilage,<sup>11</sup> and its usage, or that of D-glucosamine sulfate, on animals affected by OA would seem to enrich their cartilage tissue.<sup>12,13</sup>

Newsworthy results have come from the *in vitro* studies carried out by the research group of Prof. Anna Scotto D'Abusco on the anti-inflammatory activity of a peptidyl derivative of GlcN called 2-(N-Acetyl)-L-phenylalanyl-amido-2-deoxy-D-glucose (NAPA, figure 1.2), in the case of osteoarthritic cartilages.<sup>12,13,14</sup>

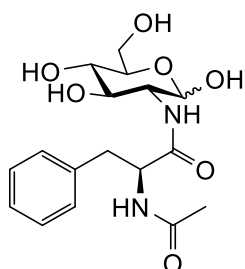


**Fig. 1.2:** Chemical structure of 2-(N-Acetyl)-L-phenylalanyl-amido-2-deoxy-D-glucose (NAPA).

Their recent investigations have highlighted that the treatment of diseased animals through intra-articular injections of NAPA was associated with a more homogeneous chondrocyte

cellularity, absence of fissures and fragmentation in tissues and more solid and smooth appearance of the matrix compared to the articular surfaces of the “control” knees treated with saline solution. The use of NAPA resulted in an enriched cartilage matrix with less injured sites through specific action on chondrocytes proliferation.<sup>15</sup> Furthermore, *in vitro* studies performed on rabbit primary chondrocytes revealed the anti-inflammatory activity of NAPA. The molecule was able to counteract the local cellular inflammation caused by induced-OA by contrasting specific cytokines production.<sup>12,14</sup>

In light of the above, the idea at the base of the PhD project was to define a chemical procedure for the synthesis of a hyaluronic acid-NAPA bioconjugate that could be used as innovative drug carrier system. In this way it could be possible to combine synergistically the viscoelastic properties of hyaluronic acid with the chondroprotective effect of NAPA in the *in vitro* treatment of osteoarthritis-induced animals cartilages, resulting in the development of an innovative bioconjugate for viscosupplementation. HA-NAPA conjugate could represent a promising therapeutic treatment in the field of arthritic diseases that could improve the standard procedures and open up on new medical strategies.

Synthetic strategies for the preparation of NAPA and HA-NAPA bioconjugates has been designed and studied in collaboration with Dr. Francesca Leonelli (Department of Chemistry, University of Rome, La Sapienza). Synthesis of NAPA, which represented the starting point of the project, revealed an unexpected racemization process that occurs during the coupling of N-Acetyl-L-phenylalanine with a glucosamine precursor. At this regard, the stereochemistry of the reaction was deepened and a general mechanism for the chirality loss of the L amino acid has been proposed. Then, NAPA was conjugated to hyaluronic acid through the use of a bivalent linker. Lastly, both NAPA diastereoisomers have been biologically tested and preliminary evaluation of the biological activity of HA-NAPA bioconjugate has been conducted.

Another problematic faced in the PhD project, dealt with the chemical modification of hyaluronic acid and the production of HA hydrogels to apply for tissue engineering. As explained above, hyaluronic acid has unique properties in terms of molecular weight, viscoelasticity and biocompatibility but it is also characterized by high solubility, poor mechanical stability and rapid degradation behavior *in vivo*.<sup>16</sup> Thus, synthetic procedures that

are able to change polymeric structure are required to empower hyaluronic acid applications, such as the viscosupplementation. The chemical modification of HA can provide new polymeric properties, influencing its ability to resist the fast *in vivo* degradation<sup>17,18</sup> and to interact better with cells or other biomaterial.<sup>19</sup> For example, some studies suggested that the introduction of sulphate<sup>20</sup> or sulfonic groups<sup>21</sup> onto the HA molecular chain increases the resistance to the activity of glycolytic enzymes, such as hyaluronidases and chondroitinase, in *in vitro* degradation analysis. The HA-SO<sub>3</sub>H half-life was triplicated respect to that of un-sulfonated HA in physiological concentration of hyaluronidase. In addition, new negatively charged groups in polymeric backbone have important effect on the physicochemical behavior of HA. Not only the sulfation or sulfonation cause the improvement of enzymatic resistance. Schanté and coworkers<sup>22</sup> demonstrated that the grafting of different amino acids towards amidation on HA increases the stability of HA-based products against enzymatic digestion defining the hyaluronic acid derivatives as promising material for viscosupplementation or drug delivery.

Although the numerous procedures described in literature for chemical modification of hyaluronic acid, only few examples regard the sulfation or sulfonation of the polysaccharide. At this regards, we defined a method for the synthesis of a series of novel sulfonated HA-based material through the amidation of taurine (Tau), a natural amino sulfonic acid, in water. The coupling efficiency of two water soluble coupling reagents was compared and a preliminary physico-chemical characterization of the new sulfonated-HA bioconjugates was carried out. The HA-SO<sub>3</sub>H derivatives represent interesting candidates for biomedical application. Sulfonation was faced not only for the synthesis of injectable HA derivatives. In fact, a one-pot procedure for the crosslinking and sulfonation of sodium hyaluronate was presented. Sulfonated hydrogels, prepared using BDDE as crosslinker, resulted to be valid candidates for chondrocytes and fibroblasts growth.

## 1.1 Hyaluronic acid: general properties

Hyaluronic acid [HA – hyaloid (vitreous) – uronic acid] is a negatively charged linear polysaccharides composed by a disaccharide units of D-glucuronic acid and N-acetyl-D-glucosamine linked by  $\beta(1,4)$  and  $\beta(1,3)$  glucosidic bonds (figure 1.3). HA is the only non-sulfated glycosaminoglycan presents in the body and it has a high molecular weight, usually in the order of millions of Daltons, and interesting viscoelastic properties influenced by its polymeric and polyelectrolyte characteristics.<sup>4</sup> Hyaluronate solutions in water show high viscosity due to the high molecular weight, the semi-flexible chain and the strong intramolecular interaction, with non-Newtonian flow properties.<sup>23</sup>

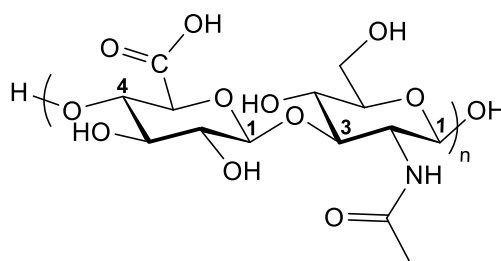


**Fig. 1.3:** Repeating unit of hyaluronic acid (HA).

HA was isolated in high molecular weight from the vitreous humor of bovine eyes by Meyer and Palmer in the 30s, without the use of strong hydrolytic agents.<sup>24</sup> It is synthesized at the plasma membrane of cells including fibroblasts, keratinocytes or chondrocytes by the enzyme Hyal synthetase and it is secreted outside the cells without any post-synthetic modification. HA is synthesized by cells in the Golgi network together with other GAG.<sup>25,26</sup> The biopolymer is characterized by high water solubility and therefore it can absorb a large amount of water expanding up to 1000 times its solid volume and forming a loose hydrated network.<sup>27</sup> Hyaluronic acid is primarily presents in the extracellular matrix (ECM) of soft connective tissues<sup>27</sup> and due to its unique viscoelastic properties, it is particularly abundant in almost all biological fluids and tissues such as in the synovial fluid of joints, skin dermis, vitreous body of eye, cartilage, tendons and umbilical cord. In physiological condition, HA is in the form of sodium salt, known as sodium hyaluronate. Its main role in body is structural and hydrating due to the high hydrophilicity that gives to the polymer the capacity to maintain water. It assures an open, hydrated and stable extracellular space in which cells and other extracellular matrix (ECM) components, such as collagen and elastin fibers, are firmly maintained, and

acts as a lubricant and shock absorber, especially in joints.<sup>28</sup> Degradation of HA leads to the lowering of molecular weight and it can occur via enzymatic or non-enzymatic reactions. Fast enzymatic digestion by hyaluronidase enzymes and HA cell internalization by CD44 cell surface receptors<sup>29</sup> explain the short half-life of HA after injection in body. Non-enzymatic degradation of HA is mainly caused by alteration of pH and oxidative damages. The hydrolytic degradation under the effect of pH occurs via random chain scission both in strong acidic or alkaline conditions but HA seems to tolerate better acidic pH. Base-catalyzed hydrolysis promotes degradation on the N-acetylglucosamine unit while hydrolytic degradation in acidic conditions affects mainly the glucuronic unit causing less chain fragmentation.<sup>30</sup>

## **1.2 Chemical modification of hyaluronic acid**

HA is a multipurpose materials with key characteristics that can be tuned deeply thanks to its chemical versatility. Chemical interventions are largely used to improve mechanical, chemical or enzymatical resistance and thus modifications are required to provide hyaluronic acid with improved qualities. Modifications of HA can be done via functionalization or crosslinking. In the first case, a specific molecule is covalently bonded to a single HA chain, while in the second case, more chains of HA are linked together to form and hydrogel. This two steps are not exclusive and in some cases functionalization is followed by crosslinking in order to obtain a covalent network with tailored functions.<sup>31,32</sup> In the recent years, many efforts have been made in the development of novel synthetic strategies for HA modification and lot of authors have suggested methods for the functionalization of hyaluronan with bioactive molecules or protocols for the fabrication of crosslinked scaffolds for cells adhesion and proliferation. Other researchers<sup>33</sup> proposed different methodologies for the formation of HA nanoparticles as drug carriers.

Bearing in mind the repeating unit of HA, all the methodologies exploit the reactivity of two specific sites: the carboxylic group and the primary alcoholic function. The COOH position is generally transformed to get amide or ester derivatives<sup>34,35</sup> while the primary OH group could be converted into ether bonds to form stabile networks.<sup>36</sup> In addition, an amine position can be liberated as consequence of the deacetylation of N-position.<sup>37,38</sup>

Reactions can be performed in water, with the sodium hyaluronate, or in organic solvents, such as dimethyl sulfoxide, dimethylformamide, or N-methylpyrrolidone, if solubility of reactants and/or type of reactions require it. In the latter case, HA is usually transformed into the corresponding tetrabutylammonium salt (HA-TBA).

Amidation is generally accomplished using carbodiimides in water. Several amines have been directly linked to sodium hyaluronate such as carnosine,<sup>39</sup> doxorubicin,<sup>40</sup> or the hindered nisin.<sup>41</sup> In other cases, aminic derivatives of the desired drug is conjugated to HA<sup>5</sup> with carbodiimides. Amidation carried out by diamines, such as adipic acid dihydrazide (ADH)<sup>42</sup> or 1,3-diaminopropane,<sup>20</sup> brings about HA crosslinking. By suitable COOH activating agents, amidation can be successfully pursue both in water or organic solvents.

Esterification of HA is harder to obtain in water due to the facile hydrolysis of COO-activated intermediate and the low nucleophilicity of hydroxylic groups and, thus, organic solvents are required. Esterification is used both to functionalize HA or to crosslink the biopolymer. Alkylation of COO<sup>-</sup> is obtained with alkyl halides<sup>43</sup> and it allows the synthesis of a wide range of hyaluronan esters. For instance, a bromine alkyl derivative of paclitaxel has been esterified on HA as a consequence of nucleophilic substitution.<sup>44</sup> Esterified networks of HA can be synthesized reacting diepoxides in water in acidic environment.<sup>36</sup>

The primary hydroxylic group in the repeating unit is generally reacted to crosslink sodium hyaluronate. Some diepoxides, like 1,4-Butanediol diglycidyl ether (BDDE),<sup>45</sup> polyethylene glycol diglycidyl ether (PEGDE)<sup>46</sup> and ethylene glycol diglycidyl ether (EGDE),<sup>47</sup> are used for this purpose and the reaction is generally accomplished at pH > pK<sub>a</sub> (OH) or in slightly acidic pH, where primary OH is still enough nucleophile. Other crosslinker commonly used are divinyl sulfone (DVS)<sup>48</sup> and glutaraldehyde.<sup>49</sup> The latter has the drawback of being toxic and requires specific handling and careful purification of the final product.

An amine group can be recovered as result of deacetylation of the NHCOCH<sub>3</sub> and it can be used for further modification of hyaluronic acid. Nevertheless, deacetylation requires drastic conditions that can induce chain fragmentation and, thus, only few examples are reported in literature.

## 1.3 General applications of HA

Hyaluronic acid is a versatile materials that is widely investigated due to its biocompatibility, biodegradability and viscoelastic properties. It finds numerous applications in medicine, in the field of ophthalmology, surgery, wound healing, in cosmesis, for the preparation of lotions with high, moderate and low molecular mass, and in dermatology as well as plastic surgery, for dermal filler injections. Furthermore, the capability of HA to interact with specific cell-surface receptors, such as CD44,<sup>29</sup> which are overexpressed in tumor growth, has strongly influenced the studies of HA derivatives in the field of anti-cancer drug delivery.<sup>50,51,52</sup> In the frame of the work of thesis, viscosupplementation, drug delivery system and hydrogels preparation will be studied in deep.

### 1.3.1 Viscosupplementation

As previously reported, arthritic disorders represent one of the major health problems especially in industrialized countries with high life expectancy and they can dramatically reduce the quality of the affected patients' lives. Currently, no reliable long-term curative strategies have experienced wide clinical acceptance <sup>1</sup> and HA viscosupplementation represents the most widespread therapeutic procedure for the reduction of local pain and the restoring of synovial fluid viscoelasticity in stiff and consumed joints. High molecular weight molecules of hyaluronic acid are partially cross-linked to form a high-viscosity solution that serve both as a lubricant and as a shock absorber.<sup>3</sup> Intra-articular injections of HA are also indicated after arthroscopy. In addition, some studies on the anti-inflammatory activity showed that administration of high molecular mass hyaluronic acid promoted the synthesis of new HA in cartilage, influencing chondrocytes proliferation, and inhibiting cartilage degradation. It diminishes the gene expression of the cytokines and enzymes that are associated with osteoarthritis.<sup>53</sup> Sodium hyaluronate has an intra-articular half-life of 13 hours and this represent one of the main drawback related to hyaluronan injection. Modifications of the polysaccharide are necessary to avoid the body's robust and fast catabolic degradation, promoting long term applications.<sup>3</sup> The molar mass of HA in synovial fluid of a healthy adult person is in the range between 2 and 7 MDa and commercially available HA-based products for viscosupplementation have a molecular weight that falls into this range, e.g. Healon

(Pfizer, New York, NY) or ORTHOVISC®.<sup>4</sup> Other products, such as Synvisc® Hylan G-F 20 are composed by a high molecular weight fraction of approximately 6,000,000 Da and by a hydrated gel. The half-life of Hylan G-F 20 is 1.5 days (liquid phase) and 8.8 days (solid phase) probably because of the presence of cross-links. Lower mass products, such as Hyalgan (Fidia, Abano Terme, Italy) and Artz Dispo (Seikagaku, Tokyo, Japan), contain HA of lower molar mass (about 1 MDa). While treatment with higher molar mass preparations requires three injections over 3 weeks, the latter have to be injected at least 5 times over 5 weeks.<sup>3</sup>

Mild crosslinking degrees are commonly used for the production of dermal fillers for augmentation, to fill facial wrinkles and depressed scars. An ideal dermal filler should be temporary, but long-lasting (months to a year or longer), with minimum side effects and no allergenic responses, easy to administer, with minimum pain or no pain upon injection, and a reasonable cost for both the physician and the patient.<sup>54</sup> Crosslinking permits to transform a viscous solution into a weak hyaluronic acid gel that imparts a physical and chemical barrier to deter drainage or degradation. Therefore, residence time increases by crosslinking HA.<sup>25</sup> The most used crosslinkers are 1,4-Butanediol diglycidyl ether and divinyl sulfone, both reacted in alkaline conditions.

### 1.3.2 HA as Drug delivery system for viscosupplementation

The key aspect of hyaluronic acid is represented by the amount of chemical modification to which it can be subjected to improve its properties, making it a versatile material for biomedical applications. The presence of specific receptors on cells surface, called CD44, make HA suitable for the synthesis of drug delivery system. Conjugation of drugs to HA was reported early in 1991<sup>51</sup> and the approach is based on the fact that a specific bio-active molecule can be covalently bonded to the sodium hyaluronate to produce a pro-drug system. The bond formed should be stable enough to be cleaved only in the target site and to allow an optimal drug release. Then, conjugation would improve therapeutic effects of the drug. Many examples can be found in literature dealing with drug conjugation, from antitumor drugs such as paclitaxel<sup>44</sup> and doxorubicin<sup>40</sup> to amino acids or peptide.

Furthermore, nonsteroidal and steroidal anti-inflammatory drugs have been successfully bonded to HA. The importance of this conjugation lies in the fact that the viscosupplementation effect of hyaluronic acid can be combined with action of drugs for local injections into painful joints. From a chemical point of view, drugs with a hydroxyl group can be directly conjugated on HA<sup>5</sup> as it was described by Della Valle and coauthors<sup>43</sup> for hydrocortisone, prednisone, prednisolone, fluorocortisone, dexamethasone, betamethasone and corticosterone.

Other works suggested the amidation of hydrocortisone-hemisuccinate and of N-Succinimidyl ibuprofen with HA. Amidation on HA was carried out after functionalization of the polymer with a diamine able to react further with the COOH group, present in the hydrocortisone derivative, or directly with that in ibuprofen molecule.<sup>55</sup> Methotrexate (MTX), a drug commonly used for reducing synovial inflammation of rheumatoid arthritis, has been conjugated to hyaluronic acid with a suitable spacer composed by peptide-linker chain forming two amide bonds.<sup>56</sup>

Anti-inflammatory drugs have been loaded onto crosslinked hyaluronic acid<sup>57</sup> for the local treatment of osteoarthritic knee, and steroids<sup>58</sup> have been combined to HA-gel matrices non-covalently, in order to fabricate a combination therapy to treat OA. The first study showed positive effects of hyaluronan-loaded hydrogel, most likely as consequence of reduction of pain and discomfort. The second approach allowed the local delivery of the steroid at OA site and would overcome the side effects associated with steroid overdose. Furthermore, the local release would result in a faster pain relief compared to that provoked only by viscosupplementation.

### 1.3.3 HA-based hydrogels preparation for chondrocytes

Modification of hyaluronic acid includes also the formation of 3D hydrogels that can be used as stable scaffolds or injectable gels for tissue engineering. Porous hydrogels have several unique characteristics, including their similarity to tissue extracellular matrix (ECM), and are widely used in the regeneration of soft tissues. They are highly permeable to nutrients and water-soluble metabolites, allowing cell survival and supporting cell growth.<sup>59</sup> Injectable gels are able to control drugs or growth factors release, cause minimal mechanical irritation to

surrounding tissue, and promote nutrient diffusion to support the viability and proliferation of cells.<sup>16</sup> HA-based gels can act as scaffold for the growth and proliferation of cartilage cells and, then, for the production *ex novo* of the tissue. For this purpose, changes in the hyaluronic acid backbone should be carried out to impress key features to the scaffold in terms of porosity, mechanical and enzymatic resistance and cellular compatibility.

The carboxylic and hydroxyl group as well as  $-\text{NHCOCH}_3$  are the sites identified for the chemical modification of HA in the fabrication of 3D supports. For instance, the crosslinking via poly(ethylene glycol) diglycidyl ether (PEGDE) has brought about the fabrication of hyaluronic acid 3D hydrogels for the culture of chondrocytes, demonstrating the ability of the scaffolds to induce chondrogenic differentiation of rabbit articular chondrocytes.<sup>45</sup> Rabbit chondrocytes have been implanted also on porous sodium hyaluronic acid/sodium alginate (HA/SA) scaffold.<sup>60</sup> In this case the material have been fabricated as interpenetrating polymeric network (IPN), carrying out a combined crosslinking of HA and SA with poly(ethylene glycol) diglycidyl ether (PEGDG) and calcium chloride, respectively. The addition of sodium alginate improved significantly the mechanical and biological properties of hyaluronic acid scaffolds and slightly up-regulated the rabbit chondrogenic differentiation.

Shaoquan Bian and coworkers presented a protocol for the synthesis of self-crosslinking hyaluronic acid after the amidation with cysteamine.<sup>61</sup> The formation of disulfide bonds from free thiol groups brought about the self-crosslinking process leading to HA-modified hydrogel with tunable features. Three-dimensional hydrogels were tested for the culture of fibroblasts and chondrocytes *in vitro* and the cells showed high proliferation and secretion of extracellular matrix during culture for 21 days. Furthermore, collagen, which is the major constituent of connective tissues, could be blended to hyaluronic acid with the purpose to increase biocompatibility with cells since it is considered one of the most promising substrate for many cell types, including chondrocytes.<sup>62</sup> HA/collagen hydrogels were successfully synthesized<sup>59</sup> resulting in the increase of the chondrocytes proliferation rate and antienzyme activity.

## 1.4 Sulfonated materials

The addition of sulfate ( $\text{ROSO}_3\text{H}$ ) or sulfonated ( $\text{RSO}_3\text{H}$ ) groups to a polymeric backbone can strongly influence physicochemical and biological properties of the material. Sulfonated polymers are a current field of research and can be found in applications like membranes for fuel cells, membranes for filtration, ion-exchange resins, medical and pharmaceutical devices.<sup>63</sup> The introduction of the negative polar groups can take place during polymerization, generally accomplished by the reaction of suitable monomers, or apporating chemical modifications onto the commercial polymers. In the field of biocompatible materials, the preparation of polymers with high hemocompatibility is an important aspect to consider in the development of blood-contact devices. Materials with tailored degree of sulfation or sulfonation are able to mimic properties of heparin, which is a linear polysaccharide consisting in repeating units of uronic acid and glucosamine residues linked via 1-4 bonds (figure 1.4). Heparin, which can be considered one of the most known member of glycosaminoglycans, was firstly discovered at the beginning of XX century and soon employed as anticlotting drugs due to its anticoagulant or antithrombotic activity. Still today, heparin and its low molecular weight analogous (LMWH) are the most commonly used clinical anticoagulants and are administered intravenously, subcutaneously or parenterally.<sup>64</sup>

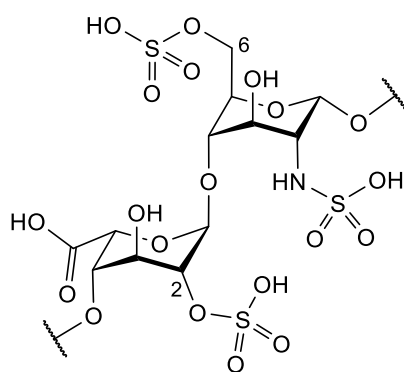


**Fig. 1.4:** Chemical structure of heparin. The disaccharide unit is composed by a 2-O-sulfated iduronic acid and 6-O-sulfated/N-sulfated glucosamine.

The anticlotting activity of heparin is the result of the ability to bind to the serine protease inhibitor antithrombin, causing the inhibitor to inactivate thrombin<sup>64</sup> and it is believed that this is possible thanks to the presence of ionic functional groups onto the polymeric backbone, such as the sulfonic, sulfonated or carboxylic moieties. At this regard, those polar groups should be present in order to impress peculiar anticoagulant properties to the biomaterials.

Several procedures for the sulfonation of materials can be found in literature, both for synthetic or natural polymers. For instance, sulfonation of polystyrene<sup>65</sup> enhances the wettability of the polymer and stimulates cell adhesion, activates cell spreading and influences cytoskeleton reorganization in fibroblasts. Poly(L-lactide) (PLLA), a highly hydrophobic material used for biomedical applications, was modified by the surface insertion of SO<sub>3</sub>H in order to enhance interactions with biomaterial such as collagen thus promoting chondrocyte adhesion and proliferation.<sup>66</sup> Zhimin Sun and coworkers<sup>67</sup> demonstrated that sulfonated chitosan exhibited higher antibacterial activities against *Escherichia coli* and *Staphylococcus aureus* than those of unmodified chitosan. In addition, chitosan exhibited selective antifungal activity after sulfonation. Sulfonation of poly( $\gamma$ -glutamic acid) ( $\gamma$ -PGA) allowed the synthesis of a useful material with anticoagulant activity usable in various medical applications, such as drug delivery, tissue engineering, and medical materials.<sup>68</sup>

### **1.5 Sulfonation of hyaluronic acid: state of the art and aim of the thesis**

Sulfonation of hyaluronic acid could represent an interesting and challenging topic for the preparation of a biocompatible material with tailored physico-chemical and biological features. As mentioned before, anticlotting properties are related to the presence of strong ionic groups in the polymeric skeleton and, thus, hyaluronic acid seems to be a suitable candidate for sulfonation process considering the natural presence of COOH and OH in the repeating unit. Furthermore, the polar SO<sub>3</sub><sup>-</sup> are considered crucial sites for the binding of growth factor in cellular culture and could strongly enhance cell compatibility of HA.

To our knowledge, only few procedures related to the functionalization of hyaluronic acid with -OSO<sub>3</sub>H or -SO<sub>3</sub>H are reported, even though the importance of sulfated and sulfonated materials in biomedical applications. Barbucci and coworkers published over the years a few articles regarding the synthesis,<sup>69</sup> properties<sup>70</sup> and applications<sup>71</sup> of a novel category of sulfated-HA derivatives. The HA-SO<sub>4</sub>H products were synthesized in dimethyl formamide starting from the tributylammonium salt of HA in the presence of sulfur trioxide pyridine complex (SO<sub>3</sub>-Py), which is generally used as source of sulfur trioxide in the synthesis of organosulfate compounds from alcohols. Degree of sulfation resulted to be very high, ranging from 1 to 4 -OSO<sub>3</sub>H groups per repeating unit, and led to an increase of glycolytic enzymes resistance in *in vitro* degradation experiments under the action of both hyaluronidases and

chondroitinase.<sup>72</sup> Additionally, crosslinked sulfated-HA hydrogels showed to have optimal properties for a possible applications in tissue engineering.<sup>73</sup>

HA-SO<sub>3</sub>H derivative synthesis could be undertaken following the procedure given from Amit K. Jha and coworkers.<sup>21</sup> In the patent the authors suggested that chemical modification of sodium hyaluronate could be performed in a two-step synthesis. The sulfonation provides a first conversion of sodium hyaluronate into an aldehyde derivative by means of sodium periodate oxidation. Then, 2-aminoethyl hydrogen sulfate was reacted with the aldehydic derivative of HA in the presence of sodium cyanoborohydride as oxidant agent. The HA-SO<sub>3</sub>H derivative showed a half-life triplicated respect to that of non-sulfonated HA in physiological concentration of hyaluronidase, confirming the importance of the chemical modification for biomedical purposes.

Nevertheless, even with optimal functionalization degrees, both procedures require drastic conditions for the treatment of hyaluronic acid, necessitate the use of organic solvent and lead to a radical change in the polymeric skeleton, in particular with strong oxidation agents. Furthermore, it has to consider that not only the sulfation or sulfonation cause the improvement of enzymatic resistance. Schanté and coworkers<sup>22</sup> demonstrated that the increase of enzymatic stability of hyaluronic acid could be achieved as a consequence of amino acids amidation. The amidated-HA derivatives revealed to be promising materials for viscosupplementation or drug delivery.

At this regards, we focused on the synthesis of HA-SO<sub>3</sub>H derivatives, towards amide bond formation, with a process that could take place in water. In addition, a one pot procedure for the synthesis of sulfonate HA-based hydrogels was developed. Taurine (2-aminoethanesulfonic acid, Tau) and N,N-Bis(2-hydroxyethyl)-2-aminoethanesulfonic acid (Bes) were used (figure 1.5) for this purpose. The first is a natural amino sulfonic acid occurring in mammalian cells while the latter is commonly used for the preparation of bio-buffered solutions.<sup>74</sup> Both molecules bear a sulfonic group in the structure, are fully water soluble, biocompatible and could be easily reacted to give sulfonated-HA derivatives through the reaction of aminic and hydroxylic groups.

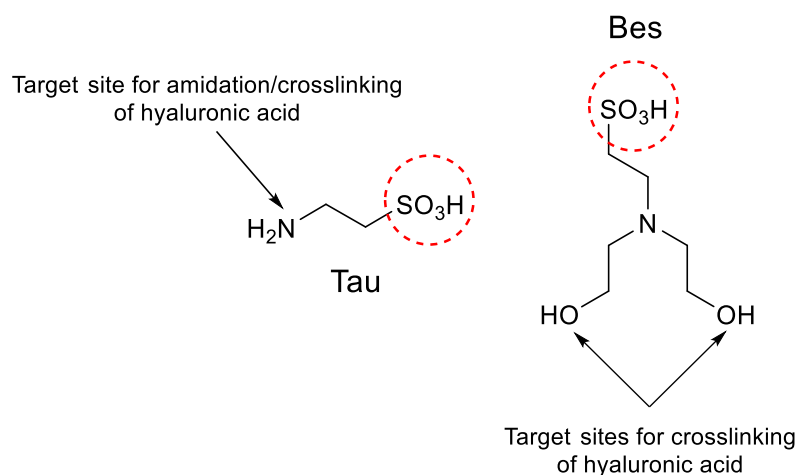


**Fig. 1.5:** Chemical structure of 2-aminoethanesulfonic acid (Tau) and N,N-Bis(2-hydroxyethyl)-2-aminoethanesulfonic acid (Bes). Tau and Bes have been used for the sulfonation of hyaluronic in order to obtain water soluble ha-Tau derivatives by exploiting the aminic function of Tau. Additionally, sulfonated HA hydrogels have been prepared in the presence of Tau and Bes.

In the present study, taurine will be linked directly on HA through amide bond formation in water to form soluble sulfonated-HA derivatives, reasonably enhancing hyaluronidase stability. Tau and Bes were also crosslinked with HA in the presence of BDDE to form porous matrices enriched in  $\text{SO}_3\text{H}$  groups, exploiting aminic and hydroxylic functions, respectively.

In mammals, taurine is near ubiquitous in distribution with a low concentration in body fluids, such as plasma, cerebrospinal fluid, and extracellular fluid. The highest concentrations are usually found in the heart or brain, but the bulk of the taurine is in the musculature.<sup>75</sup> It is the abundant in bile, being one of the major component of bile salts. Taurine has demonstrated to perform an antioxidant function in certain tissues, probably because its membrane stabilizing role<sup>76</sup> both in vitro and in vivo models of inflammation<sup>77</sup> When blended with chitosan, it enhanced the acceleration effect of the biopolymer on wound healing at early periods.<sup>78</sup> and also has effects on cell proliferation, inflammation and collagenogenesis.<sup>79</sup> The local administration of a tau-chitosan gel positively affected wound healing process in mice as result of taurine release over a period of one week. The tensile strength of wound tissues increases, the autoxidation processes diminishes and hydroxyproline, which is the main component of collagen, is stimulated.<sup>80</sup> Furthermore, a mixture of taurine and hyaluronic acid was used to investigate protective effects of ophthalmic formulations for ocular surface in dry eye models. Tau showed relevant antioxidant effect in corneal epithelial cells and osmoprotective activity, preventing the ocular surface damage elicited by atropine.<sup>81</sup> On the other hand, Bes is largely used in the modification and crosslinking of synthetic materials for

the preparation of ionic membranes<sup>82</sup> but no references of its use has been found for biopolymers modification, although its non-toxic nature. The modification of hyaluronic acid with SO<sub>3</sub>H-bearing molecules could represent the starting point for the synthesis of biomaterials with enhanced cytocompatibility and anticlotting properties.

## 1.6 References

- (1) Schulz, R. M., & Bader, A. (2007). Cartilage tissue engineering and bioreactor systems for the cultivation and stimulation of chondrocytes. *European Biophysics Journal*, 36(4-5), 539-568.
- (2) Hamburger, M. I., Lakhanpal, S., Mooar, P. A., & Oster, D. (2003, April). Intra-articular hyaluronans: a review of product-specific safety profiles. In *Seminars in arthritis and rheumatism* (Vol. 32, No. 5, pp. 296-309). WB Saunders.
- (3) de Rezende, M. U., & de Campos, G. C. (2012). Viscosupplementation. *Revista Brasileira de Ortopedia (English Edition)*, 47(2), 160-164.
- (4) Kogan, G., Šoltés, L., Stern, R., & Gemeiner, P. (2007). Hyaluronic acid: a natural biopolymer with a broad range of biomedical and industrial applications. *Biotechnology letters*, 29(1), 17-25.
- (5) Mero, A., & Campisi, M. (2014). Hyaluronic acid bioconjugates for the delivery of bioactive molecules. *Polymers*, 6(2), 346-369.
- (6) Das Jr, A., & Hammad, T. A. (2000). Efficacy of a combination of FCHG49™ glucosamine hydrochloride, TRH122™ low molecular weight sodium chondroitin sulfate and manganese ascorbate\* in the management of knee osteoarthritis. *Osteoarthritis and Cartilage*, 8(5), 343-350.
- (7) Towheed, T., Maxwell, L., Anastassiades, T. P., Shea, B., Houpt, J. B., Welch, V., ... & Wells, G. A. (2005). Glucosamine therapy for treating osteoarthritis. *Cochrane database of systematic reviews*, (2).
- (8) Lippiello, L., Woodward, J., Karpman, R., & Hammad, T. A. (2000). In vivo chondroprotection and metabolic synergy of glucosamine and chondroitin sulfate. *Clinical Orthopaedics and Related Research®*, 381, 229-240.
- (9) Oegema Jr, T. R., Deloria, L. B., Sandy, J. D., & Hart, D. A. (2002). Effect of oral glucosamine on cartilage and meniscus in normal and chymopapain-injected knees of young rabbits. *Arthritis & Rheumatism*, 46(9), 2495-2503.

- (10) Shikhman, A. R., Amiel, D., D'lima, D., Hwang, S. B., Hu, C., Xu, A., ... & Lotz, M. K. (2005). Chondroprotective activity of N-acetylglucosamine in rabbits with experimental osteoarthritis. *Annals of the rheumatic diseases*, 64(1), 89-94.
- (11) Uitterlinden, E. J., Koevoet, J. L. M., Verkoelen, C. F., Bierma-Zeinstra, S. M. A., Jahr, H., Weinans, H., ... & Van Osch, G. J. V. M. (2008). Glucosamine increases hyaluronic acid production in human osteoarthritic synovium explants. *BMC Musculoskeletal Disorders*, 9(1), 120.
- (12) Stoppoloni, D., Politi, L., Leopizzi, M., Gaetani, S., Guazzo, R., Basciani, S., ... & d'Abusco, A. S. (2015). Effect of glucosamine and its peptidyl-derivative on the production of extracellular matrix components by human primary chondrocytes. *Osteoarthritis and cartilage*, 23(1), 103-113.
- (13) Igarashi, M., Kaga, I., Takamori, Y., Sakamoto, K., Miyazawa, K., & Nagaoka, I. (2011). Effects of glucosamine derivatives and uronic acids on the production of glycosaminoglycans by human synovial cells and chondrocytes. *International journal of molecular medicine*, 27(6), 821-827.
- (14) Veronesi, F., Giavaresi, G., Maglio, M., d'Abusco, A. S., Politi, L., Scandurra, R., ... & Fini, M. (2017). Chondroprotective activity of N-acetyl phenylalanine glucosamine derivative on knee joint structure and inflammation in a murine model of osteoarthritis. *Osteoarthritis and Cartilage*, 25(4), 589-599.
- (15) d'Abusco, A. S., Corsi, A., Grillo, M. G., Cicione, C., Calamia, V., Panzini, G., ... & Scandurra, R. (2008). Effects of intra-articular administration of glucosamine and a peptidyl-glucosamine derivative in a rabbit model of experimental osteoarthritis: a pilot study. *Rheumatology international*, 28(5), 437-443.
- (16) Khunmanee, S., Jeong, Y., & Park, H. (2017). Crosslinking method of hyaluronic-based hydrogel for biomedical applications. *Journal of tissue engineering*, 8, 2041731417726464.
- (17) Liu, C., Bae, K. H., Yamashita, A., Chung, J. E., & Kurisawa, M. (2017). Thiol-Mediated Synthesis of Hyaluronic Acid–Epigallocatechin-3-O-Gallate Conjugates for the Formation of Injectable Hydrogels with Free Radical Scavenging Property and Degradation Resistance. *Biomacromolecules*, 18(10), 3143-3155.

- (18) Lee, H. Y., Hwang, C. H., Kim, H. E., & Jeong, S. H. (2018). Enhancement of bio-stability and mechanical properties of hyaluronic acid hydrogels by tannic acid treatment. *Carbohydrate polymers*, 186, 290-298.
- (19) Shin, J., Lee, J. S., Lee, C., Park, H. J., Yang, K., Jin, Y., ... & Yang, H. S. (2015). Tissue adhesive catechol-modified hyaluronic acid hydrogel for effective, minimally invasive cell therapy. *Advanced Functional Materials*, 25(25), 3814-3824.
- (20) Barbucci, R., Rappuoli, R., Borzacchiello, A., & Ambrosio, L. (2000). Synthesis, chemical and rheological characterization of new hyaluronic acid-based hydrogels. *Journal of Biomaterials Science, Polymer Edition*, 11(4), 383-399.
- (21) Jha, A. K., Altiok, E. I., Jackson, W. M., & Healy, K. E. (2018). U.S. Patent No. 10,000,582. Washington, DC: U.S. Patent and Trademark Office.
- (22) Schanté, C. E., Zuber, G., Herlin, C., & Vandamme, T. F. (2012). Improvement of hyaluronic acid enzymatic stability by the grafting of amino-acids. *Carbohydrate polymers*, 87(3), 2211-2216.
- (23) Cowman, M. K., Schmidt, T. A., Raghavan, P., & Stecco, A. (2015). Viscoelastic properties of hyaluronan in physiological conditions. *F1000Research*, 4.
- (24) Meyer, K., & Palmer, J. W. (1934). The polysaccharide of the vitreous humor. *Journal of Biological Chemistry*, 107(3), 629-634.
- (25) Fakhari, A., & Berkland, C. (2013). Applications and emerging trends of hyaluronic acid in tissue engineering, as a dermal filler and in osteoarthritis treatment. *Acta biomaterialia*, 9(7), 7081-7092.
- (26) Knudson, C. B., & Knudson, W. (1993). Hyaluronan-binding proteins in development, tissue homeostasis, and disease. *The FASEB Journal*, 7(13), 1233-1241.
- (27) Laurent, T. C., & Fraser, J. R. E. (1992). Hyaluronan 1. *The FASEB journal*, 6(7), 2397-2404.
- (28) Schanté, C. E., Zuber, G., Herlin, C., & Vandamme, T. F. (2011). Chemical modifications of hyaluronic acid for the synthesis of derivatives for a broad range of biomedical applications. *Carbohydrate polymers*, 85(3), 469-489.

- (29) Aruffo, A., Stamenkovic, I., Melnick, M., Underhill, C. B., & Seed, B. (1990). CD44 is the principal cell surface receptor for hyaluronate. *Cell*, 61(7), 1303-1313.
- (30) Stern, R., Kogan, G., Jedrzejewski, M. J., & Šoltés, L. (2007). The many ways to cleave hyaluronan. *Biotechnology advances*, 25(6), 537-557.
- (31) Kurisawa, M., Chung, J. E., Yang, Y. Y., Gao, S. J., & Uyama, H. (2005). Injectable biodegradable hydrogels composed of hyaluronic acid–tyramine conjugates for drug delivery and tissue engineering. *Chemical communications*, (34), 4312-4314.
- (32) Loebel, C., D'Este, M., Alini, M., Zenobi-Wong, M., & Eglin, D. (2015). Precise tailoring of tyramine-based hyaluronan hydrogel properties using DMTMM conjugation. *Carbohydrate polymers*, 115, 325-333.
- (33) Choi, K. Y., Min, K. H., Na, J. H., Choi, K., Kim, K., Park, J. H., ... & Jeong, S. Y. (2009). Self-assembled hyaluronic acid nanoparticles as a potential drug carrier for cancer therapy: synthesis, characterization, and in vivo biodistribution. *Journal of Materials Chemistry*, 19(24), 4102-4107.
- (34) Testa, G., Di Meo, C., Nardecchia, S., Capitani, D., Mannina, L., Lamanna, R., ... & Dentini, M. (2009). Influence of dialkyne structure on the properties of new click-gels based on hyaluronic acid. *International Journal of Pharmaceutics*, 378(1-2), 86-92.
- (35) Li, J., Shin, G. H., Chen, X., & Park, H. J. (2015). Modified curcumin with hyaluronic acid: combination of pro-drug and nano-micelle strategy to address the curcumin challenge. *Food research international*, 69, 202-208.
- (36) Tomihata, K., & Ikada, Y. (1997). Preparation of cross-linked hyaluronic acid films of low water content. *Biomaterials*, 18(3), 189-195.
- (37) Zhang, W., Mu, H., Zhang, A., Cui, G., Chen, H., Duan, J., & Wang, S. (2013). A decrease in moisture absorption–retention capacity of N-deacetylation of hyaluronic acid. *Glycoconjugate journal*, 30(6), 577-583.
- (38) Crescenzi, V., Francescangeli, A., Renier, D., & Bellini, D. (2002). New cross-linked and sulfated derivatives of partially deacetylated hyaluronan: Synthesis and preliminary characterization. *Biopolymers: Original Research on Biomolecules*, 64(2), 86-94.

- (39) Sciuto, S., Greco, V., Rizzarelli, E., Bellia, F., Lanza, V., Vaccaro, S., & Messina, L. (2016). Derivatives obtained from hyaluronic acid and carnosine. WO2016016847A1
- (40) D'Este, M., Eglin, D., & Alini, M. (2014). A systematic analysis of DMTMM vs EDC/NHS for ligation of amines to hyaluronan in water. *Carbohydrate polymers*, 108, 239-246.
- (41) Lequeux, I., Ducasse, E., Jouenne, T., & Thebault, P. (2014). Addition of antimicrobial properties to hyaluronic acid by grafting of antimicrobial peptide. *European polymer journal*, 51, 182-190.
- (42) Hahn, S. K., Park, J. K., Tomimatsu, T., & Shimoboji, T. (2007). Synthesis and degradation test of hyaluronic acid hydrogels. *International journal of biological macromolecules*, 40(4), 374-380.
- (43) Della Valle, F., & Romeo, A. (1989). U.S. Patent No. 4,851,521. Washington, DC: U.S. Patent and Trademark Office.
- (44) Leonelli, F., La Bella, A., Migneco, L. M., & Bettolo, R. M. (2008). Design, synthesis and applications of hyaluronic acid-paclitaxel bioconjugates. *Molecules*, 13(2), 360-378.
- (45) Kang, J. Y., Chung, C. W., Sung, J. H., Park, B. S., Choi, J. Y., Lee, S. J., ... & Kim, D. D. (2009). Novel porous matrix of hyaluronic acid for the three-dimensional culture of chondrocytes. *International journal of pharmaceutics*, 369(1-2), 114-120.
- (46) Ström, A., Larsson, A., & Okay, O. (2015). Preparation and physical properties of hyaluronic acid-based cryogels. *Journal of Applied Polymer Science*, 132(29).
- (47) Tavsanlı, B., & Okay, O. (2016). Preparation and fracture process of high strength hyaluronic acid hydrogels cross-linked by ethylene glycol diglycidyl ether. *Reactive and Functional Polymers*, 109, 42-51.
- (48) Longin, F., & Schwach-Abdellaoui, K. (2013). U.S. Patent No. 8,481,080. Washington, DC: U.S. Patent and Trademark Office.
- (49) Tomihata, K., & Ikada, Y. (1997). Crosslinking of hyaluronic acid with glutaraldehyde. *Journal of Polymer Science Part A: Polymer Chemistry*, 35(16), 3553-3559.

- (50) Benitez, A., Yates, T. J., Lopez, L. E., Cerwinka, W. H., Bakkar, A., & Lokeshwar, V. B. (2011). Targeting hyaluronidase for cancer therapy: antitumor activity of sulfated hyaluronic acid in prostate cancer cells. *Cancer research*, 71(12), 4085-4095.
- (51) Drobnik, J. (1991). Hyaluronan in drug delivery. *Advanced Drug Delivery Reviews*, 7(2), 295-308.
- (52) Yadav, A. K., Mishra, P., & Agrawal, G. P. (2008). An insight on hyaluronic acid in drug targeting and drug delivery. *Journal of drug targeting*, 16(2), 91-107.
- (53) Wang, C. T., Lin, Y. T., Chiang, B. L., Lin, Y. H., & Hou, S. M. (2006). High molecular weight hyaluronic acid down-regulates the gene expression of osteoarthritis-associated cytokines and enzymes in fibroblast-like synoviocytes from patients with early osteoarthritis. *Osteoarthritis and cartilage*, 14(12), 1237-1247.
- (54) Tezel, A., & Fredrickson, G. H. (2008). The science of hyaluronic acid dermal fillers. *Journal of Cosmetic and Laser Therapy*, 10(1), 35-42.
- (55) Pouyani, T., & Prestwich, G. D. (1994). Functionalized derivatives of hyaluronic acid oligosaccharides: drug carriers and novel biomaterials. *Bioconjugate chemistry*, 5(4), 339-347.
- (56) Homma, A., Sato, H., Okamachi, A., Emura, T., Ishizawa, T., Kato, T., ... & Watanabe, T. (2009). Novel hyaluronic acid-methotrexate conjugates for osteoarthritis treatment. *Bioorganic & medicinal chemistry*, 17(13), 4647-4656.
- (57) Barbucci, R., Fini, M., Giavaresi, G., Torricelli, P., Giardino, R., Lamponi, S., & Leone, G. (2005). Hyaluronic acid hydrogel added with ibuprofen-lysine for the local treatment of chondral lesions in the knee: In vitro and in vivo investigations. *Journal of Biomedical Materials Research Part B: Applied Biomaterials: An Official Journal of The Society for Biomaterials, The Japanese Society for Biomaterials, and The Australian Society for Biomaterials and the Korean Society for Biomaterials*, 75(1), 42-48.
- (58) Dhal, P. K., Gianolio, D. A., & Miller, R. J. (2012). Polymer based therapies for the treatment of chronic pain. *Pain Manag. Curr. Issues Opin*, 28, 27-42.

- (59) Zhang, J., Ma, X., Fan, D., Zhu, C., Deng, J., Hui, J., & Ma, P. (2014). Synthesis and characterization of hyaluronic acid/human-like collagen hydrogels. *Materials Science and Engineering: C*, 43, 547-554.
- (60) Chung, C. W., Kang, J. Y., Yoon, I. S., Hwang, H. D., Balakrishnan, P., Cho, H. J., ... & Kim, D. D. (2011). Interpenetrating polymer network (IPN) scaffolds of sodium hyaluronate and sodium alginate for chondrocyte culture. *Colloids and Surfaces B: Biointerfaces*, 88(2), 711-716.
- (61) Bian, S., He, M., Sui, J., Cai, H., Sun, Y., Liang, J., ... & Zhang, X. (2016). The self-crosslinking smart hyaluronic acid hydrogels as injectable three-dimensional scaffolds for cells culture. *Colloids and Surfaces B: Biointerfaces*, 140, 392-402.
- (62) Tan, H., Wan, L., Wu, J., & Gao, C. (2008). Microscale control over collagen gradient on poly (L-lactide) membrane surface for manipulating chondrocyte distribution. *Colloids and Surfaces B: Biointerfaces*, 67(2), 210-215.
- (63) Sulfonated polymers: simple chemistry for high tech materials & applications
- (64) Capila, I., & Linhardt, R. J. (2002). Heparin–protein interactions. *Angewandte Chemie International Edition*, 41(3), 390-412.
- (65) Kowalczyńska, H. M., & Nowak-Wyrzykowska, M. (2003). Modulation of adhesion, spreading and cytoskeleton organization of 3T3 fibroblasts by sulfonic groups present on polymer surfaces. *Cell biology international*, 27(2), 101-114.
- (66) Pellegrino, L., Cocchiola, R., Francolini, I., Lopreiato, M., Piozzi, A., Zanoni, R., ... & Martinelli, A. (2017). Taurine grafting and collagen adsorption on PLLA films improve human primary chondrocyte adhesion and growth. *Colloids and Surfaces B: Biointerfaces*, 158, 643-649.
- (67) Sun, Z., Shi, C., Wang, X., Fang, Q., & Huang, J. (2017). Synthesis, characterization, and antimicrobial activities of sulfonated chitosan. *Carbohydrate polymers*, 155, 321-328.
- (68) Matsusaki, M., Serizawa, T., Kishida, A., Endo, T., & Akashi, M. (2002). Novel functional biodegradable polymer: synthesis and anticoagulant activity of poly ( $\gamma$ -glutamic acid) sulfonate ( $\gamma$ -PGA-sulfonate). *Bioconjugate chemistry*, 13(1), 23-28.

- (69) Barbucci, R., Magnani, A., CASOLARO, R., Marchettini, N., Rossi, C., & Bosco, M. (1995). Modification of hyaluronic-acid by insertion of sulfate groups to obtain a heparin-like molecule. 1. Characterization and behavior in aqueous-solution towards H<sup>+</sup> and Cu<sup>2+</sup> ions. *Gazzetta Chimica Italiana*, 125(4), 169-180.
- (70) Magnani, A., Lamponi, S., Rappuoli, R., & Barbucci, R. (1998). Sulphated hyaluronic acids: a chemical and biological characterisation. *Polymer international*, 46(3), 225-240.
- (71) Cen, L., Neoh, K. G., Li, Y., & Kang, E. T. (2004). Assessment of in vitro bioactivity of hyaluronic acid and sulfated hyaluronic acid functionalized electroactive polymer. *Biomacromolecules*, 5(6), 2238-2246.
- (72) Abatangelo, G., Barbucci, R., Brun, P., & Lamponi, S. (1997). Biocompatibility and enzymatic degradation studies on sulphated hyaluronic acid derivatives. *Biomaterials*, 18(21), 1411-1415.
- (73) Barbucci, R., Rappuoli, R., Borzacchiello, A., & Ambrosio, L. (2000). Synthesis, chemical and rheological characterization of new hyaluronic acid-based hydrogels. *Journal of Biomaterials Science, Polymer Edition*, 11(4), 383-399.
- (74) Roy, R. N., Swensson, E. E., LaCross, G., & Krueger, C. W. (1975). Standard buffer of N, N-bis (2-hydroxyethyl)-2-aminoethanesulfonic acid (Bes) for use in the physiological pH range 6.6 to 7.4. *Analytical Chemistry*, 47(8), 1407-1410.
- (75) Huxtable, R. J. (1992). Physiological actions of taurine. *Physiological reviews*, 72(1), 101-163.
- (76) Sturman, J. A. (1993). Taurine in development. *Physiological reviews*, 73(1), 119-147.
- (77) Son, M. W., Ko, J. I., Doh, H. M., Kim, W. B., Park, T. S., Shim, M. J., & Kim, B. K. (1998). Protective effect of taurine on TNBS-induced inflammatory bowel disease in rats. *Archives of pharmacal research*, 21(5), 531-536.
- (78) Özmeriç, N., Özcan, G., Haytaç, C. M., Alaaddinoğlu, E. E., Sargon, M. F., & Şenel, S. (2000). Chitosan film enriched with an antioxidant agent, taurine, in fenestration defects. *Journal of Biomedical Materials Research: An Official Journal of The Society for*

Biomaterials, The Japanese Society for Biomaterials, and The Australian Society for Biomaterials and the Korean Society for Biomaterials, 51(3), 500-503.

(79) Dinçer, S., Babül, A., Erdoğan, D., Özoğul, C., & Dinçer, S. L. (1996). Effect of taurine on wound healing. *Amino Acids*, 10(1), 59-71.

(80) Değim, Z., Celebi, N., Sayan, H., Babül, A., Erdoğan, D., & Take, G. (2002). An investigation on skin wound healing in mice with a taurine-chitosan gel formulation. *Amino acids*, 22(2), 187-198.

(81) Bucolo, C., Fidilio, A., Platania, C. B. M., Geraci, F., Lazzara, F., & Drago, F. (2018). Antioxidant and osmoprotecting activity of taurine in dry eye models. *Journal of Ocular Pharmacology and Therapeutics*, 34(1-2), 188-194.

(82) Lee, C. H., Park, H. B., Chung, Y. S., Lee, Y. M., & Freeman, B. D. (2006). Water sorption, proton conduction, and methanol permeation properties of sulfonated polyimide membranes cross-linked with N, N-bis (2-hydroxyethyl)-2-aminoethanesulfonic acid (BES). *Macromolecules*, 39(2), 755-764.

## 2. SYNTHESIS OF HA-NAPA BIOCONJUGATE

Figure 2.1 shows retrosynthetic pathway for the preparation of hyaluronic acid and 2-(N-Acetyl)-L-phenylalanylamido-2-deoxy-D-glucose (NAPA) bioconjugate. Steps **VI** to **III** concern synthesis of NAPA **III** via amide bond formation from N-Acetyl-L-phenylalanine (N-Ac-L-Phe) and D-glucosamine hydrochloride (D-Glu HCl). Our aim was to modify and simplify the already existing procedure <sup>1</sup> in order to couple D-Glu HCl and N-Ac-L-Phe in a one-step synthesis that involves only intermediate **III** and precursor **IV**, avoiding protection and deprotection steps of alcoholic functions of glucosamine (Strategy 1). This approach demonstrated to be an easy process but had some drawbacks related to the purification of **III** with crystallization or silica column. So, this led to the need of a coupling reaction that includes protection/deprotection reaction of the amino sugar **IV** (Strategies 2/3).

Intermediate **II** was obtained by regioselective esterification in HO-C(6) of **III** with a n-bromo acyl derivative of suitable length.<sup>2</sup>

Finally, n-bromo derivative **II** was esterified on hyaluronic acid through nucleophilic substitution in organic solvent to give desired bioconjugate **I**.

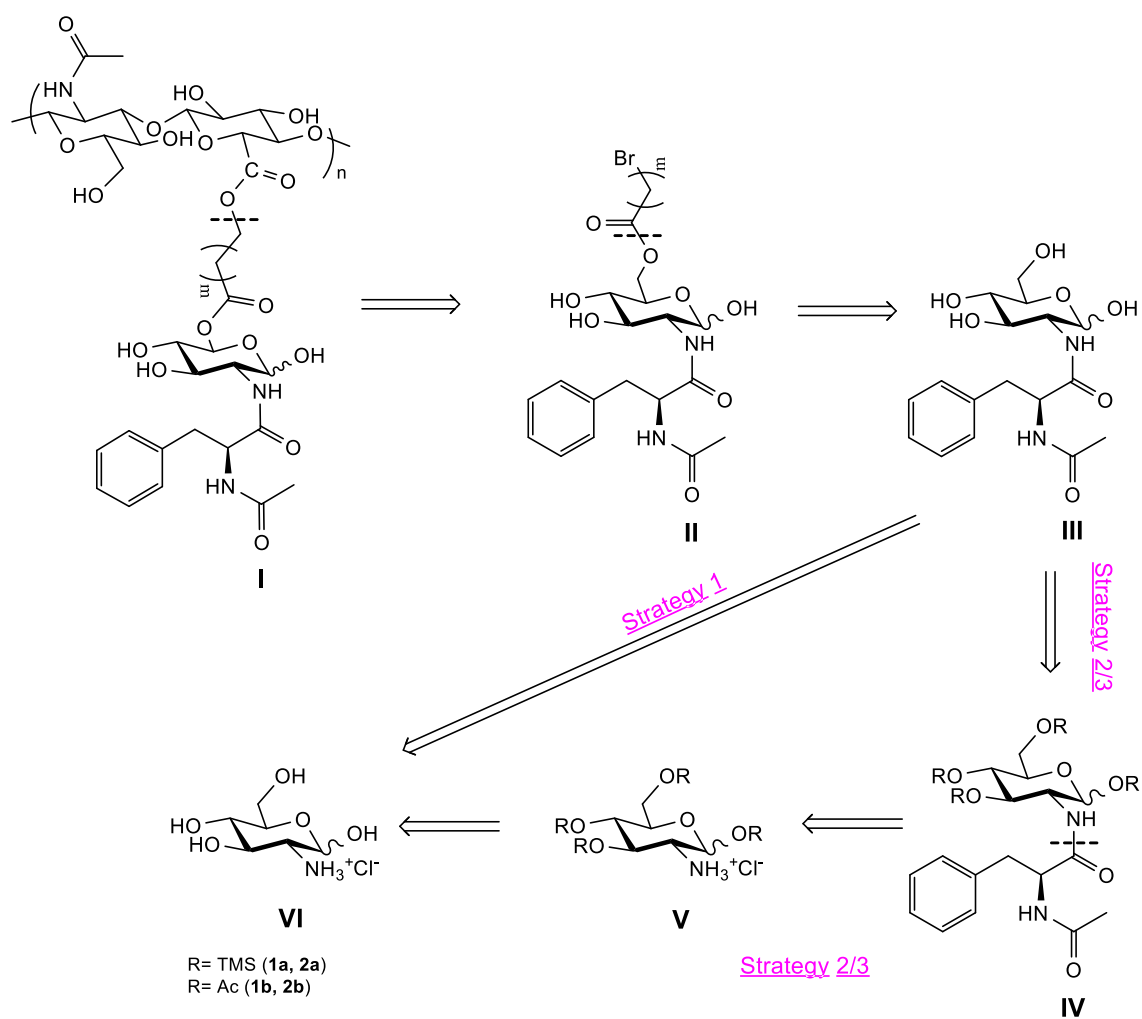


**Fig. 2.1:** Retrosynthetic pathway for the preparation of HA-NAPA bioconjugate I. Synthesis starts from D-glucosamine hydrochloride VI and included two alternative strategies: the direct preparation of NAPA III by means of coupling with N-Acetyl-L-phenylalanine (strategy 1), or protection/deprotection steps of D-glucosamine and consecutive coupling to obtain NAPA precursor IV (strategies 2/3). Then, NAPA underwent regioselective esterification in HO-C(6) to get the n-bromine derivative II. Finally, esterification of II on hyaluronic acid give desired compound I.

## 2.1 Synthesis of NAPA

### 2.1.1 Synthesis of compound **III**: direct preparation of NAPA

#### Strategy 1

As mentioned above, first studies aimed to obtain NAPA from direct conjugation of D-Glu HCl and N-Ac-L-Phe, exploiting the higher reactivity of aminic function instead of the alcoholic group in the amino sugar, thus preventing protection/deprotection steps of OH groups. General procedure for amidation is reported in figure 2.2. NAPA synthesis through direct coupling was investigated using carbodiimide (condition **A**) and mixed anhydride (condition **B**) methods. Two different solutions were prepared, one for the amine and the other for peptide activation. Water and methanol were selected as best solvent for D-Glucosamine hydrochloride, due to its high polarity, while activation of N-Acetyl-L-phenylalanine with coupling agent was carried out in THF.<sup>3</sup>

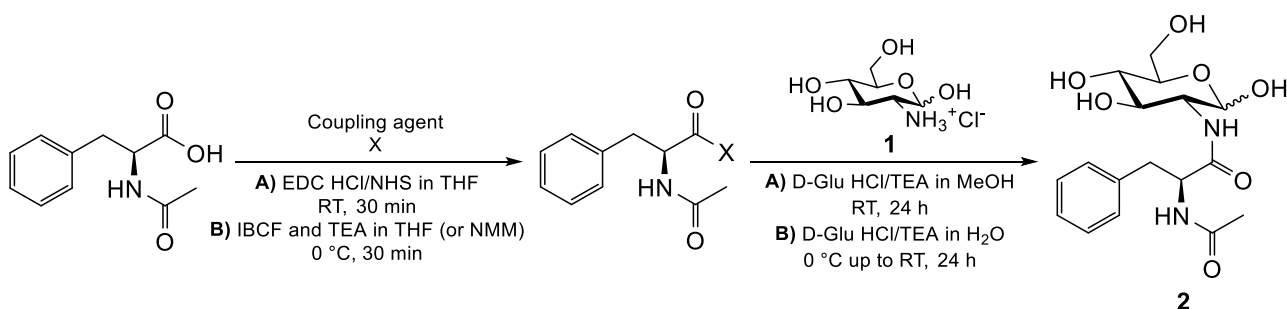


**Fig. 2.2:** Schematic representation of the direct amidation of D-Glu HCl (**1**) and N-Acetyl-L-phenylalanine by means of isobutyl chloroformate in water/tetrahydrofuran mixture to obtain NAPA (**2**).

At first, amidation was performed using 1-Ethyl-3-(3-dimethylaminopropyl)carbodiimide hydrochloride (EDC HCl) and N-Hydroxysuccinimide (NHS)<sup>4</sup> in a methanol/THF (vol/vol) mixture. A certain amount of the L-peptide was activated with a slight molar excess of EDC/NHS in THF for 30 minutes at room temperature. Then, an equimolar amount of **1** and triethylamine in water was added. Reaction was left under stirring at room temperature until formation of product **2** was revealed by TLC. Reaction couldn't be separated by silica chromatography, due to the high polarity of the molecules involved in, but crystallization in EtOH or MeOH allows the obtainment of the final product. Mass and NMR spectroscopy confirmed the synthesis of **2** although with low purity. Signals attributed to the N-acyl group of phenylalanine unit along with HO-C(6) proton and H-N(2)/H-N(2') amide protons can be

detected in the  $^1\text{H}$  spectrum as well as signals of the two amidic carbons in  $^{13}\text{C}$  spectrum. Poor yield could be ascribed to the partial solubilization of EDC HCl in THF, indicating the need to use more polar solvents to solubilize the coupling agent.

Therefore, the coupling was conducted in water/THF mixture.<sup>5</sup> In this case, the amino acid was activated by isobutyl chloroformate (IBCF) and TEA with a conventional two-steps procedure (scheme 2.3).

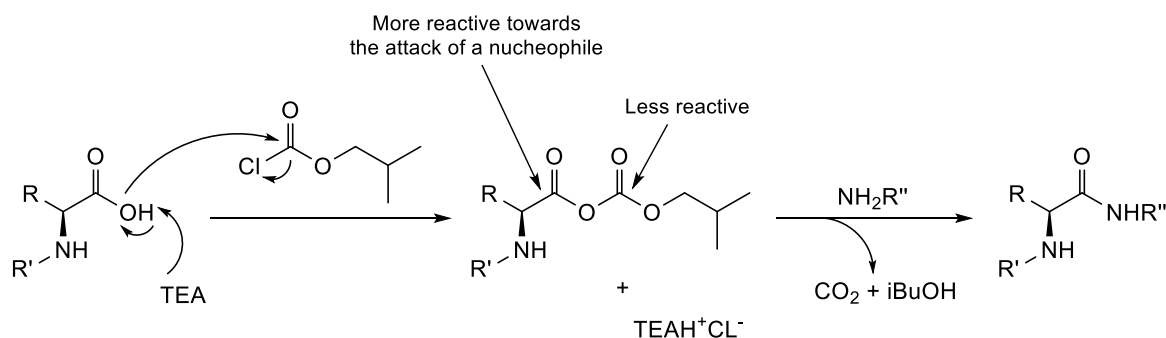


**Fig. 2.3:** Coupling mechanism with isobutyl chloroformate in the presence of TEA.

In the first step, the carboxylic group reacts with IBCF in presence of tertiary amine TEA to form an asymmetrical anhydride, more electrophilic than the starting peptide, that can undergo nucleophilic attack by  $\text{NH}_2$  group of the amino sugar **1** in water, with  $\text{CO}_2$  and isobutanol (iBuOH) as by-products. The synthesis of **2** was verified by mass spectroscopy and NMR. In particular,  $^1\text{H}$  NMR of the crude reaction in  $\text{D}_2\text{O}$  showed signals of two sets of anomeric peaks ascribable to the  $\alpha$  and  $\beta$  protons of two different diastereoisomers of peptide unit, pointing out that coupling reaction proceeds reasonably without retention of stereochemistry. Figure 2.4 shows the anomeric region in the NMR proton spectra of D-NAPA, a mixture of D and L diastereoisomers and the crude coupling reaction.

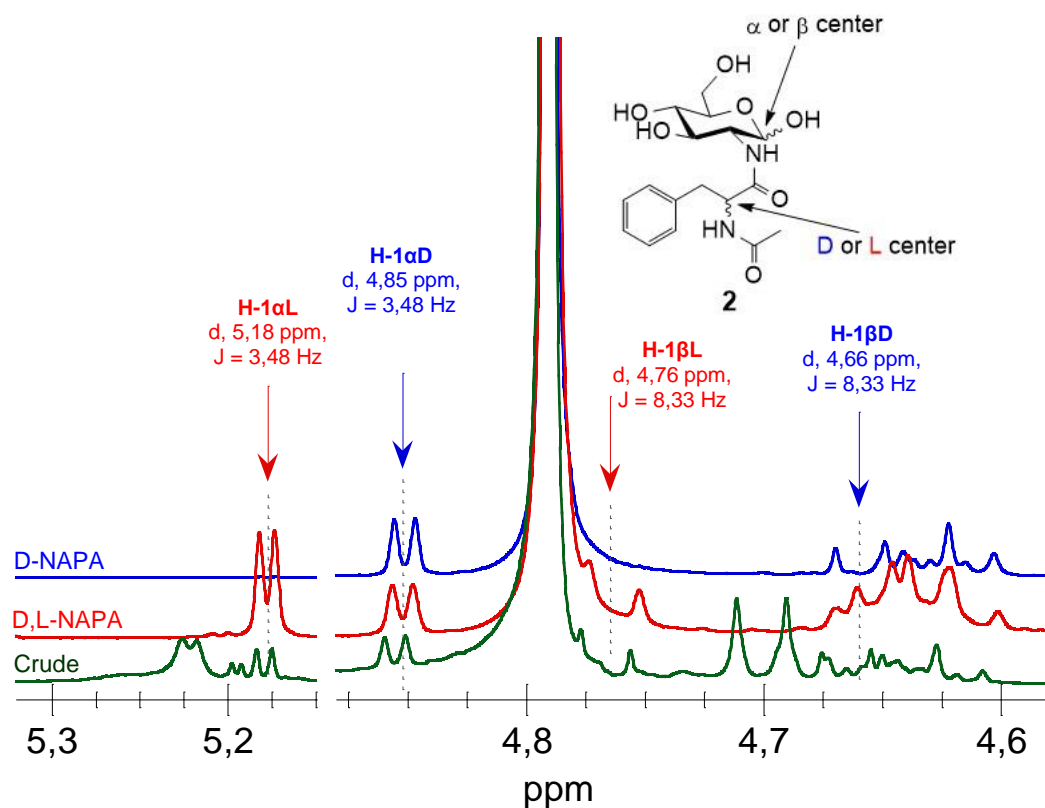


**Fig. 2.4:**  $^1\text{H}$  NMR spectra of D-NAPA (blue), mixture of D and L NAPA (red) and NAPA in the crude reaction obtained via IBCF coupling (green) between 5.35 and 4.55 ppm. The NAPA structure is also reported and chiral centers of interest are evidenced.

In addition, purification of target molecule by silica column or crystallization was hard to achieve. These strategies, even if promising, had to be changed due to the isolation difficulties of product.

### 2.1.2 Synthesis of compound **III**: preparation of precursor **IV**

#### Strategy 2

Second attempt to obtain 2-(N-Acetyl)-L-phenylalanyl-amido-2-deoxy-D-glucose was based on the synthesis of the intermediate **V** (Strategies 2 and 3). In this case, a suitable O-protector should be stable during amidation and the cleavage should not interfere with the two amide bonds in the target molecule. Ideally, protector group should be selective for hydroxylic functions instead of amine; in this regard, O-silylation was performed.

Thereby the four OH groups of D-Glucosamine hydrochloride were selectively protected using chlorotrimethylsilane (TMSCl) in presence of triethylamine in dry DMF.<sup>6</sup> Tetra-O-silylation procedure is shown in figure 2.5.

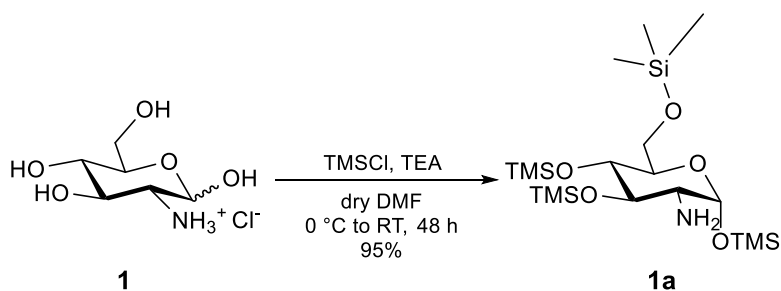


**Fig. 2.5:** Tetra-O-silylation of D-glucosamine hydrochloride using chlorotrimethylsilane in DMF.

Product **1a** was obtained in high yields and characterized by FTIR, NMR and mass spectroscopy. As result of silylation, infrared analysis showed the disappearing of the broad OH stretching band between 3200 and 3000  $\text{cm}^{-1}$ , the sharpening of methyl groups stretching bands in the region between 2990 and 2800  $\text{cm}^{-1}$ , and the appearance of strong absorption peaks at 1245 and 830  $\text{cm}^{-1}$  attributed to the stretching and bending of Si-C bond and at 1150  $\text{cm}^{-1}$  for Si-O bond stretching. It is interesting to note that the  $\alpha$  form of the amino sugar is the major product of reaction as verified by  $^1\text{H}$  NMR (doublet at 5,11 ppm,  $J=3,25$  Hz in  $\text{CDCl}_3$ ).<sup>7,8</sup>

Then, tetra-O-silylated derivative **1a** underwent amidation as follows:

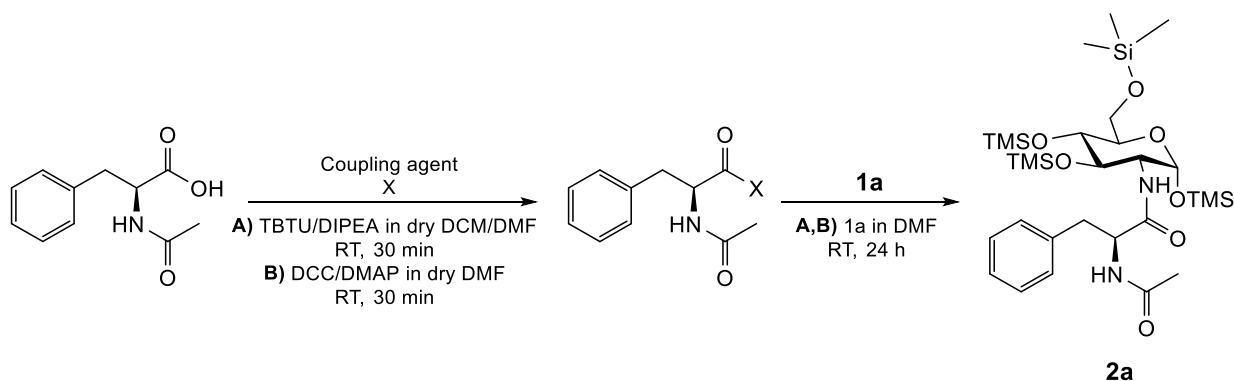


**Fig. 2.6:** Synthesis of tetra-O-silylated NAPA precursor **2a** by means of N-acetyl-L-phenylalanine and tetra-O-trimethylsilyloxy glucosamine **1a** coupling.

Different coupling agents and conditions have been used to obtain **2a**. At first, amidation with the L amino acid was carried out in the presence of O-(Benzotriazol-1-yl)-N,N,N',N'-tetramethyluronium tetrafluoroborate (TBTU) and N,N-Diisopropylethylamine (DIPEA) in DCM/DMF mixture but  $^1\text{H}$  NMR analysis didn't reveal any methyl signal related to TMS. Thus, coupling reaction was performed using N,N'-Dicyclohexylcarbodiimide (DCC) and N,N-Dimethylpyridin-4-amine (DMAP) but even in this case NMR characterization didn't show any signals ascribable to molecules **2a**. Most likely, the bond between silicon and

oxygen is not stable during coupling reaction so as to define O-silylation not suitable for our purposes.

### Strategy 3

Third approach aimed to use most stable protector groups for D-glucosamine HCl, taking into account purification limits of NAPA via strategy 1 and low stability of TMS protections explored in strategy 2. In particular, acetylic groups seemed to be suitable to endure the coupling and they require controllable deprotection conditions that do not interfere with other functional groups in the molecule. The process starts from a commercially available product, 1,3,4,6-Tetra-O-acetyl-2-amino-2-deoxy- $\beta$ -D-glucopyranose hydrochloride **1b** that would have been coupled to N-Acetyl-L-phenylalanine with IBCF and TEA (or NMM) to form 2-(N-Acetyl)-L-phenylalanyl-amido-2-deoxy-1,3,4,6-tetra-O-acetyl- $\beta$ -D-glucose **2b** in a two steps reaction, illustrated in figure 2.7. [1]

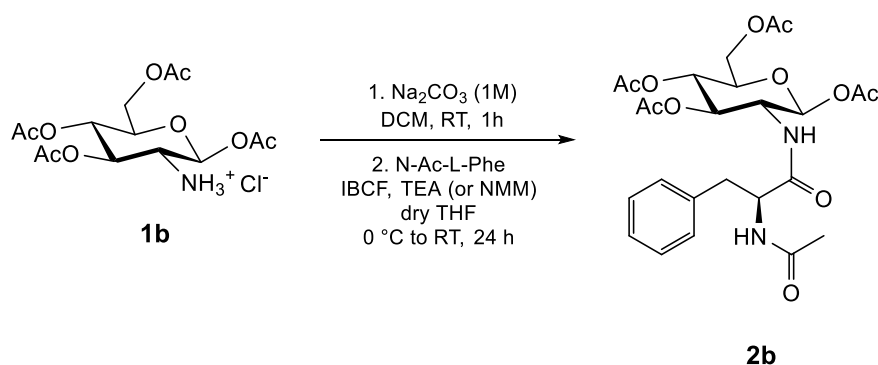


**Fig. 2.7:** Synthesis of tetra-O-acetylated NAPA precursor **2b** from O-acetylated glucosamine hydrochloride and N-Ac-L-Phe with IBCF.

Synthesis of **2b**, purified by crystallization or silica column, was confirmed by NMR and mass spectroscopy. Unfortunately,  $^1\text{H}$  NMR spectrum of purified molecule showed unexpected and unclear peaks also present in the spectrum of the starting commercial material. More extensive analysis, along with the dramatically low yield of coupling, demonstrated the high impurity of commercial product.

However, this attempt proved the stability of O-acetylic protection during the coupling reaction and the capability to obtain **2b** as precursor of NAPA.

Tetra-O-acetylated glucosamine **1b** was obtained from D-glucosamine hydrochloride by selective protection of amine moiety, via imide formation using p-anisaldehyde (**1a'**),

followed by tetra-O-acetylation of hydroxylic groups with acetic anhydride in pyridine (**1a''**) and regeneration of the amine function in aqueous acidic condition (**1b**). Finally, **1b'** could be isolated through alkaline treatment of **1b** in H<sub>2</sub>O/DCM (figure 2.8).<sup>9</sup>

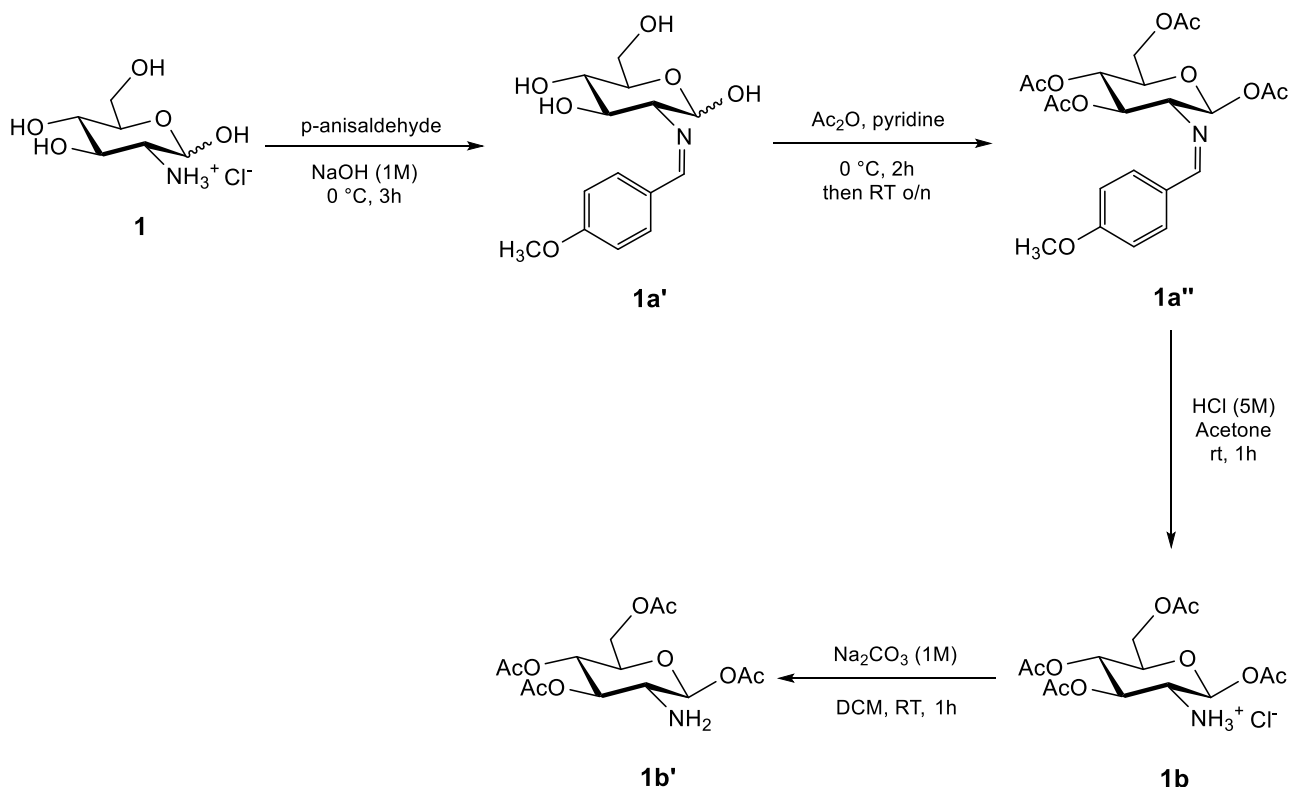


**Fig. 2.8:** Synthesis of tetra-O-acetyloxy glucosamine **1b'** from D-glucosamine hydrochloride **1**.

Structure and purity of the intermediates were confirmed by NMR, mass and FTIR spectroscopy. It should be noted that the only diastereoisomer obtained from esterification with acetic anhydride is the  $\beta$  anomer of Schiff base **1a''** (doublet at 6,07 ppm,  $J=8,25$  in DMSO- $d_6$ ).<sup>10</sup> In each reaction the tetra-O-acetyl-2-amino-2-deoxy- $\beta$ -D-glucosamine **1b'**, freshly prepared and purified, was coupled to the L-amino acid with isobutyl chloroformate, following conditions exposed at the beginning of strategy 3.

Again, NMR, FTIR and mass spectroscopy confirmed synthesis of 2-(N-Acetyl)-L-phenylalanylamido-2-deoxy-1,3,4,6-tetra-O-acetyl- $\beta$ -D-glucose **2b**, this time in higher yields. However, <sup>1</sup>H and <sup>13</sup>C NMR spectra of **2b** displayed two sets of peaks which could be assigned to:

- Presence of amide rotamers caused by rotational restriction in the molecule;

- Epimerization of N-Acetyl-L-phenylalanine resulting in a mixture of diastereoisomers of **2b** (labelled as **2b-L** and **2b-D**).

To understand the mechanism at the base of signals splitting, 2-(N-Acetyl)-L-phenylalanyl-amido-2-deoxy-1,3,4,6-tetra-O-acetyl- $\beta$ -D-glucose was studied by variable temperature  $^1\text{H}$  NMR from 25 to 90 °C in DMSO- $d_6$ . Conformational conversion of amide rotamers could be facilitate heating the sample, thus inducing the coalescence of all the signals. In hindered amide derivatives of glucosamine, coalescence of peaks has been found to occur at 95 °C with an average  $\Delta G = 20.9 \text{ kcal}\cdot\text{mol}^{-1}$ .<sup>11</sup> Otherwise, splitting could be explained with a change of amino acid residue chirality. Selected peaks in spectra acquired at room temperature and 90 °C are shown in figure 2.9. Peaks reported are those of CH and  $\text{CH}_2$  of phenylalanine residue and the anomeric proton.

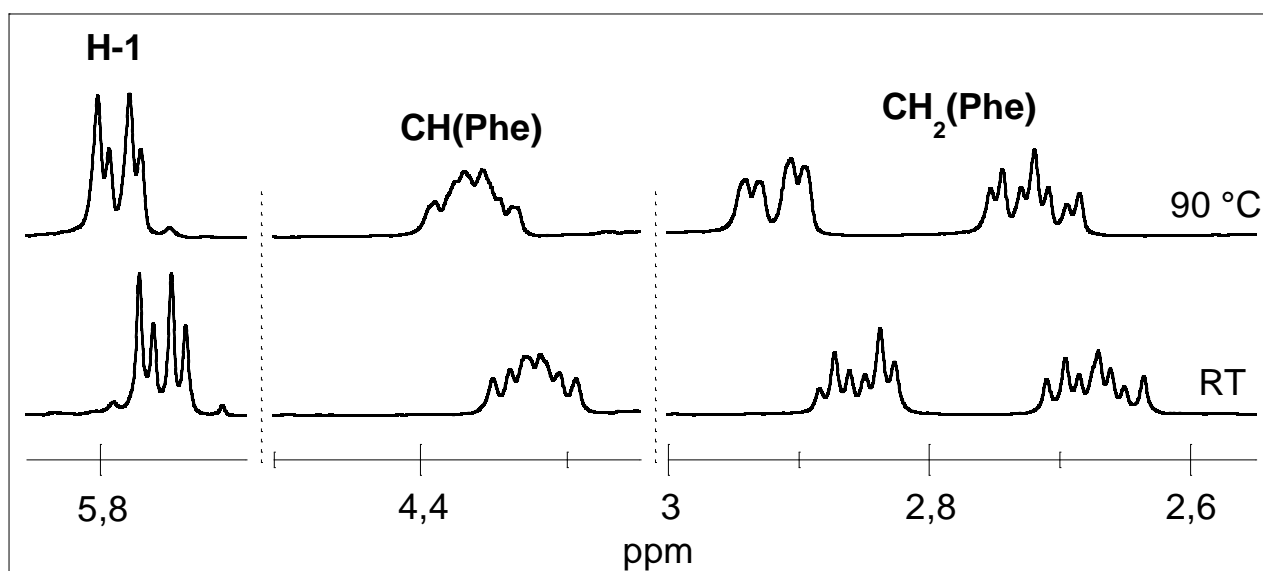


**Fig. 2.9:** Variable temperature  $^1\text{H}$  NMR of molecule **2b-D,L** in DMSO- $d_6$ . No coalescence of peaks occurs in spectra at the highest temperature. Peaks shift is caused by temperature growth.

Anomeric, CH and methylene peaks remain similar in the shape and coalescence does not occur even at high temperature and, thus, the presence of amide rotamers was excluded. The stereochemistry of amidation was then deepen in order to understand the causes at the base of N-Acetyl-L-phenylalanine epimerization. The anomeric proton at 5,76 ppm is associated to the sugar residue in L-phenylalanine-bearing isomer while anomeric proton at 5,75 ppm to the D-isomer (anomeric protons in  $\text{CDCl}_3$  spectra are located at 5,88 and 5,75 ppm, respectively).

### 2.1.3 Racemization of N-Acetyl-L-phenylalanine

Chirality lost through amide formation had to be ascribed to the exchange of the labile  $\alpha$  hydrogen in an amino acid or in a peptide, resulting in the formation of both D and L form of the starting carboxylic compound. Epimerization during amide synthesis is generally accomplished on the amino acid-coupling agent reactive intermediate generated in the presence of a tertiary base. Condensation of the activated-amino acid with the desired amine is known to be accompanied by substantial racemization.<sup>12</sup> Two mechanisms have been identified to explain peptide racemization during activation of amino acid carboxylate, as summarized in scheme 2.10 below:

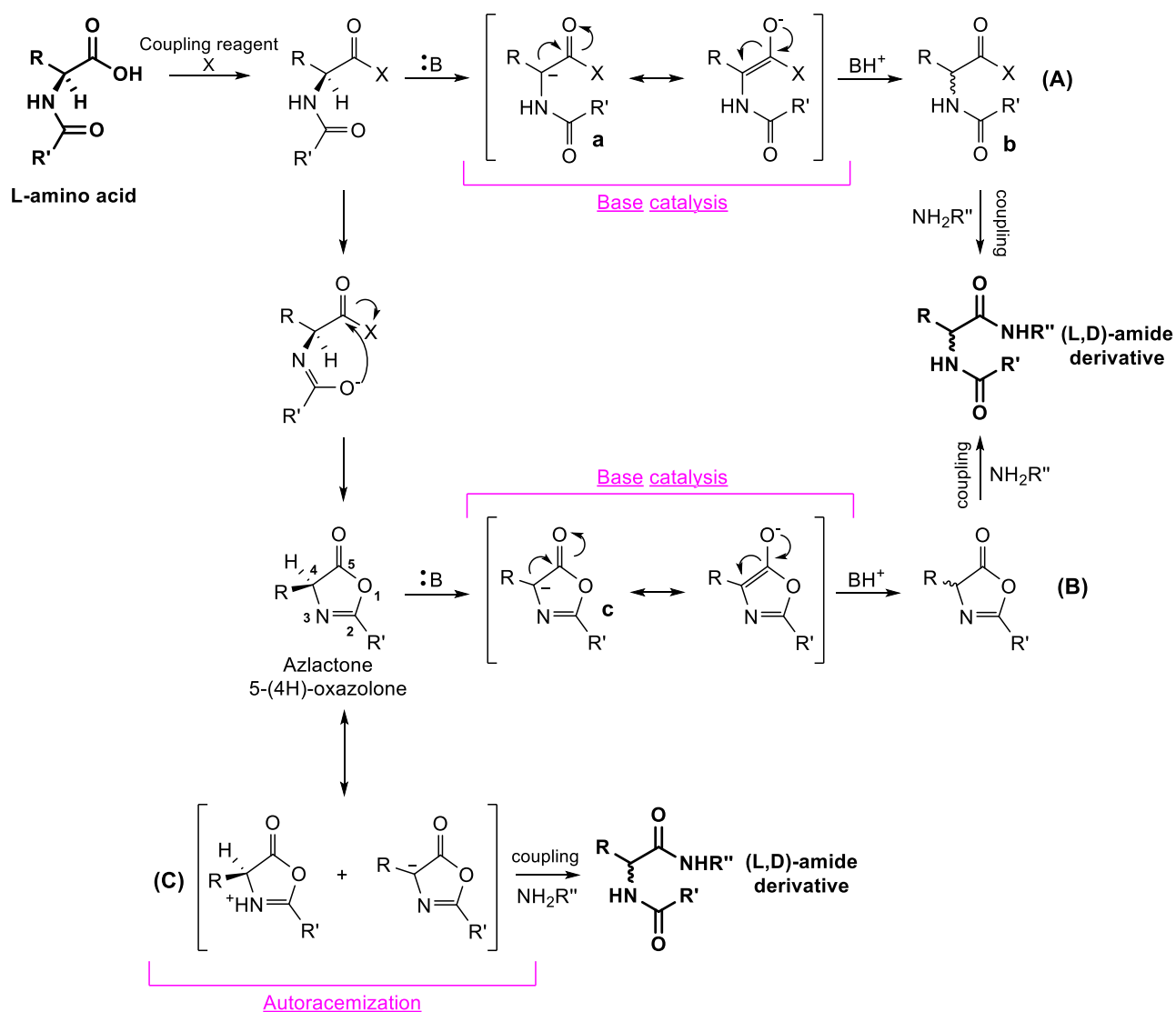


**Fig. 2.10:** Representation of racemization process that occurs in chiral substrates. **A)** Racemization via base catalysis on activated amino acid. **B)** Racemization via azlactone formation and consecutive base effect. **C)** Autoracemization of azlactone without base intervention.

Once the amino acid is activated, change in the chirality can be manifested in the abstraction of the  $\alpha$  proton by excesses of base and/or amino acidic anion attendant in activation (path **A**), or in the formation of an azlactone, also known as oxazolone, that can be deprotonated by excess of base (path **B**)<sup>13</sup> or endure autoracemization (path **C**).<sup>14</sup>

Mechanism **A** takes place when an excess of tertiary amine base, of adequate basicity, and/or amino acid is used with respect to the coupling reagent. Stereogenic proton can be removed in alkaline condition leading to the formation of carbanion **a** that can rapidly rearrange into amino acid racemate **b**. Racemization suppression can be carried out using proper amine. In fact, the lower the basicity the smaller is the racemization. In several cases, racemization can be avoided by adjusting the addition order of the reagents<sup>15</sup> or with 1-Hydroxy-7-azabenzotriazole (HOAt) or hydroxybenzotriazole (HOBt) as additive.<sup>16,17</sup> Their role in the racemization suppression is mainly based on the fact that they could react with the activated amino acid to give a more active ester which enhances the possibility of amine attack.

Additionally, activated amino acids easily cyclize into heterocyclic 5-(4H)-oxazolones since they have a nitrogen atom in the  $\beta$ -position of the ring and two electrophilic sites, respectively in 2 and 5.<sup>18</sup> The  $\alpha$ -hydrogen of an oxazolone is characterized by moderated acidity ( $pK_a \approx 9$ ), attributed to the aromatic character of the corresponding enolate tautomer (structure **c**),<sup>19</sup> and it can be potentially removed by free-base. Deprotonation of the oxazolone, or autoracemization, generates a carbanion that can undergo enolate resonance (path **B** and **C**, respectively). Again, oxazolone intermediate rearranges into an epimeric/racemic compound that reacts to give the desired amide, as mixture of enantiomers or diastereoisomers with stereochemistry of products that depends upon chirality and/or reactivity of reactant involved. Anyway, independently from the type of mechanism involved, if racemization of 5-(4H)-oxazolone is fast, the stereochemical outcome of the coupling is determined by the relative rates of the reaction of 5-(4H)-oxazolone stereoisomers with the amino component.<sup>20</sup> The formation of oxazolones is strictly related to the type of N-protector in the amino acid. Some studies suggested that azlactone formation is favored when N-acetyl peptides are reacted because of the stabilizing effect of acetyl group on carbanion **c**. Consequently, the C-5 of oxazolones is the center that is attacked by the nucleophile amine during coupling. Carbanion stability is decreased by alkoxy carbonyl groups, like benzyloxycarbonyl, tert-butoxycarbonyl, due to their electron release effect<sup>21</sup> and synthesis of chiral pure products is

attained. At this regard, if oxazolone formation is considered, an epimerization/racemization-free synthesis has never been achieved when the C-2 substituent is an aryl or alkyl group. In the enantiomerically pure oxazolones, a modification of the C-2 substituent of the cycle is necessary to make racemization less likely to occur, affording 2-alcoxy-azlactones by the cyclization of carbamate-protected amino acids.<sup>19</sup>

#### 2.1.4 Coupling of N-Acetyl-L-phenylalanine using TBTU

5-(4H)-oxazolones formation is largely described with chloroformates or carbodiimides,<sup>22,23</sup> but, to our knowledge, no studies on azlactone formation or stereochemistry retention with TBTU are presents. Only few works report cases of epimerization and/or racemization when uronium salts are used as coupling agent.<sup>24,25,26</sup> For our purposes, we decided to test the efficiency of TBTU coupling, which is considered a racemization suppressor<sup>27,28</sup> on N-Acetyl-L-phenylalanine, chose as model for amino acid that are epimerization/racemization prone.<sup>29</sup> The hypothetical TBTU/DIPEA mechanism for synthesis of **2b** is reported below:

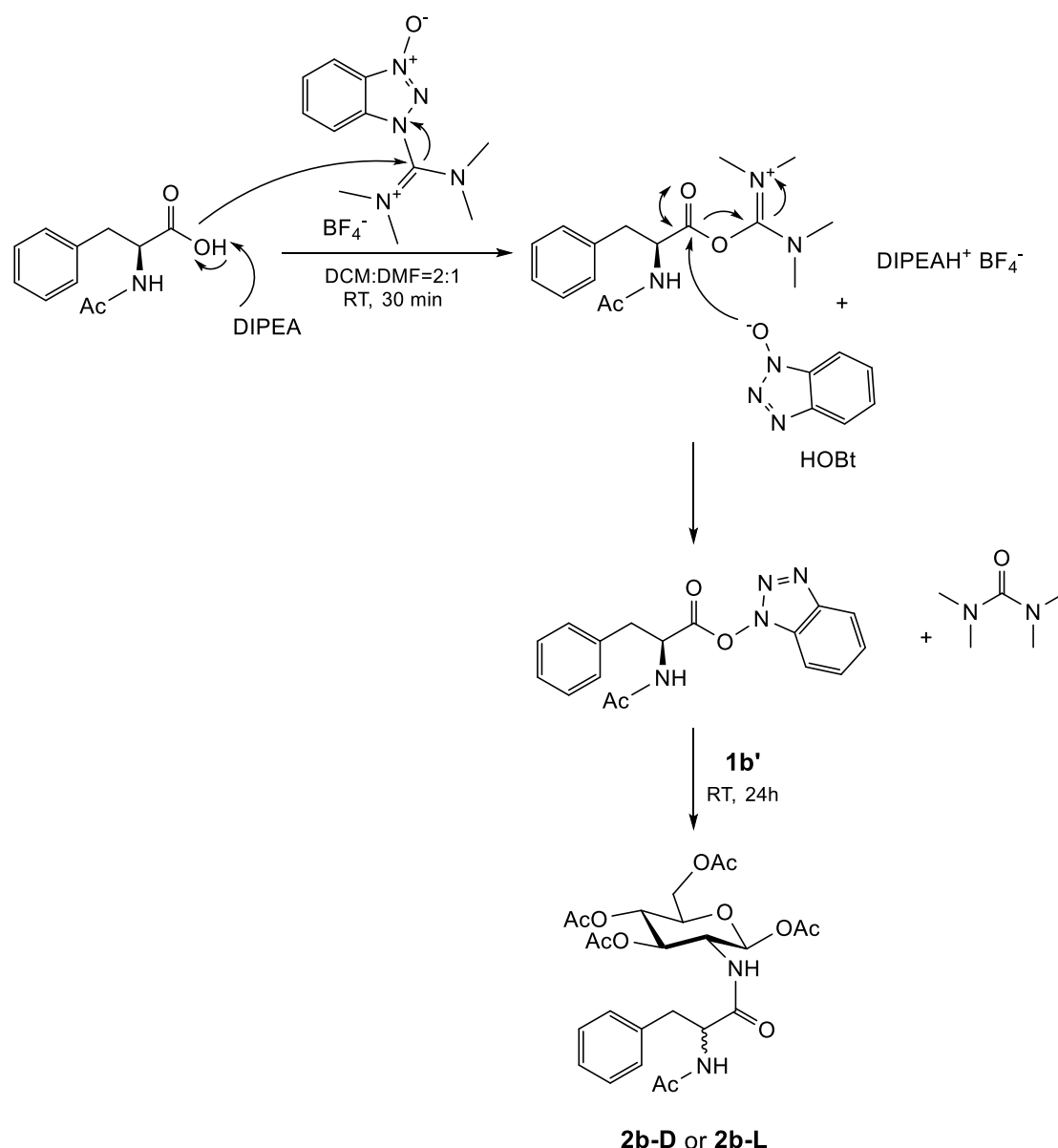


**Fig. 2.11:** Synthesis of NAPA precursor **2b** in the presence of TBTU and DIPEA. Activation with TBTU leads to the formation of a tetramethyl urea as byproduct.

After deprotonation of the amino acid by a suitable base, activation starts with the attack of imide carbonyl carbon of TBTU. Then, benzotriazole N-oxide anion reacts with electrophile carbonyl to give an active ester, forming tetramethyl urea as byproduct. Aminolysis of the HOBt ester gives the desired amide.

Thus, we decided to test TBTU coupling on N-Acetyl-L-phenylalanine, because of its racemization-prone character,<sup>29,30</sup> and DIPEA was chosen as base. At first, synthesis of **2b** was studied following general procedure described for TBTU<sup>27,31</sup> with DIPEA in large excess respect to the N-acetylated L or D amino acids, and with an activation period of 30 minutes. Further studies were conducted lowering the base equivalents. Mixture of dry

DCM:DMF=2:1 was used as solvent, with reaction times ranging from 3 to 7 and 24 hours. Work up consisted in several washes with distilled water, HCl 1M, saturated bicarbonate and brine. Typically, synthesis of **2b**, with low side-products although with a certain degree of epimerization/racemization, was revealed by NMR.

Reaction specifics are summarized in table 2.1. **R-L** and **R-D** refer to amidation of N-Ac-L-Phe or N-Ac-D-Phe, respectively. NAPA precursors are indicated as **2b-D** or **2b-L** according to the chirality of the amino acid stereocenter.

**Table 2.1:** List of conditions explored for TBTU/DIPEA coupling to synthesize derivative **2b**.  $T_{act}$  = activation temperature,  $T_R$  = reaction temperature,  $t_R$  = reaction time,  $R^D$  = **2b-L:2b-D** diastereoisomeric ratio. The yield is defined as the sum of diastereoisomers.

Reaction	N-Ac-L-Phe:DIPEA:TBTU (eq)	$T_{act}$ (°C)	$T_R$ (°C)	$t_R$ (h)	Yield (%)	$R^D$ (L:D)
<b>R1-L</b>	1:3:1,4	RT	RT	24	88	32:68
<b>R2-L</b>	1:1,4:1,4	-15	5	24	83	25:75
<b>R3-L<sup>a</sup></b>	1:3:1,4	RT	RT	24	89	42:58
<b>R4/5-L</b>	1:2:1	RT	RT	24	88	34:66
<b>R6-L<sup>b</sup></b>	1:1:1	0 °C	RT	24	85	57:43
<b>R7-L</b>	1:1:1	RT	RT	24	92	52:48
<b>R8/9-L</b>	1:1:1	RT	RT	7	87	60:40
<b>R10-L</b>	1:1:1	RT	RT	3	83	63:37
<b>R11-L<sup>c</sup></b>	1:1:1	RT	RT	24	80	37:63
<b>R12-L</b>	1:1:1	0	5	15	89	63:37
<b>R13-L</b>	1:2:1	RT	RT	3	84	43:57
<b>R14-L</b>	1:1:1	-15	5	24	86	49:51
<b>R15-L<sup>d</sup></b>	1:1:1	RT	RT	24	89	31:69
<b>R1-D</b>	1:2:1	RT	RT	24	93	35:65
<b>R2-D</b>	1:1:1	RT	RT	24	93	24:76
<b>R3-D</b>	1:1:1	RT	RT	3	82	26:78

<sup>a</sup> HOBt (2 eq) is added during activation of amino acid.

<sup>b</sup> DMF as solvent

<sup>c</sup> One pot \*\*\*

<sup>d</sup> HOBt (2 eq) is added during activation of amino acid.

Amidation of N-Acetyl-L-phenylalanine by means of TBTU/DIPEA always resulted in a mixture of **2b** diastereoisomers, with **D-2b** as major product when excess of base was used (**R1,2,3,4-L**). In contrast, equimolar amount of DIPEA led to a racemic mixture of **L,D-2b** after 24 hour (**R7-L**). It is worth to notice that conversion of **1b'** into the desired amide was almost complete with yields always close to 90%, showing high coupling efficiency of the uronium salt system. Reduction of DIPEA from 3 to 2 equivalents did not change the L:D ratio that attests at 32:68 and 34:66, respectively for **R1-L** and **R4/5-L**. The amount of the L isomer slightly increases when HOBt is added to the activation (**R3-L**) but **D-2b** diastereoisomer is again the more abundant product (probably because of the excess of base). Finally, change of activation temperature from RT to -15 °C (**R2-L**) did not enhance stereochemistry retention.

Thus, the amount of DIPEA was reduced considering that the chirality loss of the amino acid could be caused by base-promoted deprotonation of an oxazolone, which is the result of amino acid cyclization during activation (see general scheme for epimerization/racemization in figure 2.10). At this regard, the same amount of tertiary base and amino acid were used in order to have the complete consumption of DIPEA after deprotonation of amino acid, thus preventing base-catalyzed epimerization/racemization of oxazolone.

Despite what expected, **R6,7-L** (N-Ac-L-Phe:DIPEA:1:1) resulted in a racemized mixture of diastereoisomers demonstrating that excess of base has an essential role in the inversion of chirality but also that chirality loss of L-oxazolone could depend on a mechanism independent from free-base, such as autoracemization.<sup>14</sup> Furthermore, it can be assumed that N-acetylated oxazolones rearranges very rapidly into a racemic activated compound when base is in excess, as happens in the case of **R1,3,4/5,13-L**, and diastereoselectivity in the process is guided by reactivity of D-oxazolone isomer toward glucosamine **1b'** to give **D-2b** as major product.<sup>30</sup> On the other hand, when base and amino acid are equimolar (**R6,7,8/9,10,14-L**), oxazolone is still formed but no inversion of chirality takes place, most likely because racemization is slower. Autoracemization could be taken into account to explain the chirality loss of oxazolone. In addition, it has to be mentioned the existence of a side reaction that involves TBTU and the amine to give a guanidinium by-product (figure 2.12). In this case, the amine acts as nucleophile and attacks the electron-deficient carbon of the imine leading to the formation of a basic compound. The generation of a free tertiary base could strongly influence

the stereochemistry course of the reaction, as illustrated above, thus order of addition and timing are crucial.<sup>17</sup> A similar explanation was provided by Pedro P. de Castro and coworkers<sup>19</sup> for the coupling of a N-Bz amino acid by 1-ethyl-3-(3-dimethylaminopropyl)carbodiimide (EDC) with equimolar base. In this case, an urea is formed as a by-product of activation and the compound, which has both the urea and a tertiary amine moiety, might act as the base for the racemization process (figure 2.12).

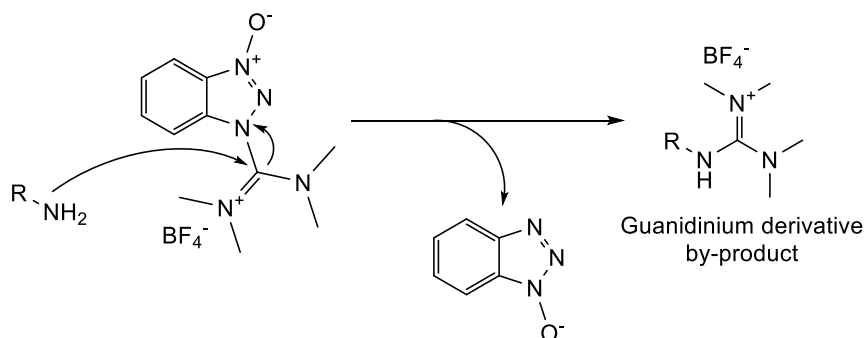


**Fig. 2.12:** Guanidinium formation with TBTU as coupling reagent.

Conditions of **R7-L** were repropose for **R8/9,10-L** and **R11-L** with a reaction time of 7 or 3 h in order to study the evolution of amide product formation in terms of L:D ratio during first hours of amidation. Additionally, **R4/5-L** (L-amino acid:base:activator = 1:2:1) was replicated and quenched after 3 hour (**R13-L**).

For the 3 and 7 h with equimolar base, the L:D ratio decreases with increasing reaction time thus demonstrating how the racemization of oxazolone isn't immediate when no free-base is present. Nevertheless, the D-oxazolone isomer reacts more rapidly with amine 1b' and **D-2b** is still very abundant after 3 h, with a reaction yield close to 80%. With 2 equivalents of DIPEA, the crude product is already enriched in **D-2b** after three hours of reaction, meaning that racemization is fast and catalyzed by free base (**R13-L**).  $T_{act}$  and  $T_R$  seem to have no effect on the L:D ratio since a racemic mixture was obtained even with activation at  $-15\text{ }^{\circ}\text{C}$  and reaction carried out at  $5\text{ }^{\circ}\text{C}$  (**R14-L**). The addition of HOBt doesn't lead to an enhancement of stereochemistry retention (**R15-L**). This result could be explained considering the action mechanism of TBTU, reported in figure 2.11. Generally, HOBt is added in order to catalyze the activation step in a coupling reaction in the presence of carbodiimides since they suffer the formation of stabile N-urea as by-products (see figure 4.3 in section 4.2.1 for the EDC mechanism. HOBt acts similarly to the N-hydroxysuccinimide)

<sup>17</sup> thus, the formation of a more reactive activated-ester is desirable. Nevertheless, in the case of TBTU coupling, the HOBt is intrinsically released during activation and the addition of more HOBt could interfere with reaction stereochemistry.

To confirm this mechanism, 2-(N-Acetyl)-L-phenylalanyl-amido-2-deoxy-1,3,4,6-tetra-O-acetyl- $\beta$ -D-glucose (**D-2b**) was synthesized from N-Acetyl-D-phenylalanine both with excess or equimolar DIPEA. Stereochemistry retention was attained for N-Ac-D-Phe demonstrating major reactivity of D-oxazolone toward aminolysis, regardless of a fast racemization or epimerization (excess or equimolar base, respectively). Higher L:D ratio of **R1-D** could be explained bearing in mind that the quantity of L-oxazolone during activation is higher when excess of base is used. Epimerization of N-Ac-D-Phe with equimolar base is complete after 3 hours considering that the L:D ratio assets at about 24:76, as shown by **R2-D** and **R3-D**.

The proposed mechanism for epimerization/racemization of activated N-Ac-D,L-Phe is proposed in figure 2.13.

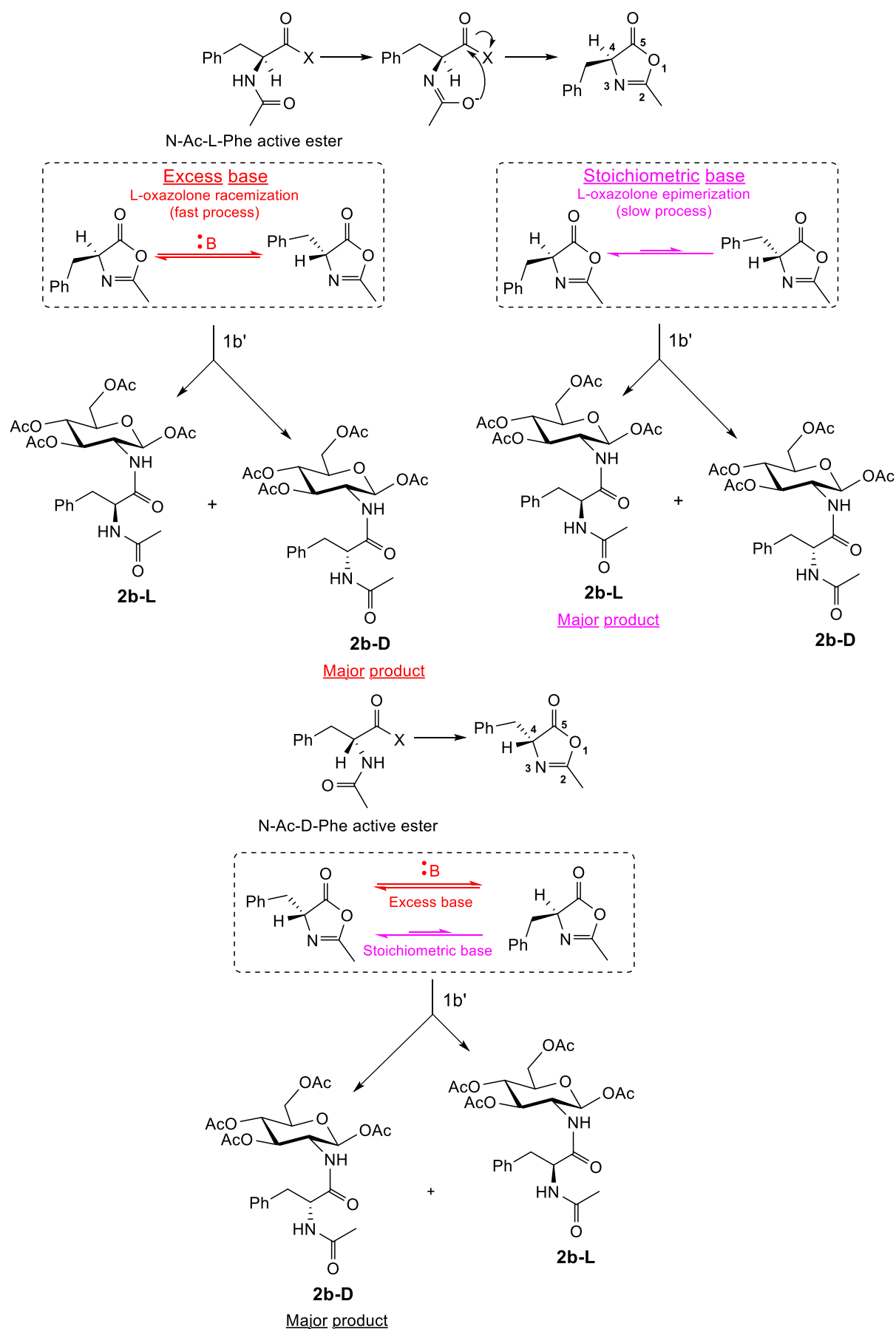


**Fig. 2.13:** Proposed mechanism for the epimerization/racemization of N-Acetyl-D,L-phenylalanine in TBTU/DIPEA mediated coupling.

Since no biological analysis have been performed on 2-(N-Acetyl)-D-phenylalanyl-amido-2-deoxy- $\beta$ -D-glucose (D-NAPA), we focused on the purification via crystallization of its tetra-O-acetylated precursor (see section 3.2.1 and 3.2.2 for the biological results). Several solvents or solvent mixtures have been tested and results are listed in table 2.2. Crystallization studies were carried out on crude reactions with **2b-D** as major product.

**Table 2.2:** Solvents/solvents mixtures used for crystallization of tetra-O-acetylated NAPA and diastereoisomeric ratios of precipitated crystals.

Solvent	D:L
DMC/Hexane	19:81
DCM/Diethyl ether	20:80
DCM/Isopropyl alcohol THF	-
Ethyl acetate	50:50
Ethanol	80:20
Methanol	100:0
Acetone	100:0

**2b-D** was efficiently crystallized in methanol or acetone, and the latter gave the higher yield of crystallization. Purification via crystallization was performed several times on crude reaction up to achieve a coupling yield of 50%. The diastereoisomeric pure product was individually characterized by  $^1\text{H}$  and  $^{13}\text{C}$  NMR.

## 2.1.5 Coupling of N-(Carbobenzyloxy)-L-phenylalanine using TBTU

Stereochemistry retention in a TBTU mediated coupling was also tested in the case of carbamate protector groups, which are known to endure easily racemization.<sup>32,21</sup>

At this regard, L-phenylalanine bearing a N-carbamate protecting group (N-(Carbobenzyloxy)-L-phenylalanine, N-Cbz-L-Phe) was coupled to **1b'** repeating same procedure proposed for **R7-L** and **R4/5-L** (figure 2.14). Reactions specifics are listed in table 2.3.

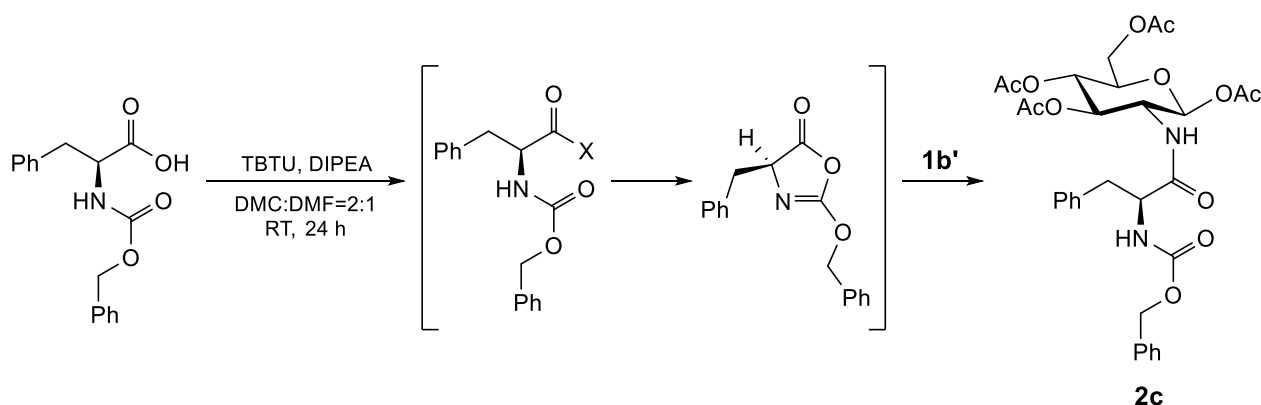


**Fig. 2.14:** Synthesis of tetra-O-acetylated-Cbz-NAPA precursor **2c** by means of TBTU/DIPEA coupling. DIPEA is used in excess respect to the amino acid in order to evaluate a possible racemization.

**Table 2.3:** Specifics for N-Cbz-L-Phe and **1b'** coupling in the presence of TBTU/DIPEA.  $T_{act}$  = activation temperature,  $T_R$  = reaction temperature,  $t_R$  = reaction time,  $R^D = 2b-L:2b-D$  diastereoisomeric ratio. The yield is defined as the sum of diastereoisomers.

Reaction	Cbz-L-Phe:DIPEA:TBTU (eq)	$T_{act}$ (°C)	$T_R$ (h)	$t_R$ (h)	Yield (%)	$R^D$ (L:D)
<b>R1-Cbz</b>	1:1:1	RT	RT	24	81	100:0
<b>R2-Cbz</b>	1:2:1	RT	RT	24	83	100:0

As expected, synthesis of **2c** occurs in high yields and without the detection of epimerization, both for **R1** or **R2-Cbz**. This results could be explained considering the higher stability of 2-alcoxy-azlactones, if oxazolone mechanism is considered, with or without excess of tertiary base.

### 2.1.6 T3P for the coupling of N-Acetyl and N- Carbobenzyloxy amino acids

Several reports demonstrated that in some cases a side reaction of TBTU with amine can afford in the formation of a guanidine byproduct, with a mechanism shown in figure 2.11. Formation of basic molecules can invalidate the study of chiral retention and, thus, 1-Propanephosphonic anhydride (T3P) was used (structure in figure 2.15). T3P is a highly reactive n-propyl phosphonic acid cyclic anhydride that works both as coupling and as water removal reagent, offering over traditional reagents several advantages, such as high yields and purity, low toxicity, broad functional group tolerance, low epimerization tendency without any additives, and easy work-up (only water-soluble by-products, elimination of the need of chromatographic columns).<sup>33</sup> Several T3P-mediated amide bonds formation can be found in literature on epimerization-prone substrates. For instance, Dunetz and co-workers developed a scalable amide bond formation strategy, in high yield, that provided the synthesis on kilogram scale of a hepatoselective glucokinase activator starting from an epimerization prone-substrate.<sup>34</sup> In the same paper, condensation of 2-phenylpropanoic acid, N-Z-alanine, and N-Z-phenylglycine (all > 99:1 er) with achiral amines by means of T3P, provided enantiomerically pure amides in high yield. Nevertheless, authors reported that the application of T3P/pyridine to N-Ac-alanine and aniline provided azlactone byproducts.<sup>32</sup> Furthermore, Fmoc-L-amino acids, including Fmoc-Phe-OH, were coupled to an isomer of 2-(N-Acetyl)-L-phenylalanyl-amido-2-deoxy-1,3,4,6-tetra-O-acetyl- $\beta$ -D-glucose via T3P and TBTU.<sup>35</sup> Amidation with propylphosphonic acid cyclic anhydride resulted in a higher purity products and yields than the other methodologies involved and isolated products were diastereoisomerically pure.

In our preliminary experiments, tetra-O-acetylated NAPA was synthesized in excess of DIPEA, following experimental procedure described by S. M. P. Martín and coauthors<sup>35</sup> to compare and evaluate T3P effect on preventing epimerization of N-Acetylated amino acids (**R1-L-T3P**). Furthermore, coupling with T3P was performed with equimolar amount of base respect to the L amino acid (**R2-L-T3P**). For the sake of comparison, N-Cbz-L-Phe was also reacted (**R1-Cbz-T3P**). List of T3P- mediated reactions is reported in table 2.4.

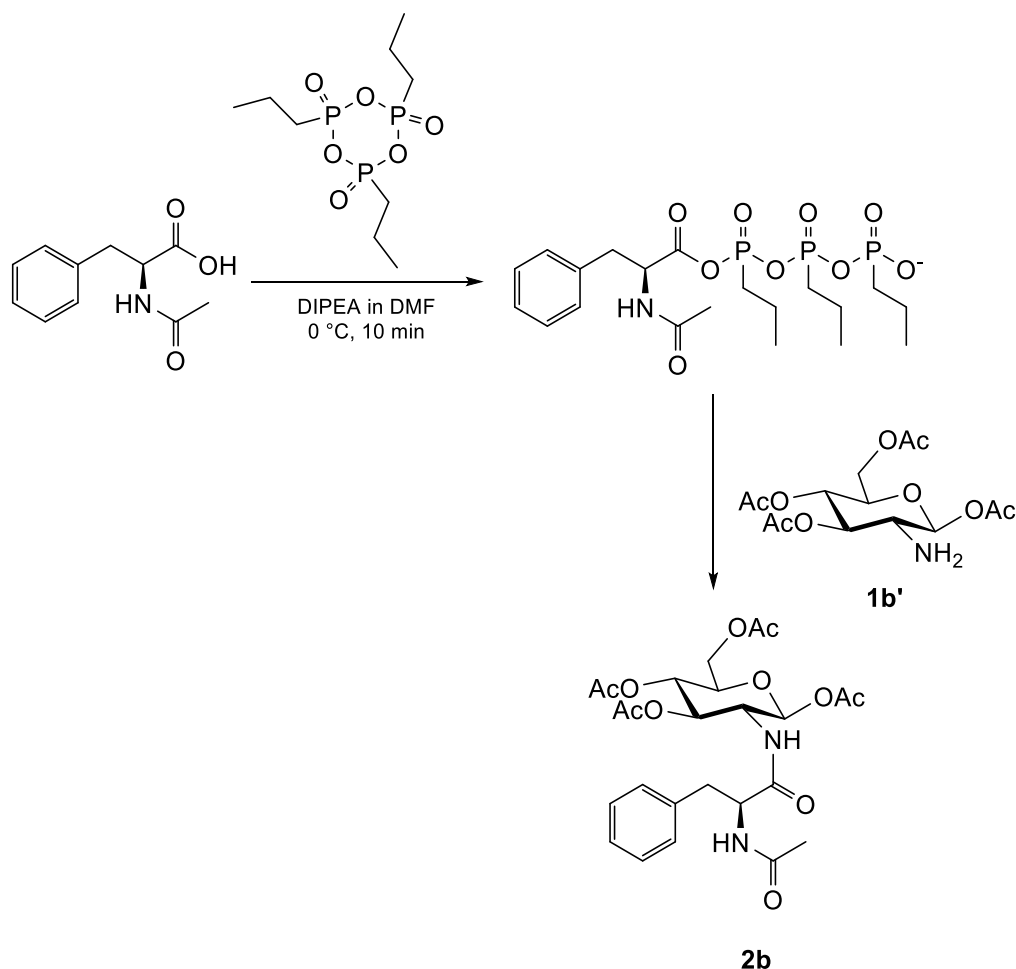


**Fig. 2.15:** Synthesis of **2b** in a coupling mediated by T3P.

N-Ac-L-Phe in DMF was mixed with 1,5 eq of T3P in the presence of DIPEA (2 equivalents) at 0 °C. Then, **1b'** was added and reaction was mixed at RT for 24 hours. Synthesis of **2b** was revealed by NMR analysis.

**Table 2.4:** List of T3P coupling specifics for the synthesis of **2b**.  $T_{act}$  = activation temperature,  $T_R$  = reaction temperature,  $t_R$  = reaction time, RD = 2b-L:2b-D diastereoisomeric ratio.

Reaction	L-Phe:DIPEA:T3P (eq)	$T_{act}$ (°C)	$T_R$ (h)	$t_R$ (h)	Yield (%)	Diastereoisomeric Ratio (L:D)
<b>R1-L-T3P</b>	1:2:1,5	RT	RT	24	84	34:66
<b>R2-L-T3P</b>	1:1:1	0	RT	24	88	47:53
<b>R1-Cbz-T3P</b>	1:2:1,5	RT	RT	24	87	100:00

Similarly to previous reactions, **2b** (yield 84%) was always obtain as mixture of diastereoisomers, with L:D ratio of 33:66 or 47:53, while **Cbz-2b** resulted in a optically pure compound. Again, racemization of N-Ac-L-Phe was obtained proving the high tendency of the L amino acid towards chirality loss.

### 2.1.7 Synthesis of compound **III**: deacetylation of **IV**

Tetra-O-acetylated intermediate **2b-D,L** was deacetylated through alkaline treatment with sodium methoxide in THF/MeOH mixture at low temperature to get target molecule **2** (figure 2.16). Low temperature and short time treatment are required to preserve amide bonds in the target molecule.

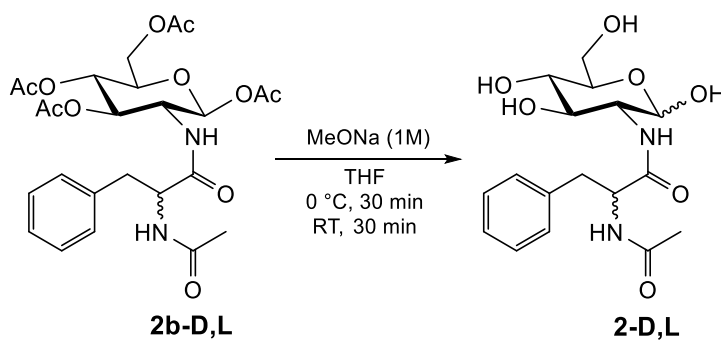


**Fig. 2.16:** deacetylation of intermediate 2b to give desired the N-peptidyl derivative of glucosamine NAPA.

2-(N-Acetyl)-D,L-phenylalanyl-amido-2-deoxy-D-glucose was purified by DCM and acetone washing and crystallization in methanol. No racemization of the peptide occurs, as confirmed by NMR (same L:D ratio is maintained before and after deacetylation), and hemiacetalic form of the amino sugar was restored.

## 2.2 Regioselective Esterification of NAPA

Conjugation of 2-(N-Acetyl)-L-phenylalanyl-amido-2-deoxy-D-glucose **III** to hyaluronic acid was attained by a regioselective esterification on 6-C with a n-bromine derivative linker (derivative **II**). Two approaches were investigated to synthesize ester **II**, as shown below (figure 2.17). Both strategies were based on selective O-acylation of the monosaccharide derivative **III**.

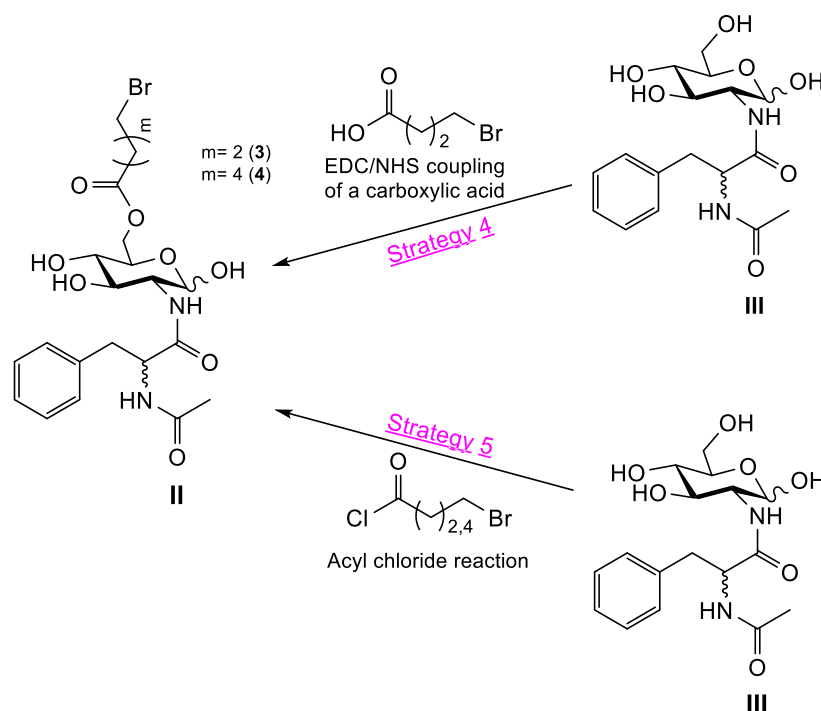


**Fig. 2.17:** General scheme for regioselective-O-esterification of NAPA with a n-bromine linker.

The main challenge in the synthesis of sugar esters lies in the differentiation of the hydroxylic groups present in the molecule. In fact, NAPA contains one primary alcohol at 6-C and three secondary alcohols at 1-C, 3-C and 4-C. Among them, the least sterically hindered position HO-C(6) is the most reactive and it could be regioselectively esterified by controlling the reaction conditions. The second reactive position through esterification is the HO-C(3).<sup>36</sup> Thereby, we focused on the definition of a method for the regioselective O-acylation of **III**, with a specific bifunctional molecule.

## 2.2.1 Esterification with 4-bromobutyric acid

### Strategy 4

At first, 4-bromobutyric acid was tested as suitable linker for esterification of NAPA. The coupling was pursued via carbodiimide as shown in figure:

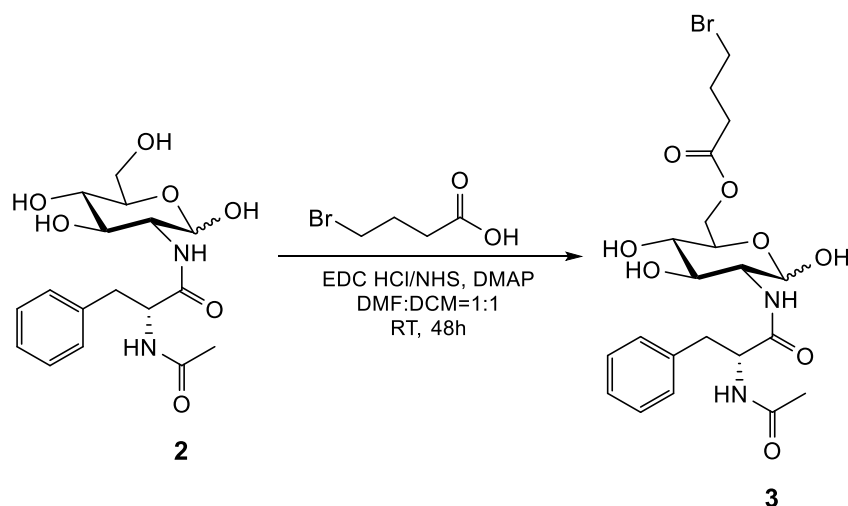


**Fig. 2.18:** Esterification of NAPA with 4-bromobutyric acid by means of EDC/NHS coupling.

To promote esterification of the primary alcoholic position, all reactants were used in defect respect to **2** (0,9 eq). Carboxylic acid was dissolved in a small volume of dichloromethane and DMF (v:v=1:1) and activated with EDC HCl/NHS and catalytic DMAP at room temperature. Then, after 15 minutes, a solution of NAPA in DMF was added. Reaction was kept under stirring at room temperature for two days but TLC didn't show the formation of any sort of product.

References for O-acylation of alcohols with 4-bromobutyric acid or similar via carbodiimide coupling can be largely found in literature reporting procedures similar to the ones employed.<sup>37,38,39,2</sup> However, in those researches, the substrates have only one or two hydroxylic groups, one of which is highly chemically inert, suggesting that carbodiimide coupling could be inappropriate when a poly-alcohol is reacted.

## 2.2.2 Esterification with acyl chlorides

### Strategy 5

HO-C(6) esterification was performed using n-bromine acyl chlorides, which are more reactive than the respective carboxylic acids owing a carbonyl position less shielded. Ester bond formation with acyl chlorides proceeds without activation step. Several works report acylation of amino sugar derivatives using acyl chlorides. They concern the total esterification of the four OH groups of the glucosamine unit<sup>40</sup> or its mono-functionalization by protecting three of the four OH positions<sup>41</sup> but only few of them deal with the regioselective esterification of amino sugar with free alcoholic positions.<sup>36</sup> To our knowledge, selective O-acylation of glucosamine derivatives with n-bromine acyl chlorides has not been described.

Molecule **2** was esterified by means of 4-bromobutyryl and 6-bromohexanoyl chloride in order to synthesize derivatives **3** and **4** (for molecule **3** m=2 while for **4** m=4) as reported in figure 2.19.

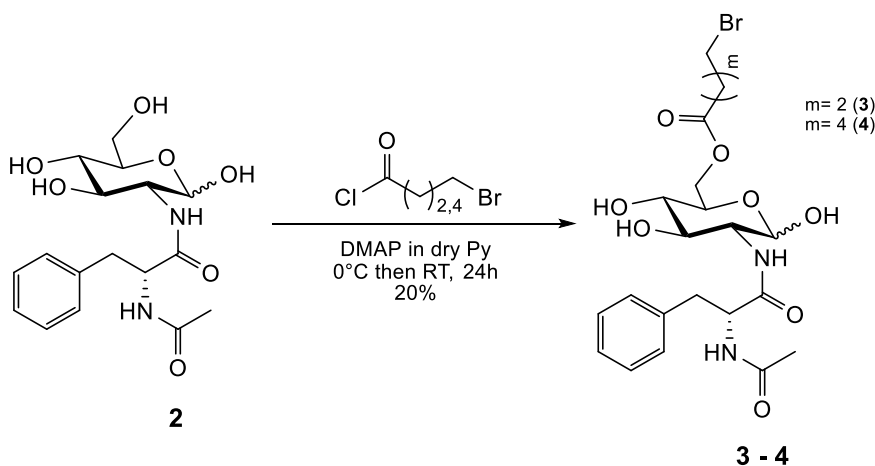


**Fig. 2.19:** Esterification of NAPA with n-bromine acyl chlorides.

Reaction was carried out in pyridine, due to the high polarity of reactants involved and to the need to work in alkaline conditions, in presence of catalytic amount of DMAP. The reaction was followed by TLC which showed that the formation of a major product rapidly occurred when 6-Bromohexanoyl chloride was used (approximately after 30 minutes from the starting of reaction). Esterification was conducted in defect and in excess of 4-bromobutyryl chloride (0,90 eq or 2 eq) respect to **2** but either conditions gave 6-O-acyl derivative as major product with similar yields. 6-bromohexanoyl chloride was used only in excess (2 eq). Nevertheless,

no consumption of starting material was detected by TLC both in excess of n-bromine acyl chlorides or after 48 h of stirring. Crude reaction was purified chromatographically by flash silica gel using a chloroform/methanol mixture as eluent.

Reaction was conducted without any tertiary bases, e.g. triethylamine, on the assumption that homogeneous acylations are faster when acetic chlorides are reacted instead of acetic anhydrides. In fact, only a catalytic amount of DMAP was added.<sup>42</sup> Mechanism proposed for O-acylation with acyl chlorides in the presence of catalytic DMAP is based on the fact that the alcoholic function of the substrate is deprotonated by the counterion generated from the DMAP-activated acyl chloride **a** and not by a tertiary base. After deprotonation, the alcohol can attack the electrophilic carbon position of the DMAP intermediate to give the desired ester, as reported in figure 2.20. If the counterion is a chloride, deprotonation of sugar occurs preferentially in most accessible position 6-C.

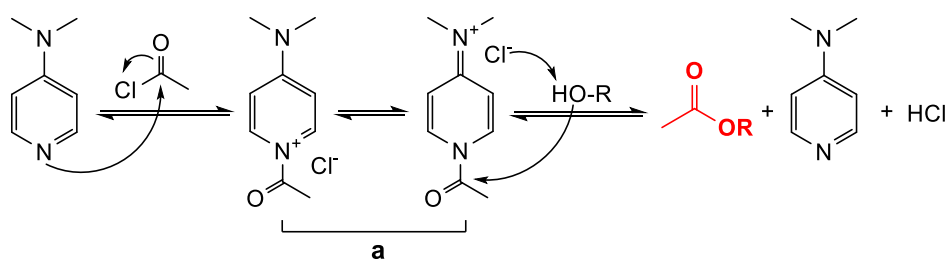


**Fig. 2.20:** Catalytic role of DMAP in the O-acylation of alcoholic substrates.

Structures of **3** and **4** were characterized by 1D, 2D NMR, FTIR and mass spectroscopy. <sup>1</sup>H spectrum of **3**, whose structure can be found in figure 2.21, showed three sets of signals related to the 8, 9 and 10-CH<sub>2</sub> groups of the 10-brominebutanoate linker covalently bonded to  $\alpha/\beta$ -NAPA, respectively centered at 2,53, 2,11 and 3,56 ppm.

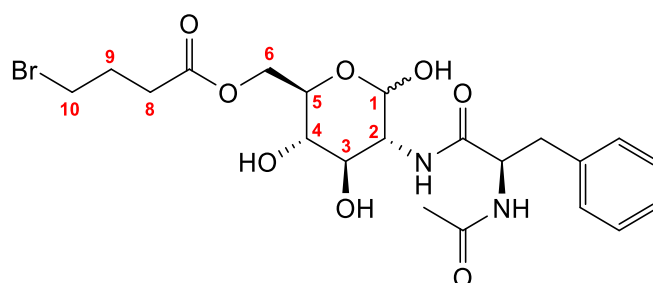


**Fig. 2.21:** Structure of mono-esterified NAPA **3**.

In addition, protons of 6-CH<sub>2</sub> were shifted in the spectrum as result of 6O-esterification. <sup>13</sup>C spectrum showed the presence of a new peak in the carbonyl region and FTIR was

characterized by the appearance of a new infrared peak at  $1730\text{ cm}^{-1}$  demonstrating that a mono 6O-acyl derivative of NAPA was obtained. The degree of esterification was calculated as the ratio between proton signal belonging to methylene group in phenylalanine ( $\text{CH}_2\text{Phe}$ ) residue and signal of 8- $\text{CH}_2$  in the linker at 2,53 ppm. The  $\alpha$  anomer resulted to be the major product with an  $\alpha/\beta$  ratio of 70:30, calculated from proton signals of 1- $\alpha\text{HC}$  at 4,89 and 1- $\beta\text{HC}$  at 4,61 ppm.

However, an unexpected splitting of some  $\text{CH}_2$  signals assigned to the 10-brominebutanoate linker occurred in both  $^1\text{H}$  and  $^{13}\text{C}$  spectra. Magnification of  $^1\text{H}$  spectrum of molecule **3** is showed in figure 2.22. Signals of 8,9 and 10- $\text{CH}_2$  groups are the in-box peaks.

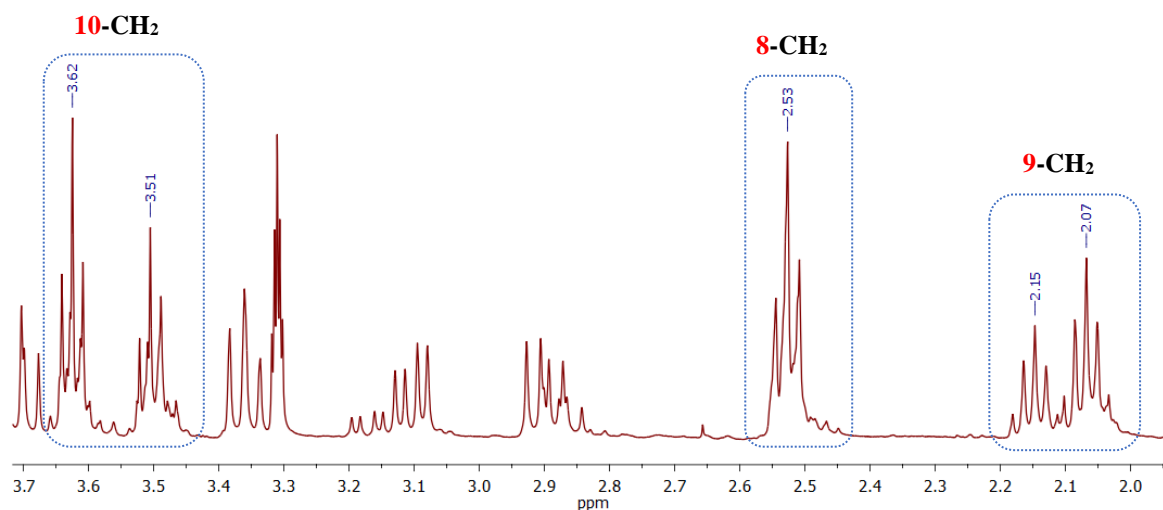


**Fig. 2.22:**  $^1\text{H}$  NMR spectrum of **3**. Evidences of chloride replacement in the lateral chain of the molecule.

Splitting can be observed in the multiplets centered at 2,11 and 3,56 ppm (9- $\text{CH}_2$ : two multiplets at 2,07 and 2,15 ppm. 10- $\text{CH}_2$ : two multiplets at 3,51 and 3,62 ppm), and the ratio between the two sets of signals does not match the one determined for  $\alpha/\beta$  anomers. The triplet at 2,53 ppm is for 8- $\text{CH}_2$ . The splitting could be ascribed to some structural changes in the mono-O-linker bonded to NAPA. Specifically, it could be related to a partially replacement of bromine by chlorine in the side chain of linker as result of chloride ion generation during 4-Bromobuteryl chloride reaction.

This hypothesis was supported by the fact that the only doubled signals belong to 9- $\text{CH}_2$  and 10- $\text{CH}_2$ , which are closer to the terminal halogen and that could have some kind of interaction with the atom. 8- $\text{CH}_2$  is not affected by halogen effect and its protons and carbon signals are not doubled.

2D NMR of **3** was also performed in order to investigate in deep its structural features. COSY spectrum highlighted that protons correlation takes place only for the methylene signals at 2,07 and 3,62 ppm and for those at 2,15 and 3,51 ppm, confirming the hypothesis that two types of carbon chains are covalently bonded to NAPA. Furthermore, two protons triplet at 2,53 ppm resulted be coupled with both signals of 9-CH<sub>2</sub> at 2,07 and 2,15 ppm, in accordance with their spatial proximity. About 40 % of **3** resulted to be 4-bromine substituted. Finally, mass spectroscopy confirmed the partial chlorine replacement in derivative **3** (ESI-MS: Calcd for C<sub>21</sub>H<sub>29</sub>BrN<sub>2</sub>O<sub>8</sub><sup>+</sup> [M+Na]<sup>+</sup>: 539,1; measured m/e: 539,3. Calcd for C<sub>21</sub>H<sub>29</sub>ClN<sub>2</sub>O<sub>8</sub><sup>+</sup> [M+Na]<sup>+</sup>: 495,2; measured m/e: 495,3).

NMR, mass and FTIR confirmed synthesis of 6-O-ester **4** as well (structure in figure 2.23).

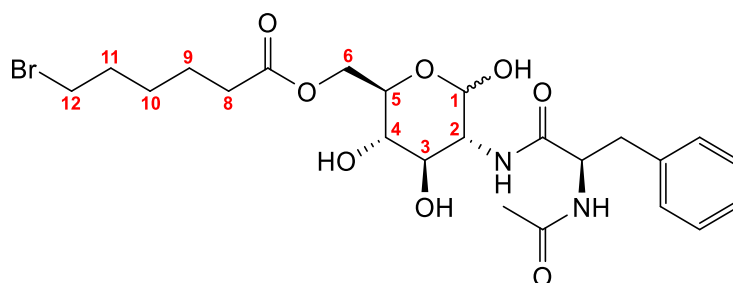


**Fig. 2.23:** Structure of mono-esterified NAPA **4**.

Multiplets related to the five methylene groups of 12-brominehexanoate linker can be found in the <sup>1</sup>H NMR spectrum of **4**. Specifically , three quintuplets, in the region between 1,38 and 1,84 ppm for 10, 9 and 11-CH<sub>2</sub>, and two triplets, centered at 2,36 and 3,56 ppm for 8 and 12-CH<sub>2</sub>, are visible. A shift in the position of 6-CH<sub>2</sub> protons can be seen in the spectrum indicating that O-acylation occurs in the least hindered position even when the longer acyl chloride is reacted. The major product is represented by the α diastereoisomer.

NMR characterization did not show the splitting of methylene signals prompting no chemical changes in the bromine-hexanoate linker or the total replacement of chlorine in 12-C position, as described above. Unfortunately, the latter was confirmed by mass spectroscopy (ESI-MS: Calcd for C<sub>23</sub>H<sub>33</sub>BrN<sub>2</sub>O<sub>8</sub><sup>+</sup> [M+H]<sup>+</sup>: 545,2; measured m/e: no peak. C<sub>23</sub>H<sub>33</sub>BrN<sub>2</sub>O<sub>8</sub><sup>+</sup> [M+Na]<sup>+</sup>: 567,1; measured m/e: no peak. Calcd for C<sub>23</sub>H<sub>33</sub>ClN<sub>2</sub>O<sub>8</sub><sup>+</sup> [M+H]<sup>+</sup>: 501,2; measured m/e: 501,2. Calcd for C<sub>23</sub>H<sub>33</sub>ClN<sub>2</sub>O<sub>8</sub><sup>+</sup> [M+Na]<sup>+</sup>: 523,2; measured m/e: 523,3). Although unexpected, chlorine replacement is not considered as an obstacle for hyaluronic acid

functionalization via nucleophilic substitution in the final step of the bioconjugation (figure 2.17 from **II** to **I**).

For both acyl chlorides reactions, low side-products, about 5%, were isolated and characterized by  $^1\text{D}$  NMR. Most likely they represent the amino sugar fraction multi-esterified.

## 2.3 Esterification of hyaluronic acid with a NAPA derivative

In the last step, bioconjugate **I** was synthesized from esterification of hyaluronic acid with n-bromine derivative **II** in organic solvent (figure 2.1).

Linkage of n-bromine ester of NAPA to hyaluronic acid was carried out in organic solvent, since nucleophilic substitutions are known to proceed well in that environment. Dimethyl sulfoxide (DMSO) was chosen as solvent, thus the native HA sodium salt has to be firstly converted into its tetrabutylammonium salt (HA-TBA).

HA-TBA was prepared mixing sodium hyaluronate with tetrabutylammonium hydroxide (TBA-OH), properly activated with Dowex®50WX-8-400 resin (figure 2.24).<sup>43</sup> Solution was filtrated and purified by extensive dialysis in distilled water to remove TBA-OH excess. Finally, HA-TBA salt was collected as a cotton-like material after freeze drying.

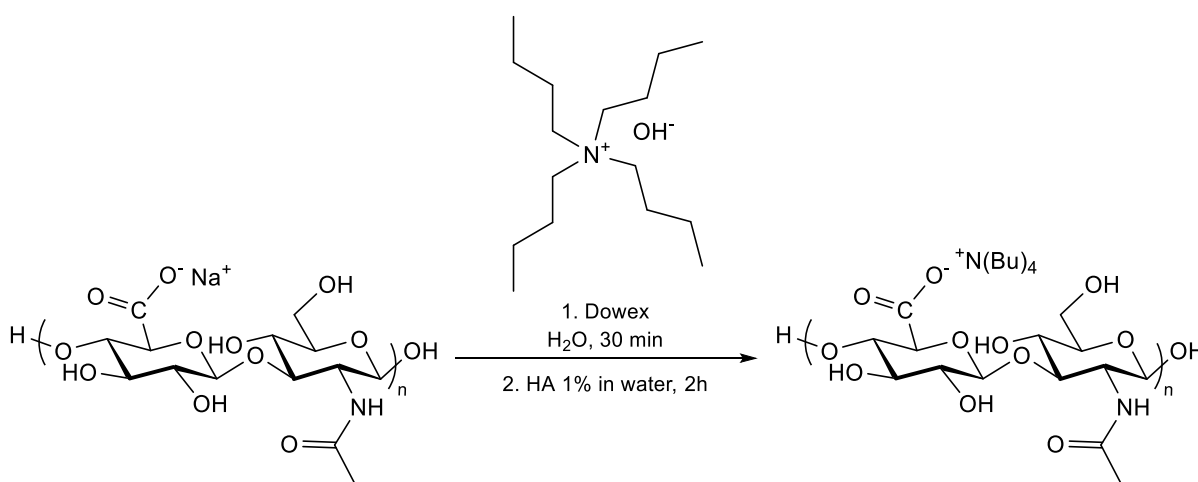


**Fig. 2.24:** Preparation of the organic salt of hyaluronic acid (HA-TBA) using tetrabutylammonium hydroxide.

TBA<sup>+</sup> ion presence was confirmed by intense stretching peaks of methyl and methylene groups between 3000 and 2880 cm<sup>-1</sup> in the infrared spectrum of HA-TBA salt. Furthermore, proton spectrum in D<sub>2</sub>O showed specific sets of signals assigned to the ammonium anion such as a triplet at 0.95 ppm for methyl groups and a sextuplet at 1.37, a quintuplet at 1.66 and a triplet at 3.20 ppm for the three methylene groups. Degree of substitution resulted to be close to 100% as indicated by <sup>1</sup>H NMR spectrum.

Functionalization of hyaluronic acid with molecule **3** or **4** was performed via esterification of the glucuronic carboxylic moiety, as shown in figure 2.25.

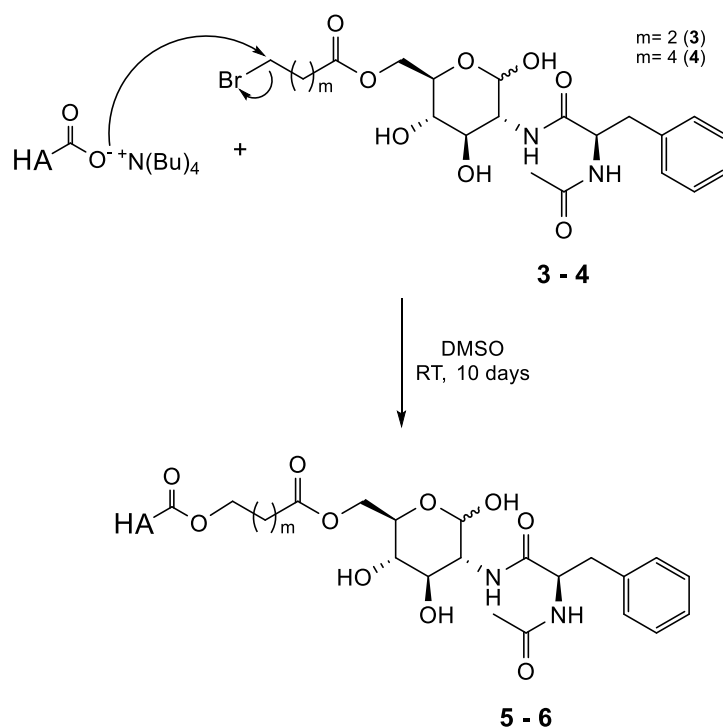


**Fig. 2.25:** Functionalization of hyaluronic acid with the n-bromine derivatives **3** or **4** toward nucleophilic substitution.

Polar aprotic solvents, such as N,N-dimethylformamide (DMF), dimethyl sulfoxide (DMSO) and N-Methyl-2-pyrrolidone (NMP) are considered the best solvents for nucleophilic substitution. At this regard, the reaction was carried out in DMSO, due to the lack of solubility of HA-TBA in the amidic solvent. HA-TBA was dissolved in DMSO at room temperature and mixed vigorously for at least three hours. Esters **3** (or **4**) was added afterwards and reaction was kept under stirring until TLC revealed consumption of the amino sugar ester **3-4**. To the crude reaction saturated NaCl solution and absolute EtOH were added and mixed for further 3 hours. Then, hyaluronic acid derivative was separated by centrifugation, purified with extensive dialysis in NaCl saturated solution and water for several days and finally freeze dried.

Functionalization of hyaluronic acid with NAPA was confirmed by FTIR and NMR spectroscopy. In the infrared spectrum of bioconjugate **5** (figure 2.26) a new peak at  $1732\text{ cm}^{-1}$  appears as result of HA esterification. Reasonably, when an ester bond is formed carboxylate is consumed and indeed, decrease of bands related to  $\text{COO}^-$  asymmetrical and symmetrical stretching are visible at  $1605$  and  $1406\text{ cm}^{-1}$ . Unfortunately, no evidences of esterification are visible for HA-NAPA derivative **6** in the FTIR spectrum.

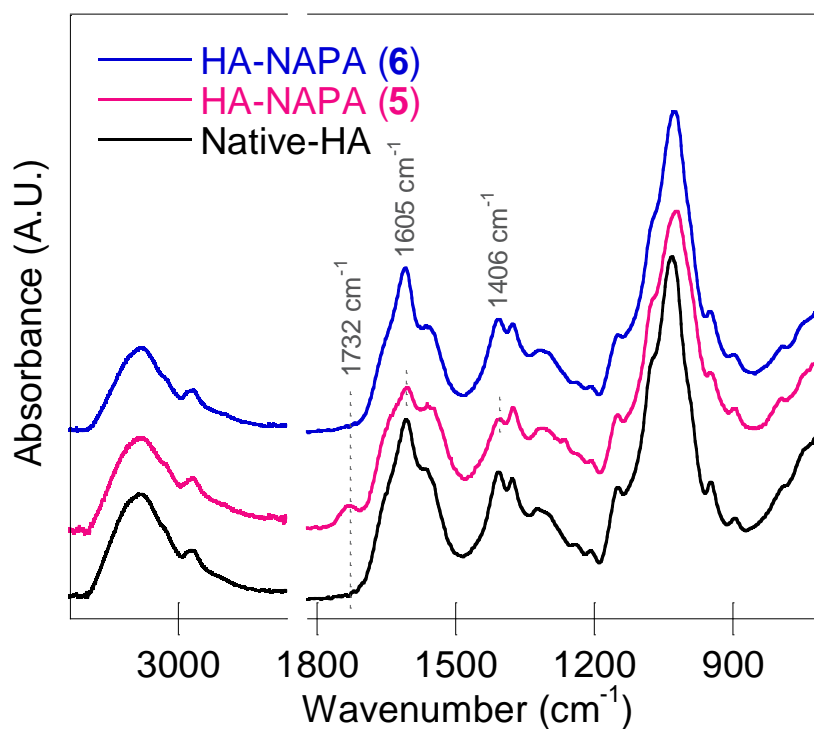


**Fig. 2.26:** FTIR spectra of native-HA (black), HA-NAPA **5** (pink) and HA-NAPA **6** (blue).

Lastly, HA-NAPA derivatives were studied using NMR spectroscopy. Proton spectra of **5** and **6** in D<sub>2</sub>O are shown in figure 2.27. Functionalization of hyaluronic acid is evidenced by the presence of methylene signals (dashed lines in figure) and by the presence of aromatic proton at around 7,35 ppm. Degree of functionalization of the samples was calculated from ratio between aromatic signal and the singlet at 1,9 ppm related to HA-CH<sub>3</sub>. Functionalization resulted to be 20 % for derivative HA-NAPA **5** and 2% for HA-NAPA **6**.

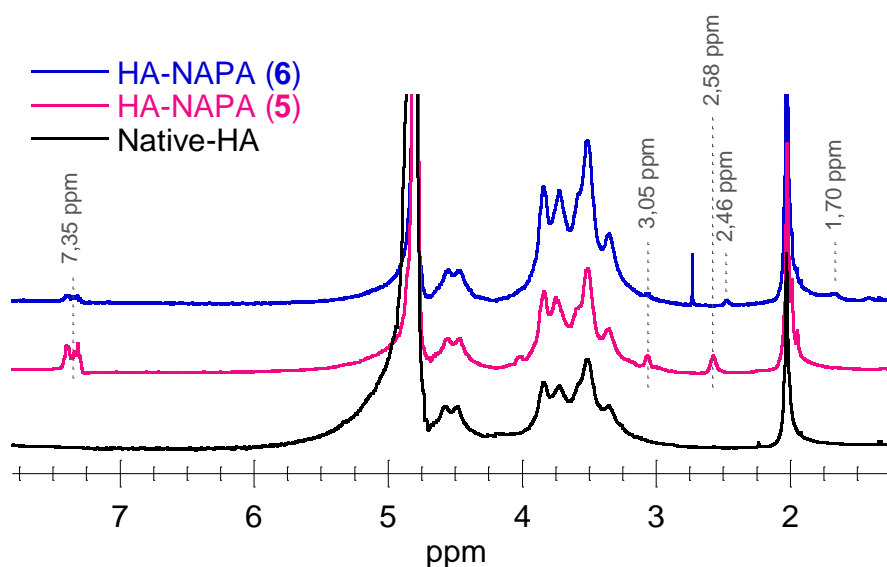


**Fig. 2.27:** <sup>1</sup>H NMR spectra in D<sub>2</sub>O of native HA (black) and esterified-NAPA derivatives **5** and **6** (pink and blue) in the region between 1,2 and 7,80 ppm.

## 2.4 Materials and methods

### 2.4.1 Strategy 1

#### Synthesis of **2**

##### EDC/NHS coupling

N-Ac-L-Phe (0,207 g, 1 mmol) was dissolved in THF (2 ml) and EDC HCl (0,230 g, 1,2 mmol) and NHS (0,138 g, 1,2 mmol) were added and kept under stirring for 30 minutes at room temperature. Then, a solution of **1** (0,216 g, 1 mmol) and TEA (0,139 ml, 1 mmol) in MeOH (2 ml) was added to peptide mixture. The reaction was stirred for 21 hours at room temperature and followed by TLC (CHL:MeOH=8:2). Crystallization in MeOH gave product **2** (or EtOH).

<sup>1</sup>H NMR (400 MHz, DMSO): δ 8,10 – 7,70 (m, 2H, 2xNH), 7,40 – 7,10 (m, 5H, ArPhe) 6,60 – 6,35 (m, 1H, OH), 5,19 – 4,25 (m, 5H, H-1, CHPhe, 3xOH), 3,86 – 3,87 (m, 5H, C-3,4,5,6,6'), 3,20 – 3,04 (m, 1H, H-2), 3,04 – 2,62 (m, 2H, CH<sub>2</sub>Phe), 1,78 – 1,71 (s, 3H, CH<sub>3</sub>Phe).

##### IBCF coupling

N-Ac-L-Phe (0,137 g, 0,66 mmol) was dissolved in THF (1 ml) at room temperature and then cooled at 0 °C in ice bath. TEA (0,181 ml, 1,3 mmol) and IBCF (0,130 ml, 1 mmol) were added to peptidyl solution and stirred for 30 minutes (white solid salt is formed when TEA is added). To this solution, **1** (0,216 g, 1 mmol) in water (1 ml) was added and the reaction was stirred at 0 °C for 30 minutes and then at room temperature for 21 hours. Crude reaction solution was dried under vacuum and product **2** was purified by crystallization in MeOH (or EtOH),

<sup>1</sup>H NMR (400 MHz, CDCl<sub>3</sub>): for NMR spectrum see spectrum before.

### 2.4.2 Strategy 2

#### Synthesis of **1a**

TEA (0,737 ml; 5,30 mmol) was added to a solution of **1** (0,216 g; 1 mmol) in dry DMF (7 ml) at 0 °C under argon atmosphere. After complete dissolution, TMS-Cl (0,551 ml; 5,30 mmol) was added dropwise and the mixture was stirred at room temperature until TLC showed complete consumption of **1** (HEX:EtAc=8:2). Reaction was extracted with pentane at 0 °C and organic layer was washed several times with NaHCO<sub>3</sub> saturated solution, dried with Na<sub>2</sub>SO<sub>4</sub>, filtrated and dried under vacuum, **1a** was obtained as white powder with a 95% yield.

**ATR-FTIR** (powder): main peaks at 2955, 1245, 1150, 1060, 960, 830 cm<sup>-1</sup>.

**<sup>1</sup>H NMR** (400 MHz, CDCl<sub>3</sub>): δ 5,11 (d, J = 3,3 Hz, 1H, H-1), 3,68 (dd, J = 5,7, 3,3 Hz, 2H, H-6,6'), 3,61 (ddd, J = 9,1, 4,3, 2,2 Hz, 1H, H-5), 3,54 (t, J = 8,8 Hz, 1H, H-3), 3,45 (t, J = 9 Hz, 1H, H-4), 2,54 (dd, J = 9,2, 3,3 Hz, 1H, H-2), 0,18, 0,15, 0,14, 0,07 (4s, 9H each, (CH<sub>3</sub>)<sub>3</sub>Si).

**<sup>13</sup>C NMR** (101 MHz, CDCl<sub>3</sub>): δ 94,51 (C-1α), 77,43 (C-3), 73,14 (C-5), 72,07 (C-4), 62,08 (C-6,6'), 57,49 (C-2), 1,41, 0,92, 0,03, 0,15 (4x(CH<sub>3</sub>)<sub>3</sub>Si).

**ESI-MS**: Calcd for C<sub>18</sub>H<sub>45</sub>NO<sub>5</sub>Si<sub>4</sub><sup>+</sup> [M+H]<sup>+</sup>: 468,2; measured m/e: 468,3, Calcd for C<sub>18</sub>H<sub>45</sub>NO<sub>5</sub>Si<sub>4</sub><sup>+</sup> [M+Na]<sup>+</sup>: 490,2; measured m/e: 490,2,

### 2.4.3 Strategy 3

#### Synthesis of **1a'**

To a solution of **1** (0,216 g, 1 mmol) in NaOH 1M (1 ml) at 0 °C, p-anisaldehyde (0,125 ml, 1,03 mmol) was added dropwise. The reaction was followed by TLC (CHL:MeOH=8:2) and the mixture was stirred until complete conversion of **1** at 0 °C (around 4 hours). The precipitate was collected by filtration, washed with cold water, cold ethanol and diethyl ether, and then dried under vacuum to give title compound as white solid (yield 90%).

**ATR-FTIR** (powder): main peaks at 3484, 3424-3050, 3030, 2930, 2890, 2880, 1640, 1604, 835 cm<sup>-1</sup>.

**<sup>1</sup>H NMR** (400 MHz, DMSO): δ 8,11 (s, 1H, N=CH), 7,68 (d, J = 8,8 Hz, 2H, 2xArCH), 6,98 (d, J = 8,8 Hz, 2H, 2xArCH), 6,52 (d, J = 6,6 Hz, 1H, OH-1), 4,91 (d, J = 5,3 Hz, 1H, OH), 4,80 (d, J = 5,6 Hz, 1H, OH), 4,69 (t, J = 7,1 Hz, 1H, H-1), 4,54 (t, J = 5,8 Hz, 1H, OH-6),

3,80 (s, 3H, OCH<sub>3</sub>), 3,72 (ddd, J = 11,6, 5,5, 1,9 Hz, 1H, H-5), 3,55 – 3,38 (m, 2H, H-6,6'), 3,28 – 3,18 (m, 1H), 3,18 – 3,09 (m, 1H), 2,79 (dd, J = 9,1, 7,9 Hz, 1H, H-2).

<sup>13</sup>C NMR (101 MHz, DMSO): δ 161,20 (2xC), 129,62 (2xArCH), 113,89 (2xArCH), 95,63 (CH), 78,19 (CH), 76,86 (CH), 74,59 (CH), 70,36 (CH), 61,27 (CH<sub>2</sub>), 55,27 (OCH<sub>3</sub>).

### Synthesis of **1a''**

Imine **1a'** (0,297 g, 1 mmol) was suspended in pyridine (1,5 ml) at 0 °C under argon atmosphere. Acetic anhydride (0,388 ml, 4,1 mmol) was added slowly at the same temperature and the mixture was stirred at 0 °C for 2 hours and then at room temperature overnight. Product **1a''** was precipitated in iced water and collected by filtration, washed with cold water and dried under vacuum as a white solid (yield 97%).

**ATR-FTIR** (powder): main peaks at 1745, 1735, 1646, 1604, 1247, 1211, 823 cm<sup>-1</sup>.

<sup>1</sup>H NMR (400 MHz, DMSO): δ 8,28 (s, 1H, CH=N), 7,66 (d, J = 8,7 Hz, 2H, 2xArCH), 6,99 (d, J = 8,7 Hz, 2H, 2xArCH), 6,07 (d, J = 8,2 Hz, 1H, H-1β), 5,45 (t, J = 9,7 Hz, 1H, H-3), 4,98 (t, J = 9,6 Hz, 1H, H-4), 4,32 – 4,16 (m, 2H, H-5,6), 4,02 (m, 1H, H-6), 3,79 (s, 3H, OCH<sub>3</sub>), 3,45 (dd, J = 9,4, 8,6 Hz, 1H, H-2), 2,02 (s, 3H, CH<sub>3</sub>), 1,98 (s, 6H, 2xCH<sub>3</sub>), 1,82 (s, 3H, CH<sub>3</sub>).

<sup>13</sup>C NMR (101 MHz, DMSO): δ 170,05 (CO), 169,45 (CO), 168,99 (CO), 168,60 (CO), 164,46 (C), 161,84 (C), 129,93 (2xArCH), 128,27 (ArC), 114,20 (2xArCH), 92,55 (C-1β), 72,36 (CH), 72,25 (CH), 71,55 (CH), 67,83 (CH), 61,66 (C-6,6'), 55,36 (OCH<sub>3</sub>), 20,52 (CH<sub>3</sub>), 20,44 (2xCH<sub>3</sub>), 20,19 (CH<sub>3</sub>).

### Synthesis of **1b**

Solution of acetoxy imine **1a''** (0,465 g, 1 mmol) in acetone (4 ml) was treated with HCl (5M, 0,150 ml) and stirred for 1 hour. Then, diethyl ether (4 ml) was added, and the mixture was stirred for two further hours. The product, in the form of a white precipitate, was collected by filtration, washed with cold diethyl ether and dried under vacuum (yield 95%).

**ATR-FTIR** (powder): main peaks at 3100-2500, 1766, 1742, 1594, 1575, 1513, 1190, 1035 cm<sup>-1</sup>.

**<sup>1</sup>H NMR** (400 MHz, DMSO):  $\delta$  8,87 (s, 3H, NH<sub>3</sub><sup>+</sup>), 5,92 (d, J = 8,6 Hz, 1H, H-1 $\beta$ ), 5,36 (t, J = 9,8 Hz, 1H, H-3), 4,92 (t, J = 9,5 Hz, 1H, H-4), 4,18 (dd, J = 12,2, 4,1 Hz, 1H, H-6), 4,07 – 3,95 (m, 2H, H-5,6'), 3,54 (dd, J = 10,0, 9,0 Hz, 1H, H-2), 2,17 (s, 3H, CH<sub>3</sub>), 2,02 (s, 3H, CH<sub>3</sub>), 1,99 (s, 3H, CH<sub>3</sub>), 1,97 (s, 3H, CH<sub>3</sub>).

**<sup>13</sup>C NMR** (101 MHz, DMSO):  $\delta$  170,03 (CO), 169,82 (CO), 169,37 (CO), 168,70 (CO), 90,12 (C-1 $\beta$ ), 71,63 (CH), 70,36 (CH), 67,83 (CH), 61,28 (C-6,6'), 52,19 (CH), 20,99 (CH<sub>3</sub>), 20,89 (CH<sub>3</sub>), 20,52 (CH<sub>3</sub>), 20,38 (CH<sub>3</sub>).

### Synthesis of **1b'**

Tetracetylated glucosamine hydrochloride **1b** (0,384 g, 1 mmol), suspended in DCM (6 ml), was treated with excess of Na<sub>2</sub>CO<sub>3</sub> (1M) at room temperature till complete consumption of the starting material. The organic layer was washed with water, dried over anhydrous Na<sub>2</sub>SO<sub>4</sub> and concentrated in vacuo to give title compound **1b'** as a white solid (yield 94%).

**ATR-FTIR** (powder): main peaks at 3280, 2942, 1756, 1743, 1616, 1580, 1535.

**<sup>1</sup>H NMR** (400 MHz, DMSO)  $\delta$  5,54 (d, J = 8,4 Hz, 1H, H-1 $\beta$ ), 5,04 (t, J = 9,8 Hz, 1H, H-3), 4,80 (t, J = 9,6 Hz, 1H, H-4), 4,15 (dd, J = 12,9, 5,1 Hz, 1H, H-6), 3,99 – 3,90 (m, 2H, H-5,6'), 2,74 (dd, J = 9,7, 8,8 Hz, 1H, H-2), 2,10 (s, 3H, CH<sub>3</sub>), 1,99 (s, 6H, 2xCH<sub>3</sub>), 1,96 (s, 3H, CH<sub>3</sub>), 1,63 (s, 2H, NH<sub>2</sub>).

**<sup>13</sup>C NMR** (101 MHz, DMSO)  $\delta$  170,04 (CO), 169,94 (CO), 169,38 (CO), 169,18 (CO), 94,73 (C-1 $\beta$ ), 74,55 (CH), 71,35 (CH), 68,33 (CH), 61,70 (C-6,6'), 55,10 (CH), 20,73 (CH<sub>3</sub>), 20,66 (CH<sub>3</sub>), 20,51 (CH<sub>3</sub>), 20,43 (CH<sub>3</sub>).

### Synthesis of **2b**

#### IBCF coupling

Amino acid activation: N-A-L-Phe (1 mmol) and N-methylmorpholine (1 mmol) were dissolved in dry THF (2 ml) and cooled at -10 °C under argon atmosphere and then IBCF (1 mmol) was added dropwise and stirred for 30 minutes.

Glucosamine solution A: **1b** (1 mmol) and NMM (1 mmol) were dissolved in dry THF (2 mmol) under argon atmosphere and after few minutes the mixture was added to the activation solution while the temperature of -10 °C was maintained.

Glucosamine solution B: **1b'** (1 mmol) was dissolved in dry THF (2 mmol) under argon atmosphere and slowly added to activation mixture while the temperature of -10 °C was maintained.

The reaction was kept at low temperature for 30 minutes, stirred for 24 h at room temperature and then filtered and concentrated at reduced pressure. The crude reaction was dissolved in ethyl acetate and washed with water, HCl 1M, saturated NaHCO<sub>3</sub> and brine. After drying on Na<sub>2</sub>SO<sub>4</sub>, the mixture was filtered and dried to obtain product **2b** as a white solid (mixture of diastereoisomers, yield 65%).

#### TBTU/DIPEA coupling

N-Ac-L-Phe (0,250 g, 1 mmol) and DIPEA (1 mmol) were dissolved in dry DCM (8 ml) and later a solution of TBTU (0,385 g, 1 mmol) in dry DMF (3 ml) was slowly added. After 30 minutes, a solution of **1b'** (1 mmol) in dry DMF (1 ml) was added dropwise to the amino sugar solution and the mixture was allowed to stir at room temperature under argon atmosphere for 24 h. Reaction was quenched with water (10 ml) and washed with HCl 1M (10 ml), saturated NaHCO<sub>3</sub> (10 ml) and abundant brine. Organic layer was dried on Na<sub>2</sub>SO<sub>4</sub>, filtered and the solvents were removed under reduced pressure. Crystallization in acetone gave product **2b-D** as pure diastereoisomer (reaction yield 87% of a mixture of D:L=50:50).

**ATR-FTIR** (powder): main peaks at 330, 1739, 1667, 1649, 1365, 1200, 1035, 700 cm<sup>-1</sup>.

Generic proton spectrum for **2b-D,L** with D:L ratio equal to 20:80.

**<sup>1</sup>H NMR** (400 MHz, CDCl<sub>3</sub>): δ 7,40 – 7,01 (m, 5H, ArPhe), 6,97 and 6,48 (2d, J = 9 Hz, 0,40H, NH-D) 6,90 and 6,26 (2d, J = 9 Hz, 1,60H, NH-L), 5,88 (d, J = 8,8 Hz, 0,80H, H-1β-L), 5,75 (d, J = 8,8 Hz, 0,2H, H-1β-D), 5,40 (~t, J = 9,6 Hz, 0,8H, H-3-L), 5,25 (~t, J = 9,6 Hz, 0,2H, H-3-D), 5,12 (t, J = 9,6 Hz, 1H, H-4), 4,57 (m, 1H, CHPhe-D,L), 4,34 – 4,17 (m, 2H, H-2,6-D,L), 4,11 (dd, J = 12,4, 2,0 Hz, 1H, H-6'-D,L), 3,85 (ddd, J = 10,0, 4,7, 2,1 Hz, 0,8H, H-5-L), 3,79 (ddd, J = 10,0, 4,7, 2,1 Hz, 0,2H, H-5-D), 3,07 (2xddd, J = 14,1, 6,3 Hz, 1H, CH<sub>2</sub>Phe), 2,88 (2xddd, J = 14,1, 8,1 Hz, 1H, CH<sub>2</sub>Phe), 2,13 – 1,85 (10 s, 15H, CH<sub>3</sub>).

Proton spectrum for **2b-D**

**<sup>1</sup>H NMR** (400 MHz, CDCl<sub>3</sub>): δ 7,40 – 7,01 (m, 5H, ArPhe), 6,73 (d, J = 9,2 Hz, 1H, NH), 6,23 (d, J = 7,3 Hz, 1H, NH), 5,73 (d, J = 8,8 Hz, 1H, H-1β-D), 5,25 (~t, J = 9,6 Hz, 1H, H-3), 5,12 (t, J = 9,6 Hz, 1H, H-4), 4,57 (~dt, J = 7,5, 6,3 Hz, 1H, CHPhe), 4,34 – 4,17 (m, 2H, H-2,6), 4,11 (dd, J = 12,4, 2,0 Hz, 1H, H-6'), 3,85 (ddd, J = 10,0, 4,7, 2,1 Hz, 1H, H-5), 3,07 (dd, J = 14,1, 6,3 Hz, 1H, CH<sub>2</sub>Phe), 2,88 (dd, J = 14,1, 8,1 Hz, 1H, CH<sub>2</sub>Phe), 2,07, 2,06, 2,03, 1,99 and 1,88 (5 s, 15H, CH<sub>3</sub>).

**<sup>13</sup>C NMR** (101 MHz, CDCl<sub>3</sub>) δ 171,90 (CO), 171,31 (CO), 170,78 (CO), 170,60 (CO), 169,46 (NHCO), 169,39 (NHCO), 136,47, 129,08, 128,81 and 127,19 (ArPhe), 92,04 (C-1β-D)\*, 72,92 (CH), 72,89 (CH), 68,09 (CH), 61,90 (C-6,6'), 54,78 (CH), 52,98 (CH), 37,44 (CH<sub>2</sub>Phe), 22,99, 21,00, 20,84 and 20,65 (CH<sub>3</sub>).

\* 91,96 (C-1β-L)

**ESI-MS:** +Q1: Calcd for C<sub>25</sub>H<sub>32</sub>N<sub>2</sub>O<sub>11</sub><sup>+</sup> [M+H]<sup>+</sup>: 537,2; measured m/e: 537,5, Calcd for C<sub>25</sub>H<sub>32</sub>N<sub>2</sub>O<sub>11</sub><sup>+</sup> [M+Na]<sup>+</sup>: 559,2; measured m/e: 559,2, Calcd for C<sub>25</sub>H<sub>32</sub>N<sub>2</sub>O<sub>11</sub><sup>+</sup> [M+K]<sup>+</sup>: 575,2; measured m/e: 575,2. -Q1: Calcd for C<sub>25</sub>H<sub>32</sub>N<sub>2</sub>O<sub>11</sub><sup>-</sup> [M]<sup>-</sup>: 535,2; measured m/e: 535,4, Calcd for C<sub>25</sub>H<sub>32</sub>N<sub>2</sub>O<sub>11</sub><sup>-</sup> [M+Cl]<sup>-</sup>: 571,2; measured m/e: 571,3.

## Synthesis of **2**

Tetracetylated derivative **2b** (1 mmol) was suspended in dry THF (10 ml) and cooled at -10 °C under argon atmosphere. MeONa 1M (4 mmol) was added dropwise to THF solution and the mixture was kept under stirring for 30 minutes at -10 °C and then, at room temperature for 30 minutes further. After complete consumption of **2b** the reaction was acidified to pH 5-6 by the addition of H<sub>2</sub>SO<sub>4</sub> 6N. The resulting Na<sub>2</sub>SO<sub>4</sub> was filtrated, and the reaction was dried under vacuum to remove residual solvents. The crude product was washed with dichloromethane and warm acetone. Finally, crystallization in methanol gave pure product **2-D,L**.

**ATR-FTIR** (powder): main peaks at 3288, 3075, 2920, 1620, 1545, 1380, 1285, 1106, 1030, 700 cm<sup>-1</sup>.

Proton spectra for **2-D**

**<sup>1</sup>H NMR** (400 MHz, D<sub>2</sub>O): δ 7,44 – 7,25 (m, 5H, ArPhe), 4,85 (d, J = 3,50 Hz, 0,7H, H-1-α-D), 4,69 – 4,58 (m, 1,3H: 4,66, d, J = 8,40 Hz, 0,3H, H-1-β-D and 4,64, dd, J = 8,70, 5,90 Hz, 0,3H CHPhe-β and 4,63, t, J = 7,70 Hz, 0,7H, CHPhe-α), 3,97 – 3,40 (m, 6H, H-2,3,4,5,6,6'), 3,22 – 2,90 (m, 2H: 3,18, dd, J = 14, 5,90 Hz, 0,3H, CH<sub>2</sub>Phe-β and 3,06, d, J = 7,70 Hz, 1,4H, CH<sub>2</sub>Phe-α and 2,98, dd, J = 14, 8,70 Hz, 0,3H, CH<sub>2</sub>Phe-β), 1,98 (s, 2,1H, CH<sub>3</sub>Phe-α), 1,95 (s, 0,9H, CH<sub>3</sub>Phe-β).

**<sup>13</sup>C NMR** (101 MHz, D<sub>2</sub>O) δ 173,93 (NHCO-β), 173,88 (NHCO-α), 173,76 (NHCO-β), 173,36 (NHCO-α), 136,45 and 136,21 (CAr-β/α), 129,26 and 129,19 (CHAR-β/α), 128,71 and 128,62 (CHAR-α/β), 127,19 and 127,07 (CHAR-α/β), 94,71 (C-1-β-D), 90,76 (C-1-α-D), 75,83 (C-β), 73,61 (C-β), 71,38 (C-α), 70,47 (C-α), 69,94 (C-α), 69,77 (C-β), 60,71 (C-β), 60,56 (C-α), 56,78 (C-β), 55,25 (C-α), 55,17 (C-β), 53,87 (C-α), 37,51 (C-α), 37,45 (C-β), 21,61 (CH<sub>3</sub>).

Proton spectrum for **2-D,L** mixture

**<sup>1</sup>H NMR** (400 MHz, D<sub>2</sub>O): δ 7,34 (m, 5H, ArPhe), 5,18 (d, J = 3,47 Hz, 1H-α-L), 4,85 (d, J = 3,5 Hz, 1H-α-D), 4,76 (d, J = 8.5 Hz, 1H-β-L), 4.70 – 4.58 (m, CHPhe and 1H-β-D), 3.97 – 3.61 (m, 6H, H-2,3,4,5,6,6'), 3.54 – 3.37 (2xddd, CH<sub>2</sub>Phe), 3.30 – 2.92 (2xddd, CH<sub>2</sub>Phe), 2.04 – 1.84 (m, CH<sub>3</sub>).

**<sup>13</sup>C NMR** (101 MHz, D<sub>2</sub>O): Spectra is similar to that of **2-D**.

**ESI-MS**: +Q1: Calcd for C<sub>17</sub>H<sub>24</sub>N<sub>2</sub>O<sub>7</sub><sup>+</sup> [M+Na]<sup>+</sup>: 391,1; measured m/e: 391,1. -Q1: Calcd for C<sub>17</sub>H<sub>24</sub>N<sub>2</sub>O<sub>7</sub><sup>-</sup> [M]<sup>-</sup>: 367,2; measured m/e: 367,5, Calcd for C<sub>17</sub>H<sub>24</sub>N<sub>2</sub>O<sub>7</sub><sup>-</sup> [M+Cl]<sup>-</sup>: 403,1; measured m/e: 403,2.

#### 2.4.4 Strategy 4

##### Synthesis of **3**

To a solution of **2** in dry DMF (200 mg, 0,54 mmol) EDC HCL (1,2 mmol) and DMAP (0,2 mmol) were added and the solution was let to mix at room temperature for 30 minutes. Then, 4-bromobutyric acid (1 mmol) was added and reaction was monitored using TLC (CHL:MeOH=80:20). No product formation was revealed after 48 h.

#### 2.4.5 Strategy 5

##### Synthesis of **3** and **4**

Molecule **2** (1 mmol), along with a catalytic mount of DMAP (0,024 g, 0,2 mmol), was dissolved in dry pyridine (7 ml) under argon atmosphere and cooled at -10 °C. Then, the n-bromine acyl chloride (2 eq) was added dropwise and carefully. The solution was mixed at -10 °C for 3 h and then allowed to warm up at room temperature and stirred for 2 h further. After that time, reaction was dried under vacuum and purified by flash silica gel column with a mixture of chloroform and methanol as eluent (5% MeOH till 20%). Products **3** and **4** were obtained as a yellowish powder in Br and Cl ester derivatives (15% yield monoacetylated).

**<sup>1</sup>H NMR: 3** (400 MHz, MeOD):  $\delta$  7,31 – 7,17 (m, 5H, ArPhe), 4,89 (d, J = 3,4 Hz, 0,7H, H-1 $\alpha$ ), 4,69 – 4,57 (m, 1,3H: 4,66, dd, J = 8,6, 6,1 Hz, 1H, CHPhe and 4,61, d, J = 8,3 Hz, 0,3H, H-1 $\beta$ ), 4,47 – 4,34 (2dd, J = 11,8 – 2,00 Hz, 1H, H-6' $\alpha/\beta$ ), 4,23 (~dd, J = 11,8, 5,3 Hz, 1H, H-6 $\alpha/\beta$ ), 3,97 (ddd, J = 9,9, 5,2, 2,2 Hz, 1H, H-5 $\alpha/\beta$ ), 3,82 (dd, J = 10,5, 3,4 Hz, ~1H, H-2), 3,70 (m, ~1H, H-3), 3,62 (m, 1,5H: t, J = 6,4 Hz, 1,2H, H-10,10'Cl and m, 0,3H, H- $\beta$ ), 3,51 (m, 1,1H: t, J = 6,6 Hz, 0,8H, H-10,10'Br and m, 0,3H, H- $\beta$ ), 3,36 (t, J = 9,4 Hz, 1H, H-4 $\alpha/\beta$ ), 3,21 – 3,05 (m, 1H: 3,17, dd, J = 14,0, 5,1 Hz, 0,3H, CH<sub>2</sub>Phe $\beta$  and 3,10, dd, J = 13,7, 6,1 Hz, 0,7H, CH<sub>2</sub>Phe $\alpha$ ), 2,90 (~dd, J = 13,7, 8,6 Hz, 1H, CH<sub>2</sub>Phe $\alpha/\beta$ ), 2,53 (t, J = 7,3 Hz, 2H, H-8,8'Br/Cl), 2,15 (p, J = 6,8 Hz, 0,8H, H-9,9'Br), 2,07 (p, J = 6,8 Hz, 1,2H, H-9,9'Cl), 1,90 (s, 2,1H, CH<sub>3</sub> $\alpha$ ), 1,88 (s, 0,9H, CH<sub>3</sub> $\beta$ ).

**<sup>13</sup>C NMR: 3** (101 MHz, MeOD):  $\delta$  174,33 , 173,77 and 173,14 (CO), 130,32, 129,41 and 127,79 (ArPhe $\alpha/\beta$ ), 96,92 (C-1 $\beta$ ), 92,53 (C-1 $\alpha$ ), 75,70 (C- $\beta$ ), 75,27 (C- $\beta$ ), 72,58 (C-3 $\alpha$ ), 72,34 (C-4 $\alpha/\beta$ ), 70,66 (C-5 $\alpha$ ), 64,91 (C-6,6' $\alpha/\beta$ ), 58,87 (C- $\beta$ ), 56,20 (CHPhe $\alpha/\beta$ ), 55,72 (C-2 $\alpha$ ),

44,83 (C-10,10'Br), 39,20 (CH<sub>2</sub>Phe $\alpha/\beta$ ), 33,31 (C-10,10'Cl), 32,02 (C-8,8'Br/Cl), 29,15 (C-9,9'Br), 28,99 (C-9,9'Cl), 22,42 (CH<sub>3</sub>Phe $\alpha/\beta$ ).

**<sup>1</sup>H NMR: 4** (400 MHz, MeOD):  $\delta$  7,32 – 7,16 (m, 5H, ArPhe), 4,90 (d, J = 3.2 Hz, 1H, H-1- $\alpha$ ), 4,71 – 4,55 (m, ~1H, CHPhe and H-1- $\beta$ ), 4,41 – 4,21 (2xddd, 1H, H-6' $\alpha/\beta$ ), 3,97 (ddd, J = 9,9, 5,2, 2,2 Hz, 1H, H-5 $\alpha/\beta$ ), 3,82 (dd, J = 10,5, 3,4 Hz, ~1H, H-2), 3,76 – 3,67 (m, ~1H, H-3), 3,55 (t, J = 6,6 Hz, 2H, CH<sub>2</sub>Br), 3,37 (t, J = 9,4 Hz, 1H, H-4 $\alpha/\beta$ ), 3,20 – 3,78 (m, 2H, CH<sub>2</sub>Phe), 2,35 (t, J = 7.4 Hz, 2H, CH<sub>2</sub>-8), 1,96 – 1,85 (2s, 3H, CH<sub>3</sub> $\alpha/\beta$ ), 1,78 (~q, 2H, CH<sub>2</sub>-11), 1,65 (~q, 2H, CH<sub>2</sub>-9), 1,48 (~q, 2H, CH<sub>2</sub>-10).

#### 2.4.6 Synthesis of HA-NAPA bioconjugates 5,6

To a solution of HA-TBA (300 mg, 1 mmol) in DMSO esters **3**, or **4**, were added (0,5 mmol). Solutions were kept under stirring until TLC revealed consumption of NAPA derivative. Generally, 10 days of reaction were needed. Then, H<sub>2</sub>O and brine were added to the reaction and stirred for further 3 h. The HA precipitate was collected after centrifugation and purified in dialysis against saturated NaCl solution for 2 days and water for additional 5 days. Finally, HA-NAPA bioconjugate was frozen in liquid nitrogen and lyophilized. (Esterification yield: bioconjugate **5**:= 40%. Bioconjugate **6**: 4%).

Signals reported below are only those of ester **3** or **4** found in the HA-NAPA derivatives spectra after esterification. For the proton spectra of HA-NAPA derivatives **5** and **6** see section 2.3, figure 2.27.

**<sup>1</sup>H NMR: 5** (400 MHz, D<sub>2</sub>O):  $\delta$  7,40 (s, ArPhe), 3,05 (m, CH<sub>2</sub>), 2,58 (m, CH<sub>2</sub>), 1,99 (s, CH<sub>3</sub>).

**<sup>1</sup>H NMR: 6** (400 MHz, D<sub>2</sub>O):  $\delta$  7.40 (s, ArPhe), 3,05 (m, CH<sub>2</sub>), 2,47 (m, CH<sub>2</sub>), 1,99 (s, CH<sub>3</sub>), 1,68 (m, CH<sub>2</sub>).

### 3. BIOLOGICAL ANALYSES

The effect of D,L-NAPA and HA-NAPA on the reduction of pro-inflammatory cytokines was evaluated *in vitro* in the case of induced OA. Analyses were conducted in collaboration with Prof. Anna Scotto d'Abusco of department of Biochemical Science, Sapienza University of Rome. Before any experiment, the safety of few synthesized compounds was tested by means of chondrocytes cytotoxicity assay (MTS). Chondrocytes, and not NIH3T3 mouse fibroblasts as indicated by ISO 10995-5:2009, were used for the cytotoxicity contact tests considering that those are the cells of interest for the research aim. Two sets of molecules were analyzed.

1) The cytotoxicity of D,L-NAPA (**2-D,L**) precursors, such as N-Acetyl-L-phenylalanine (N-Ac-L-Phe), N-Acetyl-D-phenylalanine (N-Ac-D-Phe), tetra-O-acetyl-2-amino-2-deoxy- $\beta$ -D-glucosamine hydrochloride (Tetra-O-Ac-Glu, **1b**) and 2-(N-Acetyl)-D,L-phenylalanyl-amido-2-deoxy-1,3,4,6-tetra-O-acetyl- $\beta$ -D-glucose (**2b-D,L**) (first molecule set) was evaluated and a possible action on the expression of inflammatory mediators was studied only for the molecules that showed no cytotoxicity. D-NAPA (**2-D**) was also studied in order to identify the anti-inflammatory efficiency of the diastereoisomer bearing D-aminoacidic residue.

2) Then, analyses were conducted in the presence of native hyaluronic acid, bioconjugate HA-NAPA (**5**) and D-NAPA (**2-D**) (second molecule set) in terms of cytotoxicity for chondrocytes and cytokines expression in *in vitro* models. The HA-NAPA derivatives with 15% and 20% of functionalization are indicated as HA-NAPA 20% and HA-NAPA 15%, respectively.

#### 3.1 Materials and methods

##### 3.1.1 Cell culture

Human primary cells were isolated from patients that underwent surgical treatment, and full ethical consent was obtained from all donors and the Research Ethics Committee of Sapienza University of Roma (#290/07, 29 Marzo 2007) and of ASL Lazio 2 (#005605/2019, 3 Marzo 2019) approved the study.

Human Primary Chondrocytes (HPCs) were isolated from femoral and tibial condyles and from femoral heads, obtained from patients who underwent a total knee and hip arthroplasty explanted in an aseptic environment by a team of orthopedists from the Polyclinic of Cassino with whom Prof. Scotto d'Abusco collaborates. HPCs were isolated, as previously described, from articular cartilages aseptically dissected from patients, selecting areas of macroscopically normal cartilage. The isolated chondrocytes were grown to 80% confluence in DMEM (HyClone, Logan, UT, USA) supplemented with L-glutamine, penicillin/streptomycin (SigmaAldrich) and 10% Fetal Bovine Serum (FBS). HPCs were used at first passage (p1) and primary chondrogenic phenotype of cells was evaluated by means of Collagen type II production.

### 3.1.2 Cell viability

To assess a potential cytotoxic effect of molecules on HPCs at different concentration and time points, MTS (3-[4,5-dimethylthiazol-2-yl]-5-[3-carboxymethoxyphenyl]-2-[4-sulfophenyl]-2H-tetrazolium) based colorimetric assay was performed (Promega Corporation, Madison, WI, USA). Briefly,  $5 \times 10^3$  cells per well, according to growth rate, were seeded in a 96-well plate. The day after seeding, cells were starved overnight in reduced serum medium, in order to align cell cycle progression. For the first set of molecules, cells were then left untreated (CTL – negative control) and N-Ac-L-Phe, N-Ac-D-Phe, Tetra-O-Ac-Glu **1b** and **2b-D,L** (D:L=36:64, 72:28 and 100:0) were administered at 10 mM, 5 mM, 1 mM and 0,5 mM for 24, 48 and 72h. For the second set of molecules, cells were then left untreated (CTL – negative control) and HA-NAPA 15% and 20% treated for 48 h and 72 h. HA-NAPA 15% and 20% were used at 4 different concentrations: 30 µg/ml, 10 µg/ml, 5 µg/ml and 1 µg/ml. After each time point, 100 µl MTS solution was added to the wells. Spectrophotometric absorbance was directly measured at 492 nm after 3 h incubation. Cells were monitored at 24 h, 48 h and 72 h under optical microscope, by Leica DM IL LED using AF6000 modular Microscope. From the optical density values measured, an average value subsequently normalized with respect to the control (untreated) was obtained, whose optical density was evaluated as 100.

### 3.1.3 Cells treatment and RNA extraction

In order to test the anti-inflammatory activity of the first molecule set, cells were left untreated (CTL) or pre-treated for 2 h with 1 mM and 0.5 mM N-Ac-L-Phe, N-Ac-D-Phe, D-NAPA (**2-D**) and D,L-NAPA (**2-D,L**). For the second set of molecules cells were left untreated (CTL) or pre-treated for 2 h with 2 mM HA-NAPA 20% (**5**), 0,5 mM D-NAPA and 2 mM HA. Both were then stimulated with TNF $\alpha$  10 ng/mL for 30 min. Total RNA was extracted using TRIZOL reagent (Invitrogen, Thermo Fisher Scientific), according to the manufacturers' instructions. The culture medium was removed from the capsules and washed in Phosphate Buffered Saline (Dulbecco A) (PBS) (Oxoid Ltd., Basingstoke, Hampshire, England). TRIZOL Reagent was added in an amount that depends on the cell growth area: the ratio to be respected is 1 ml/10 cm<sup>2</sup>. The cell lysate was transferred into 1,5 ml tubes and CHCl<sub>3</sub> is added to the solution in a ratio of 1:5 and shaken vigorously by hand. The samples were left at room temperature for 5 min, so as to allow the separation of the organic phase from the aqueous one, and then centrifugated at 12000 rpm for 15 min at 4 °C to facilitate complete separation between the two phases. The aqueous phase was recovered and added with isopropanol in a ratio of 1:1 with respect to the volume of the aqueous phase recovered, and again centrifuged at 12000 rpm for 12 min at 4 °C, in order to favor the formation of an opalescent white precipitate (the pellet of RNA).

The latter, once the supernatant has been removed, was washed in cold EtOH 75% and centrifuged at 7500 rpm for 5 min at 4 °C. Then, ethanol was eliminated and the RNA pellet was immediately suspended in sterile water, preventing it from drying out. Samples were stored at -80 °C until further use. The quality and quantity of RNA in the different samples is determined by spectrophotometric analysis (A260/A280) and by electrophoresis on 1% agarose gel.

### 3.1.4 Reverse transcription

The RNA samples obtained as described above are back-transcribed in complementary DNA (cDNA) using the reverse transcriptase enzyme Improm-II (Promega Corporation, Madison, WI, USA), in accordance with the protocol provided by the manufacturer. The samples thus obtained are stored at -20 °C until further use.

### 3.1.5 Quantitative Real-Time-PCR (q-RT-PCR)

Quantitative Real Time-PCR analysis was performed using an ABI Prism 7300 (Applied Biosystems, Thermo Fisher Scientific). Amplification was carried out using SensimixPlus SYBR Master mix (Bioline). Primers were designed using Primer Express software (Applied Biosystems) and synthesized by Biofab Research (Rome, Italy) (Table ). Relative expression levels were normalized with 18S as housekeeping gene. Data were analyzed by  $2^{-\Delta\Delta C_t}$  method<sup>48</sup> and expressed as fold change compared to CTL.

**Table 3.1:** GeneBank accession number and sequence of primers used to analyze gene expression by q-RT-PCR

Gene	Primer Sequences
<b>IL-6</b> NM_000600	Forward: 5'-GATGGATGCTTCCAATCTG-3' Reverse: 5'-CTCTAGGTATACCTCAAACCTCC-3'
<b>IL-8</b> NM_000584	Forward: 5'- AGATATTGCACGGGAGAATATACAAA -3' Reverse: 5'- GCAAACCCATTCAATTCCTGAA-3'
<b>ICAM1</b> NM_000201	Forward: 5'-ATACACAAGAACCAGACCCG -3' Reverse: 5'-GACAATCCCTCTCGTCCAGT -3'
<b>18S</b> NM_003286	Forward: 5'-CGCCGCTAGAGGTGAAATTC-3' Reverse: 5'-CATTCTTGGCAAATGCTTTCG-3'

### 3.1.6 Immunofluorescence

Collagen II protein was visualized by immunofluorescence. Cells were plated at a density of  $8 \times 10^3/\text{cm}^2$ , treated with 0.1 mM, 0.05 mM and 0.01 mM HA-NAPA 20% , cultured for 48 h and then washed in PBS, fixed in 4% paraformaldehyde in PBS for 15 min at 4 °C, and permeabilized with 0.5% Triton-X 100 in PBS for 10 min at room temperature. After blocking with 3% bovine serum albumin (BSA) in PBS for 30 min at room temperature, cells were incubated at 1 h, at room temperature, with mouse monoclonal anti-Collagen II antibody (Abcam, Cambridge, UK) 1:100. Cells were washed with PBS and then incubated for 1 h, at room temperature, with Alexa Fluor 595 donkey anti-rabbit antibody 1:400 (Invitrogen, Thermo Fisher Scientific), to stain protein in red. Slides were washed and then stained with DAPI (Invitrogen, Thermo Fisher Scientific) to visualize the nuclei. The images were captured by a Leica DM IL LED optical microscope, using an AF6000 modular microscope (Leica Microsystem, Milan, Italy).

The free software ImageJ (<https://imagej.nih.gov/ij/>) was used to perform the densitometric analysis of protein production. For each cell culture condition, the integrated density values of fluorescence were considered.

### 3.1.7 Micromasses

$3 \times 10^5$  HPCs were pelleted by centrifuging for 5 minutes, at 250 x g, in tubes of 15 ml and then cultured with 10% FBS, in presence of 50  $\mu\text{g/ml}$  of ascorbic acid. Micromasses were left untreated (CTL) or treated with 2 mM HA-NAPA 20%, 0.5 mM NAPA and 2 mM HA and were cultured for 2 weeks. Then were fixed with 4% paraformaldehyde and paraffin embedded. Sequentially sections were used for Hematoxylin-Eosin and for immunohistochemical analysis, staining them with mouse monoclonal anti-Collagen II antibody (Abcam).

## 3.2 HA-NAPA derivative: biological evaluation

### 3.2.1 Cells viability

In order to evaluate the time-course and dose-dependent effect of NAPA precursors (first set of molecules) and HA-NAPA derivatives (second set of molecules) on cellular viability, and therefore the potential cytotoxic effect of these molecules, human primary chondrocytes (HPCs) grown on DMEM with FBS 10% and cultured for 1 day prior to be treated. Cell viability was measured by performing an MTS assay, a colorimetric method based on the reduction of the tetrazolium salt by mitochondrial dehydrogenases of live cells, which generate a violet coloured precipitate. The control (CTL), consisting of cells attached on plate, is considered as a reference and a viability of 100% is attributed. Cytotoxicity results are showed in figure 3.1 for the NAPA precursor and in figure 3.2 for HA-NAPA derivatives, respectively.

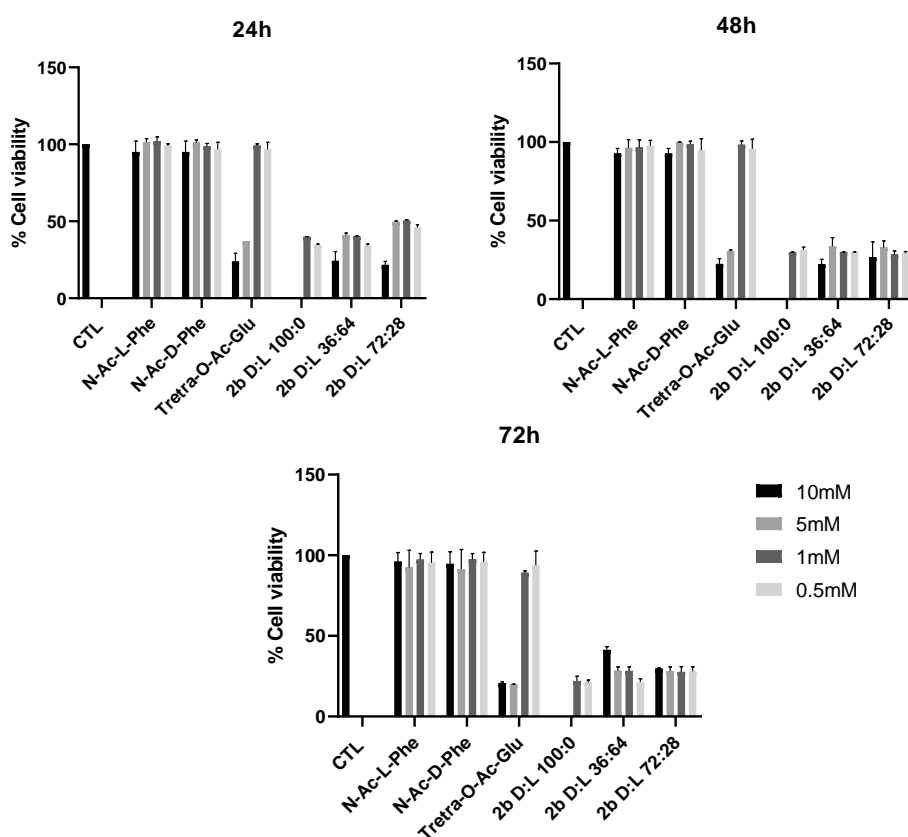


**Fig. 3.1:** Effect of N-Ac-L-Phe, N-Ac-D-Phe, Tetra-O-Ac-Glu **1b** and **2b-D,L** (D:L=36:64, 72:28 and 100:0) on cell viability. Cell viability was assessed by MTS (3-[4,5-dimethylthiazol-2-yl]-5-[3-carboxymethoxyphenyl]-2-[4-sulfophenyl]-2H-tetrazolium) based colorimetric assay. Cells were left untreated (CTL) or treated with N-Ac-L-Phe, N-Ac-D-Phe, Tetra-O-Ac-Glu **1b** and **2b-D,L** for 24 h, 48 h and 72 h. Results are reported as the ratio of the expression obtained in treated cells and in control cells. The columns and error bars represent the mean  $\pm$  D.S. of 3 independent experiments.

For the first set of molecules, cells were exposed to 10 mM, 5 mM, 1 mM and 0,5 mM of each substance for 1, 2 and 3 days. Cells treated with N-Ac-L-Phe and N-Ac-D-Phe resulted perfectly viable at all time-points analysed at different concentrations while tetra-O-acetylated glucosamine HCl **1b** showed a cytotoxic effect on cells at 10 mM and 5 mM. On the other hand, HPCs treated with 1 mM and 0,5 mM of this molecule resulted perfectly viable. Anyway, its effect on the inflammation reduction was no longer evaluated. **2b-D,L** with D:L=36:64 and 72:28 resulted cytotoxic already after 24 h of treatment and cell viability decreases over time. 10 mM and 5 mM **2b-D** (D:L=100:0) was not analysed considering low solubility of molecule into cell medium. In addition, cells at 1 mM and 0,5 mM weren't viable.

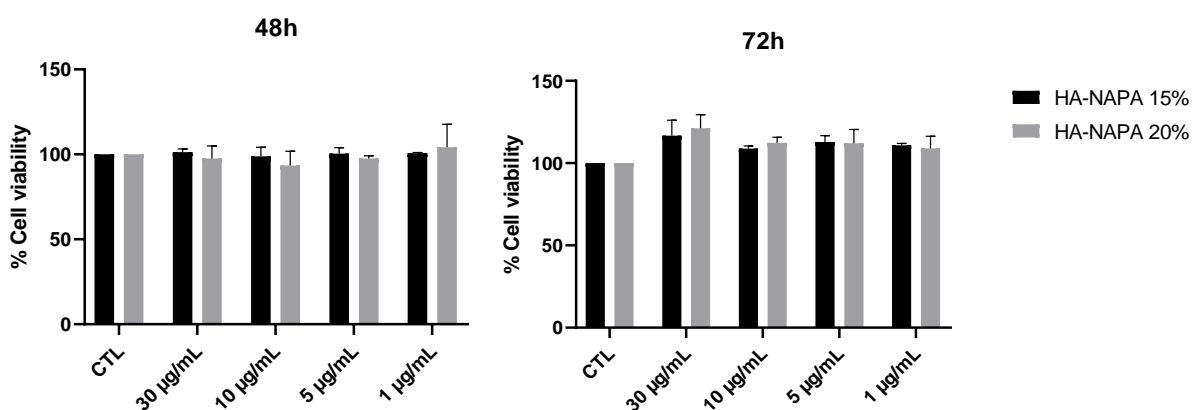


**Fig. 3.2:** Effect of HA-NAPA 15% and 20% on cell viability. Cell viability was assessed by MTS (3-[4,5-dimethylthiazol-2-yl]-5-[3-carboxymethoxyphenyl]-2-[4-sulphophenyl]-2H-tetrazolium) based colorimetric assay. Cells were left untreated (CTL) or treated with HA-NAPA 15% and 20%, for 48 h and 72 h. Results are reported as the ratio of the expression obtained in treated cells and in control cells. The columns and error bars represent the mean  $\pm$  D.S. of 3 independent experiments.

For the second set of molecules (figure 3.2), cells were exposed to 30 µg/mL, 10 µg/mL, 5 µg/mL and 1 µg/mL of HA-NAPA 15% or 20% for 2 and 3 days. The control (CTL), consisting of cells attached on plate, is considered as a reference and a viability of 100% is attributed. Cells resulted perfectly viable and did not show detrimental effects at each time-points analysed and in all tested conditions.

### 3.2.2 Effect of molecules on cytokines expression in HPCs

Following the extraction of mRNA from HPCs treated with molecules and from untreated HPCs, respectively, the gene expression of some pro-inflammatory cytokines such as Interleukin-6 (IL-6), Interleukin-8 (IL-8) and Intercellular Adhesion Molecule 1 (ICAM1) was evaluated by RT-PCR (figure 3.3 and 3.4). These inflammatory mediators are produced by chondrocytes, synovial cells and cells of other joint tissues and, in osteoarthritic patients, are also detectable in synovial fluid and plasma. The suppression of the expression of these genes indicates an anti-inflammatory effect *in vitro* of these molecules. The 18S gene was used as housekeeping.

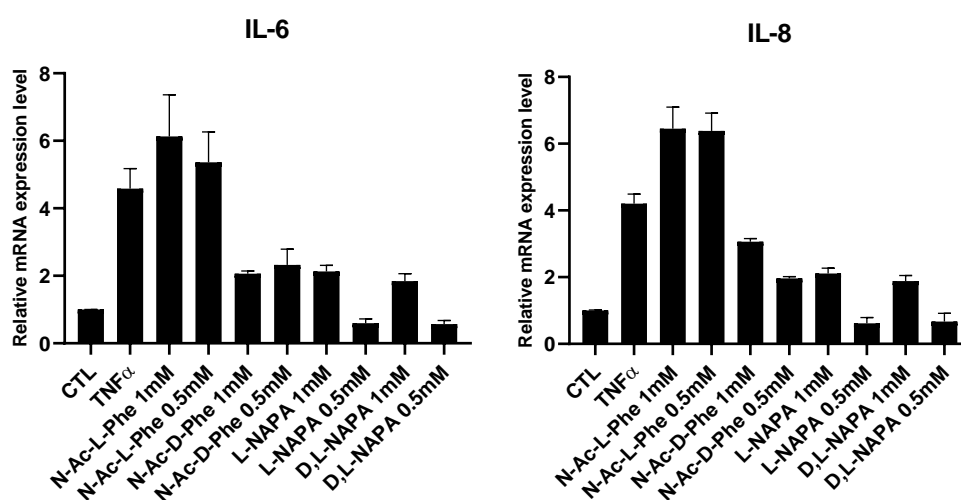


**Fig. 3.3:** Evaluation of the effect of 0,5 mM and 1 mM L-NAPA (**2-D**), D,L-NAPA (**2-D,L**), N-Ac-L-Phe and N-Ac-D-Phe on IL-6 and IL-8 expression. Human primary chondrocytes were cultured in monolayer and untreated (CTL) or exposed to 0,5 mM and 1 mM L-NAPA, D,L-NAPA, N-Ac-L-Phe, N-Ac-D-Phe for 2 h and stimulate with TNF $\alpha$  10 ng/ml for 30 min. After this time the cells were lysed and RNA was extracted for evaluation of mRNA expression levels of IL-6, IL-8 and ICAM1 by Q-RT-PCR. Results are reported as the ratio of the expression obtained in treated cells and in control cells. The columns and error bars represent the mean  $\pm$  D.S. of 3 independent experiments.

Cell cultures underwent a pre-treatment with the examined molecules for 2 h and then a stimulation with TNF $\alpha$  for 30 min, in order to simulate the inflammatory condition of osteoarthritis disease. It emerged that following the treatment of cell cultures stimulated with TNF $\alpha$  and incubated with L-NAPA and D,L-NAPA for 2 h, there is a decrease in the expression of all the inflammatory mediators examined. In particular, this anti-inflammatory effect is higher at 0,5 mM but is also appreciable at 1 mM. This results evidence that the

behaviour of pure **2-L** or mixture of D and L diastereoisomers **2-D,L** is equal within the experimental error in the *in vitro* inflammation-induced model.

N-Ac-L-Phe does not show an anti-inflammatory effect *in vitro* since it is unable to decrease the mRNA expression of pro-inflammatory cytokines. On the contrary, only the D enantiomer of N-Ac-Phe induces a decrease of the expression in mRNA level of both interleukins.

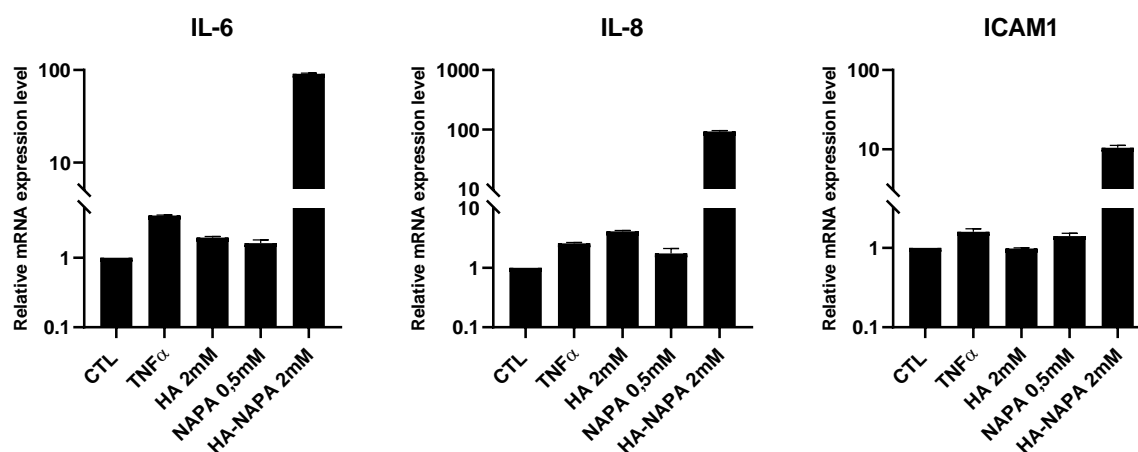


**Fig. 3.4:** Evaluation of the effect of HA 2 mM, D-NAPA (**2-D**) 0,5 mM and HA-NAPA 20% 2 mM on IL-6, IL-8 and ICAM1 expression. Human primary chondrocytes were cultured in monolayer and, untreated (CTL) or exposed to HA 2 mM, NAPA 0,5 mM and HA-NAPA 20% 2 mM for 2 h and stimulate with TNF $\alpha$  10 ng/ml for 30 min. After this time the cells were lysed and RNA was extracted for evaluation of mRNA expression levels of IL-6, IL-8 and ICAM1 by Q-RT-PCR. Results are reported as the ratio of the expression obtained in treated cells and in control cells. The columns and error bars represent the mean  $\pm$  D.S. of 3 independent experiments.

For the second set of molecules, it emerged that after the incubation of cells with 0,5 mM D-NAPA for 2 h, there is a decrease in the expression of all the inflammatory mediators examined. Similarly, the expression of the cytokine IL-6 and of ICAM1 is reduced after 2 h in the presence of 2 mM HA, following a proinflammatory stimulus with TNF $\alpha$ . Unfortunately HA-NAPA 20% does not show an anti-inflammatory effect *in vitro* as it is unable to decrease the mRNA expression of proinflammatory cytokines and ICAM1. On the contrary, a strong increase of these genes is observed in the analysed conditions.

### 3.2.3 Effect of HA-NAPA 20% on Collagen II production: an immunofluorescence analysis

The ability of HA-NAPA 20% to stimulate the synthesis of Collagen II in chondrocytes cultured in monolayer, was evaluated by the immunofluorescence analysis. Collagen II is a structural component of the articular cartilage matrix and typically decreases in osteoarthritis disease, where the tissue is destroyed with loss of function of the articular joint. It is used also as markers of chondrocytes phenotype for cells cultured in vitro. Cells, seeded in monolayer at a density of  $8 \times 10^5$  cells/well in 8 wells and kept in culture for 1 day, were then treated with 0,1 – 0,5 or 0,01 mM HA-NAPA 20% for 2 days, using cells grown in the same conditions as CTL but without any treatment. In particular, cells were analysed with indirect immunofluorescence conjugating a primary anti-Collagen II antibody and a secondary antibody to the fluorochrome. The nuclei were highlighted through the use of 4',6-diamidino-2-phenylindole (DAPI). Immunofluorescence images of cells after the treatment and intensities of the images, analysed with ImageJ, are reported in figure 3.5 in the upper and lower panel, respectively.

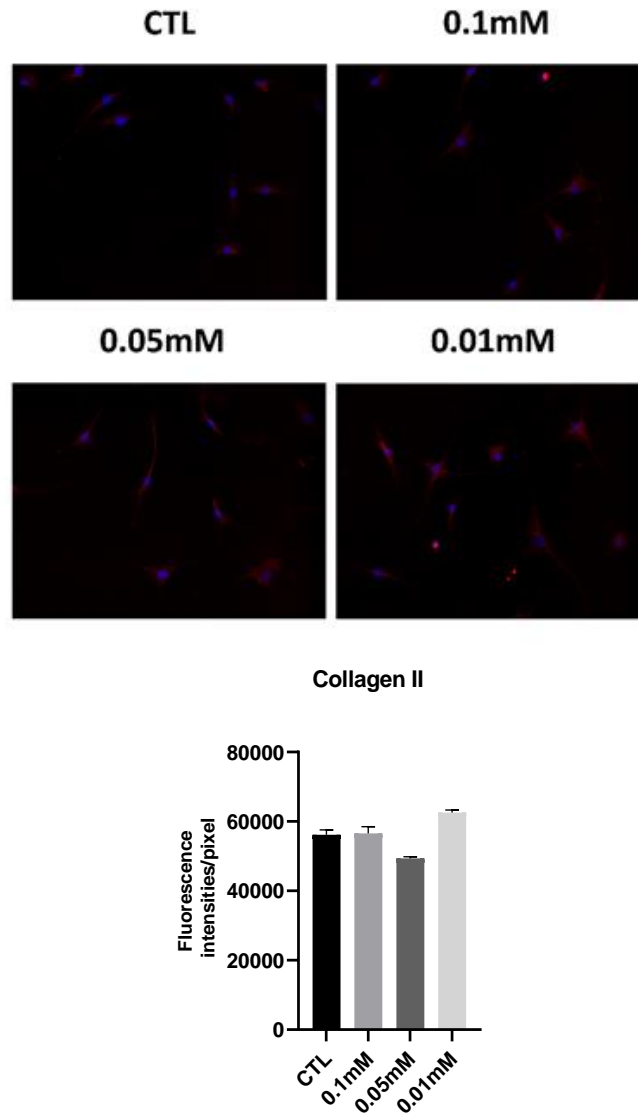


**Fig. 3.5:** Effects of HA-NAPA 20% on Collagen II protein production. Upper panel: Cells were treated with 0,1 mM, 0,05 mM and 0,01 mM of HA-NAPA 20% analysed by immunofluorescence using anti-Coll II primary antibodies and Alexa Fluor 568 (red) secondary antibody. Nuclei were stained with DAPI (original magnification 20X). Lower panel: The pixel intensities in the region of interest were obtained by ImageJ.

No evidences of Collagen II stimulation can be observed in cells, since no difference in intensity are visible in treated samples respect to the CTL. It could be supposed that the administration of bioconjugate HA-NAPA had no effect on Collagen II production at the expense or stimulated chondrocytes.

### 3.2.4 Effect of HA, NAPA and HA-NAPA 20% on Collagen II production: a 3D model

The production of collagen type II was analysed in 3D culture conditions by immunohistochemistry analysis. Cells were left untreated (CTL) or treated with 2 mM HA, or 0,5 mM D-NAPA (**2-D**) and 2 mM HA-NAPA 20% and grown in 3 dimensions. After 14 days sections were stained with Hematoxylin-Eosin (figure 3.6, **A**) as well as antibody staining (figure 3.6, **B**) and analysed by immunohistochemistry to evaluate their morphological characteristics and the production on Collagen type II.

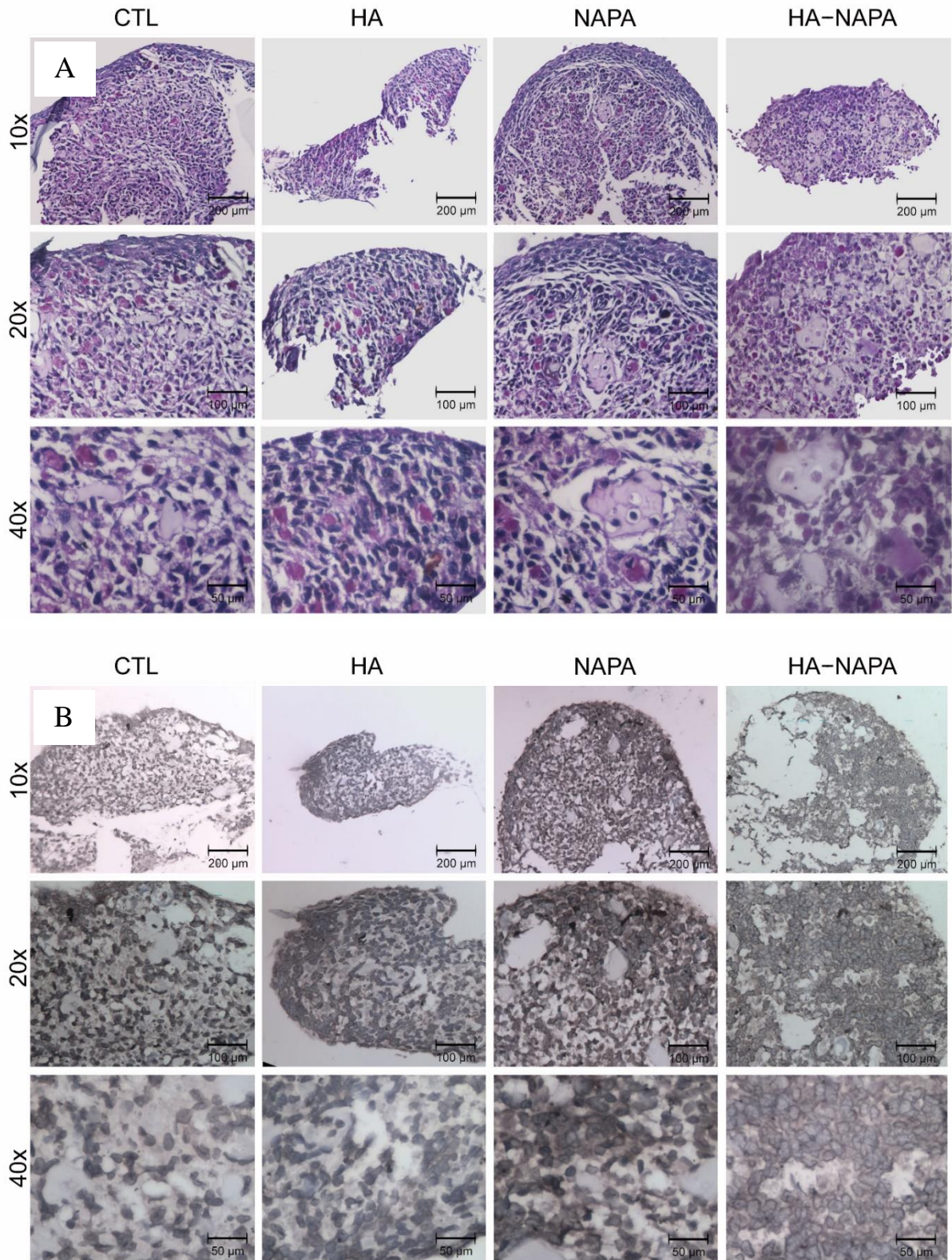


**Fig. 3.6:** Effect of HA, D-NAPA and HA-NAPA 20% on collagen type II. A, Chondrocyte micromasses untreated (CTL) or treated with 2 mM HA or with 0,5 mM D-NAPA or with 2 mM HA-NAPA 20% were stained with HE (original magnification 10, 20 and 40 X). B, Collagen type II was revealed by antibody staining (original magnification 10, 20 and 40X). The picture is a representative image of 3 independent experiments.

As shown by Hematoxylin-Eosin staining, all the micromasses are characterized by chondrocytes (dark dots) with high cellular regularity and homogeneity. Furthermore, all

treated samples have revealed strong staining. Cells treated with D-NAPA appeared disposed around extracellular deposits of self-produced matrix components (light pink zone) (fig. 3.6 – **A**, NAPA 40x). A similar response is observed in cells treated with HA-NAPA 20% albeit with less staining (fig. 3.6 - **A**, HA-NAPA 40x).

The sections analysed with anti-collagen type II antibody showed a stronger brown staining in NAPA-treated sample compared to all other samples due to the strong presence of Collagen type II. Furthermore, the section edges are well defined (fig. 3.6 - **B**, NAPA 10x) as consequence of a compact cellular structure. The brown staining is also visible in the samples treated with HA and bioconjugate HA-NAPA 20 % as results of Collagen II production.

### 3.3 Conclusion

A new method for the synthesis of NAPA, an amino acidic derivative of D-glucosamine, was described. NAPA was synthesized from tetra-O-acetylated glucosamine and N-Acetyl-L-phenylalanine, with TBTU as coupling reagent and DIPEA as tertiary base. Racemization of the L-amino acid, which resulted to occur in all the experimental conditions explored, was also deepened. In particular, the influence of tertiary base on the racemization products was presented, on the assumption that the chirality loss depends upon the azlactone formation during the activation step of the amino acid. Experimental results evidenced that the azlactone racemization is fast when an excess of base is used and NAPA enriched in the D-phenylalanine-bearing isomer is the major product. On the other hand, in the presence of stoichiometric amount of tertiary base, the epimerization of azlactone occurs and the major diastereoisomer is that with the L-amino acid residue. Nevertheless, the coupling diastereoselectivity was associated to the relative rate of D,L-azlactone and glucosamine reaction. When the uronium salt was used for the coupling of a non-epimerization prone L-phenylalanine to glucosamine, epimeric products were neglectable, as evidenced by NMR. In fact, the reaction of N-protected phenylalanine bearing a N-carbamate protecting group gave as result diastereo-pure products, independently from base excess, confirming that racemization affects preferentially N-acetylated amino acids. The conditions proposed could be used to accomplish the synthesis of stereoisomeric molecules bearing N-acetylated-D-amino acidic residues.

The biological evaluation of the D-diastereoisomer activity was conducted *in vitro* using HPCs and results evidenced that the anti-inflammatory efficiency of D-NAPA was comparable to that of L diastereoisomer activity. Thus, a procedure for the grafting of NAPA to hyaluronic acid was carried out. First attempts were made in order to esterify regioselectively the HO-C(6) position of NAPA using a n-bromine carboxylic acid but no reaction was evidenced. Then, the more reactive n-bromine acyl chlorides were used and esterification was successfully obtained.

Finally, esterification of NAPA derivative by means of nucleophilic substitution in organic solvent was accomplished. The potentiality of HA-NAPA bioconjugate was evaluated in terms of cytokines reduction in *in vitro* experiments. In particular, an inflammatory action of the

bioconjugate occurred as evidenced by biological analysis. This result could be explained supposing a decrease in the molecular weight of hyaluronic acid during treatment in organic solvent, or a non-suitability of the linker chosen. Further studies to understand and to improve activity of HA-NAPA bioconjugate are in progress.

### 3.4 References

- (1) Giordano, C., Gallina, C., Consalvi, V., & Scandurra, R. (1991). Synthesis and properties of D-glucosamine N-peptidyl derivatives as substrate analog inhibitors of papain and cathepsin B. *European journal of medicinal chemistry*, 26(8), 753-762.
- (2) Leonelli, F., La Bella, A., Francescangeli, A., Joudioux, R., Capodilupo, A. L., Quagliariello, M., ... & Renier, D. (2005). A new and simply available class of hydrosoluble bioconjugates by coupling paclitaxel to hyaluronic acid through a 4-hydroxybutanoic acid derived linker. *Helvetica chimica acta*, 88(1), 154-159.
- (3) Anderson, G. W., Zimmerman, J. E., & Callahan, F. M. (1967). Reinvestigation of the mixed carbonic anhydride method of peptide synthesis. *Journal of the American Chemical Society*, 89(19), 5012-5017.
- (4) Ke, B., Chen, W., Ni, N., Cheng, Y., Dai, C., Dinh, H., & Wang, B. (2013). A fluorescent probe for rapid aqueous fluoride detection and cell imaging. *Chemical Communications*, 49(25), 2494-2496.
- (5) Kurosawa, W., & Ubagai, R. (2020). U.S. Patent No. 10,787,476. Washington, DC: U.S. Patent and Trademark Office.
- (6) Uchiyama, T., & Hindsgaul, O. (1996). Per-o-trimethylsilyl- $\alpha$ -l-fucopyranosyl iodide: a novel glycosylating agent for terminal  $\alpha$ -l-fucosylation. *Synlett*, 1996(06), 499-501.
- (7) Bhat, A. S., & Gervay-Hague, J. (2001). Efficient syntheses of  $\beta$ -cyanosugars using glycosyl iodides derived from per-O-silylated mono- and disaccharides. *Organic letters*, 3(13), 2081-2084.
- (8) Irmak, M., Groschner, A., & Boysen, M. M. (2007). glucoBox ligand—a new carbohydrate-based bis (oxazoline) ligand. Synthesis and first application. *Chemical communications*, (2), 177-179.
- (9) Biswas, N. N., Yu, T. T., Kimyon, Ö., Nizalapur, S., Gardner, C. R., Manefield, M., ... & Kumar, N. (2017). Synthesis of antimicrobial glucosamides as bacterial quorum sensing mechanism inhibitors. *Bioorganic & medicinal chemistry*, 25(3), 1183-1194.

- (10) Dang, C. H., Nguyen, C. H., Nguyen, T. D., & Im, C. (2014). Synthesis and characterization of N-acyl-tetra-O-acyl glucosamine derivatives. *RSC Advances*, 4(12), 6239-6245.
- (11) Jones, R. A., Thillier, Y., Panda, S. S., Rosario, N. R., Hall, C. D., & Katritzky, A. R. (2014). Synthesis and characterisation of glucosamine–NSAID bioconjugates. *Organic & biomolecular chemistry*, 12(41), 8325-8335.
- (12) Krasnov, V. P., Zhdanova, E. A., Solieva, N. Z., Sadretdinova, L. S., Bukrina, I. M., Demin, A. M., ... & Kodess, M. I. (2004). Study of the effect of the nature of the side chain in esters of  $\alpha$ -amino acids on the diastereoselectivity of condensation with 5 (4H)-oxazolone in the synthesis of dipeptides with N-terminal N-acetylphenylalanine. *Russian chemical bulletin*, 53(6), 1331-1334.
- (13) CHEN, F. M., & BENOITON, N. L. (1987). <sup>1</sup>H nmr long-range coupling in 2, 4-disubstituted-5 (4H)-oxazolones and 4-alkyl-5 (2H)-oxazolones generated therefrom by the action of triethylamine. *International journal of peptide and protein research*, 30(5), 683-688.
- (14) Katritzky, A. R. (1984). *Advances in heterocyclic chemistry*. Academic Press.
- (15) Anderson, G. W., Zimmerman, J. E., & Callahan, F. M. (1967). Reinvestigation of the mixed carbonic anhydride method of peptide synthesis. *Journal of the American Chemical Society*, 89(19), 5012-5017.
- (16) Windridge, G., & Jorgensen, E. C. (1971). 1-Hydroxybenzotriazole as a racemization-suppressing reagent for the incorporation of im-benzyl-L-histidine into peptides. *Journal of the American Chemical Society*, 93(23), 6318-6319.
- (17) Valeur, E., & Bradley, M. (2009). Amide bond formation: beyond the myth of coupling reagents. *Chemical Society Reviews*, 38(2), 606-631.
- (18) de Castro, P. P., Carpanez, A. G., & Amarante, G. W. (2016). Azlactone reaction developments. *Chemistry–A European Journal*, 22(30), 10294-10318.
- (19) de Castro, P. P., Batista, G. M., Dos Santos, H. F., & Amarante, G. W. (2018). Theoretical Study on the Epimerization of Azlactone Rings: Keto–Enol Tautomerism or Base-Mediated Racemization?. *ACS omega*, 3(3), 3507-3512.

- (20) Krasnov, V. P., Zhdanova, E. A., Solieva, N. Z., Sadretdinova, L. S., Bukrina, I. M., Demin, A. M., ... & Kodess, M. I. (2004). Study of the effect of the nature of the side chain in esters of  $\alpha$ -amino acids on the diastereoselectivity of condensation with 5 (4H)-oxazolone in the synthesis of dipeptides with N-terminal N-acetylphenylalanine. *Russian chemical bulletin*, 53(6), 1331-1334.
- (21) Joullié, M. M., & Lassen, K. M. (2010). Evolution of amide bond formation. *Arkivoc*, 8(189-250), 75.
- (22) Chen, F. M., Slebioda, M., & Benoiton, N. L. (1988). Mixed carboxylic-carbonic acid anhydrides of acylamino acids and peptides as a convenient source of 2, 4-dialkyl-5 (4H)-oxazolones. *International Journal of Peptide and Protein Research*, 31(3), 339-344.
- (23) Kaskiw, M. J., Tassotto, M. L., Th'ng, J., & Jiang, Z. H. (2008). Synthesis and cytotoxic activity of diosgenyl saponin analogues. *Bioorganic & medicinal chemistry*, 16(6), 3209-3217.
- (24) Thaler, A., Seebach, D., & Cardinaux, F. (1991). Lithium-salt effects in peptide synthesis. Part I. conditions for the use of lithium-salts in coupling reactions. *Helvetica chimica acta*, 74(3), 617-627.
- (25) Jablonski, J. A., Shpritzer, R., & Powers, S. P. (2002). Racemization induced by excess base during activation with uronium salts. In *Peptides Frontiers of Peptide Science* (pp. 323-324). Springer, Dordrecht.
- (26) Xiao, N., Jiang, Z. X., & Yu, Y. B. (2007). Enantioselective synthesis of (2R, 3S)- and (2S, 3R)-4, 4, 4-trifluoro-N-Fmoc-O-tert-butyl-threonine and their racemization-free incorporation into oligopeptides via solid-phase synthesis. *Peptide Science: Original Research on Biomolecules*, 88(6), 781-796.
- (27) Ivanov, A. S., Zhalnina, A. A., & Shishkov, S. V. (2009). A convergent approach to synthesis of bortezomib: the use of TBTU suppresses racemization in the fragment condensation. *Tetrahedron*, 65(34), 7105-7108.

- (28) Chinchilla, R., Dodsworth, D. J., Nájera, C., & Soriano, J. M. (2000). Polymer-bound TBTU as a new solid-supported reagent for peptide synthesis. *Tetrahedron Letters*, 41(14), 2463-2466.
- (29) Garrett, C. E., Jiang, X., Prasad, K., & Repič, O. (2002). New observations on peptide bond formation using CDMT. *Tetrahedron letters*, 43(23), 4161-4165.
- (30) Zhdanova, E. A., Solieva, N. Z., Sadretdinova, L. S., Ezhikova, M. A., Kodess, M. I., & Krasnov, V. P. (2006). Study of the influence of the alkyl ester group in (S)-valinates on diastereoselectivity of their condensation with N-acetylphenylalanine by the mixed anhydride method. *Russian chemical bulletin*, 55(5), 925-927.
- (31) Novelli, F., De Santis, S., Punzi, P., Giordano, C., Scipioni, A., & Masci, G. (2017). Self-assembly and drug release study of linear l, d-oligopeptide-poly (ethylene glycol) conjugates. *New biotechnology*, 37, 99-107.
- (32) Dunetz, J. R., Xiang, Y., Baldwin, A., & Ringling, J. (2011). General and scalable amide bond formation with epimerization-prone substrates using T3P and pyridine. *Organic Letters*, 13(19), 5048-5051.
- (33) Garcia, A. L. L. (2007). T3P: A convenient and useful reagent in organic synthesis. *Synlett*, 2007(08), 1328-1329.
- (34) Waghmare, A. A., Hindupur, R. M., & Pati, H. N. (2014). Propylphosphonic anhydride (T3P®): An expedient reagent for organic synthesis. *Review Journal of Chemistry*, 4(2), 53-131.
- (35) Martín, S. M. P., Medina, R. F., Castro, C. A. I., Monroy, Z. J. R., & Castañeda, J. E. G. (2018). Novel synthesis of N-glycosyl amino acids using T3P®: Propylphosphonic acid cyclic anhydride as coupling reagent. *International Journal of Peptide Research and Therapeutics*, 24(2), 291-298.
- (36) AlFindee, M. N., Zhang, Q., Subedi, Y. P., Shrestha, J. P., Kawasaki, Y., Grilley, M., ... & Chang, C. W. T. (2018). One-step synthesis of carbohydrate esters as antibacterial and antifungal agents. *Bioorganic & medicinal chemistry*, 26(3), 765-774.

- (37) Tsepaeva, O. V., Nemtarev, A. V., Abdullin, T. I., Grigor'eva, L. R., Kuznetsova, E. V., Akhmadishina, R. A., ... & Mironov, V. F. (2017). Design, synthesis, and cancer cell growth inhibitory activity of triphenylphosphonium derivatives of the triterpenoid betulin. *Journal of natural products*, 80(8), 2232-2239.
- (38) Mincione, F., Benedini, F., Biondi, S., Cecchi, A., Temperini, C., Formicola, G., ... & Supuran, C. T. (2011). Synthesis and crystallographic analysis of new sulfonamides incorporating NO-donating moieties with potent antiglaucoma action. *Bioorganic & medicinal chemistry letters*, 21(11), 3216-3221.
- (39) Calce, E., Monfregola, L., & De Luca, S. (2013). Synthetic Strategy to Prepare DOTA-Based Bifunctional Chelating Agent Ready to Bind Biomolecular Probes. *International Journal of Peptide Research and Therapeutics*, 19(3), 199-202.
- (40) Yang, L., Dong, Y., Hu, X., & Liu, A. (2012). Synthesis and liquid crystallinity of dendronized carbohydrate liquid crystal. *Carbohydrate research*, 347(1), 40-46.
- (41) Chen, A., Samankumara, L. P., Garcia, C., Bashaw, K., & Wang, G. (2019). Synthesis and characterization of 3-O-esters of N-acetyl-d-glucosamine derivatives as organogelators. *New Journal of Chemistry*, 43(21), 7950-7961.
- (42) Lawandi, J., Rocheleau, S., & Moitessier, N. (2016). Regioselective acylation, alkylation, silylation and glycosylation of monosaccharides. *Tetrahedron*, 41(72), 6283-6319.
- (43) Oh, E. J., Park, K., Choi, J. S., Joo, C. K., & Hahn, S. K. (2009). Synthesis, characterization, and preliminary assessment of anti-Flt1 peptide–hyaluronate conjugate for the treatment of corneal neovascularization. *Biomaterials*, 30(30), 6026-6034.
- (44) Schmittgen, T. D., & Livak, K. J. (2008). Analyzing real-time PCR data by the comparative C T method. *Nature protocols*, 3(6), 1101.

## 4. SULFONATION OF HYALURONIC ACID: AMIDATION WITH TAURINE

Sulfonation of hyaluronic acid was performed through taurine amidation in water in order to synthesize sulfonated-HA derivatives (HA-Tau, figure 4.1). Reactions were carried out using water soluble coupling reagents (WSC) such as N-(3-Dimethylaminopropyl)-N'-ethylcarbodiimide hydrochloride (EDC HCL) and 4-(4,6-Dimethoxy-1,3,5-triazin-2-yl)-4-methylmorpholinium chloride (DMTMM). Firstly, EDC HCl coupling was studied but improvement of amidation degree was achieved with DMTMM. Physico-chemical characterization of HA-Tau was performed in terms of taurine amidation degree, using NMR and FTIR spectroscopy, and thermal behavior.

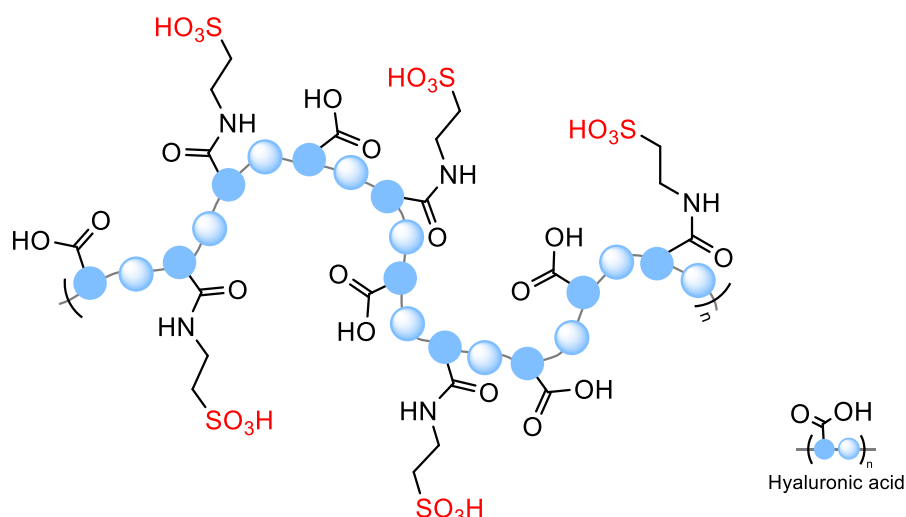


**Fig. 4.1:** Schematic illustration of hyaluronic acid-taurine derivative structure (HA-Tau). Functionalization has been achieved by means of amide bond formation on the glucuronic unit of sodium hyaluronate.

### 4.1 Materials and methods

Hyaluronic acid was bought from Flower Tales Cosmetics (Milan, Italy) with an average MW of 1200 – 1500 kDa. Taurine (Tau), N-(3-Dimethylaminopropyl)-N'-ethylcarbodiimide hydrochloride (EDC HCL), N-hydroxysuccinimide (NHS), 4-(4,6-Dimethoxy-1,3,5-triazin-2-yl)-4-methylmorpholinium chloride (DMTMM), 2-(N-morpholino)-ethanesulfonic acid (MES), phosphate-buffered saline (PBS) and dialysis membrane (cut-off 14 kDa) were purchased by Sigma Aldrich (Milan, Italy). All materials were used without any further purification.

#### 4.1.1 General procedure for amidation of HA: coupling with EDC HCl and DMTMM

Generally, a 1% (wt/v) water solution of sodium hyaluronate with desired pH was prepared and, after complete dissolution of the biopolymer, the coupling reagent and taurine were added consecutively. The activation step lasted 30 minutes while amidation with Tau was let to proceed at room temperature for a period from one to five days. General pathway for the synthesis of hyaluronic acid-taurine derivative is shown in figure 4.2. Purification of HA bioconjugates was obtained with extensive dialysis against saturated NaCl solution and distilled water (membranes cut-off of 14 kDa, 5 d dialysis). Finally, samples were freeze-dried to obtain taurinated hyaluronic acid (HA-Tau).

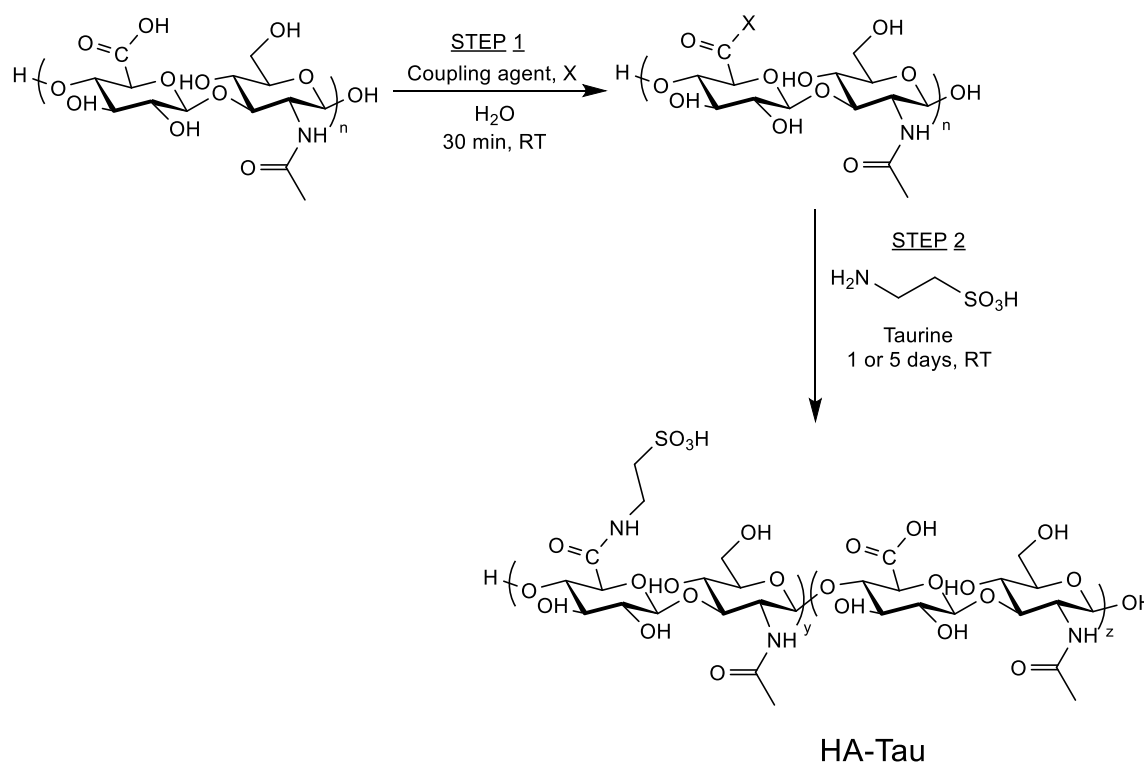


**Fig. 4.2:** General procedure for the coupling of hyaluronic acid with taurine using water soluble coupling reagent. STEP 1: activation of COOH with coupling agent to form an activated ester intermediate. STEP 2: reaction with taurine from 1 to 5 days to form the desired amidic derivative HA-Tau.

Four different water media were investigated with a pH ranging from 4 to 7,4. Acidic conditions are favorable when EDC hydrochloride is used <sup>1</sup> and, thus, we decide to compare coupling efficiency at pH 4, with MES buffer, and 5,5, by pH adjustment with HCl 0,1 M. In the latter case, a pH correction was necessary after EDC addition, due to its basic nature, and in some cases after Tau addition, depending on the amine molar ratio required for the reaction.

Taurine grafting was also studied in distilled water without pH control, with an initial pH of 6,5, and in PBS (isotonic solution, 0.01 M, pH 7,4).

The list of HA-Tau derivatives synthesized by means of EDC/NHS coupling is summarized in table 4.1. Samples are grouped in terms of pH, molar ratio of reactants and reaction time ( $t_R$ ). Molar ratios are referred to 1 mmol of hyaluronic acid repeating unit (R.U.). EDC hydrochloride is always abbreviated as EDC. EDC and NHS are always used equimolar, except for sample HA-Tau 8 where NHS is double respect to the carbodiimide.

**Table 4.1:** Acronyms for of HA-Tau derivatives synthesized using EDC/NHS. Samples are sorted from lower to higher pH and with increasing reagents quantity. Derivatives obtained with the 5 days reaction are differentiated from the correspondents one day reaction by the letter a.  $t_R$  = reaction time.

pH	Sample	EDC:Tau	$t_R$ (days)
4 MES buffer	HA-Tau 1	1:6	1
	HA-Tau 2	3:6	1
	HA-Tau 3	6:6	1
5,5 Acidified water with HCl 0,1 M	HA-Tau 4	1:1	1
	HA-Tau 4a	1:1	5
	HA-Tau 5	1:3	1
	HA-Tau 6	1:6	1
	HA-Tau 6a	1:6	5
	HA-Tau 7	3:6	1
	HA-Tau 8*	3:6	1
	HA-Tau 9	1:12	1
	HA-Tau 10	3:12	1
	HA-Tau 10a	3:12	5
6,5 Distilled water	HA-Tau 11	3:6	1
	HA-Tau 11a	3:6	5g
7,4 PBS buffer	HA-Tau 12	1:6	1
	HA-Tau 13	3:6	1

\* EDC:NHS:Tau=3:6:6

Coupling with DMTMM was performed reproducing few conditions used in EDC reactions in order to compare the efficiency of coupling reagents, following the same synthetic steps. HA-Tau derivatives were synthesized in acidified water (pH = 5,5) and in distilled water without pH adjustment. Samples are summarized in table 4.2 (molar ratios of reactants are referred to 1 mmol of hyaluronic acid repeating unit).

**Table 4.2:** Acronyms for of HA-Tau derivatives synthesized using DMTMM. Samples are sorted from lower to higher pH and with increasing reagents quantity. Samples are compare to the correspondents obtained with EDC/NHS.

pH	Sample	DMTMM:Tau	t <sub>R</sub> (days)	EDC reference
5,5 Acidified water with HCl 0,1 M	HA-Tau 14a	1:1	5	HA-Tau 4a
	HA-Tau 15a	1:6	5	HA-Tau 6a
	HA-Tau 16a	3:12	5	HA-Tau 10a
6,5 Distilled water	HA-Tau 17a	3:6	5	HA-Tau 11a

#### 4.1.2 <sup>1</sup>H-NMR Measurements

Water soluble HA-Tau samples were dissolved in D<sub>2</sub>O at room temperature (6 mg in 0,6 ml of D<sub>2</sub>O). <sup>1</sup>H NMR analyses were performed on a 400 MHz Bruker Avance III spectrometer and spectra were processed using MestReNova 6.0.2 (Mestrelab Research SL). Third order polynomial fit was used to correct base line.

#### 4.1.3 Infrared spectroscopy (FTIR)

Fourier-transform infrared spectroscopy (FTIR) was used to characterized HA-Tau derivatives. Spectra, before and after chemical modification/acidification in HCl 0,1 M, were acquired in attenuated total reflection (ATR) using a Nicolet 6700 (Thermo Fisher Scientific, Waltham, MA, USA) equipped with a Golden Gate single reflection diamond ATR accessory. All spectra were recorded in absorption mode with 200 scans/spectrum and at 4 cm<sup>-1</sup> resolution in the region between 4000 – 650 cm<sup>-1</sup>. The software Omnic 8.0 (Thermo Fisher Scientific Inc.) was used for the elaboration of spectra.

#### 4.1.4 Thermo gravimetric measurements (TGA)

Thermal response of sulfonated hyaluronic acid was examined using thermo-gravimetric analysis (TGA) with a Mettler TG 50 thermobalance (Mettler Toledo, Columbus, OH, USA). Briefly, 5-7 mg of the sample were placed in a ceramic pan and heated from 30 to 500 °C with a heating rate of 10 °C/min, under N<sub>2</sub> flow. Before the scan, specimens were vacuum dried at 80 °C for 24 hours in order to remove excess of water. The weight loss was recorded as function of temperature for each sample. Degradation temperature (T<sub>d</sub>) were measured from the derivative of weight loss curves as function of temperature.

#### 4.1.5 Cell viability investigations

Safety of HA-Tau derivatives was evaluated using MTS assay. For cell culture, cell viability and MTS assay see chapter 3 (sections 3.1.1 and 3.1.2). Briefly, in the case of HA-Tau derivatives, seeded cells were treated with pristine HA and with HA-Tau17a<sub>100%</sub>, HA-Tau11a<sub>51%</sub> and HA-Tau10<sub>31%</sub> at 3 µg/µl, 1 µg/µl, 0,3 µg/µl and 0,15 µg/µl. Then, the MTS assay was performed after 48 h. Cells were then left untreated (CTL) as control.

## 4.2 Results

### 4.2.1 Coupling with EDC: mechanism and NMR analysis

Reaction with water soluble carbodiimide EDC HCl/NHS is considered the standard method to link amine to carboxylic function of HA and it represents a very well established wide-ranging bioconjugation method.<sup>2</sup> Amidation of carboxylic group of HA starts with its activation by EDC, that lead to the formation of an O-acylisourea as intermediate. This first step requires acidic pH to occurs because EDC reacts with COOH, acting as base, and, hence, the carboxylic moiety should be protonated. Then, the reactive O-intermediate undergoes nucleophilic attack by the amine R-NH<sub>2</sub> leading to the formation of target amide. However, the O-acylisourea intermediate is highly reactive and also reacts with water quickly rearranging into a stable N-acylurea by-product, thus preventing any further reaction with the amine. The reaction is strongly pH-dependent and needs acidic pH for the activation step, while the attack of amine is favored in alkaline condition, where the NH<sub>2</sub> group is deprotonated and it can exploit nucleophilic properties. The compromise is therefore not easy to define and amines with high pK<sub>a</sub> values are not easily conjugated to HA using this method.<sup>3</sup> Rearrangement into N-acylurea by-product can be reduced adding N-hydroxysuccinimide (NHS) to EDC allowing for a more efficient amidation of carboxylic compounds. NHS reacts with O-acylisourea intermediate forming a hydrolysis-resistant and non-rearrangeable active ester that couples easier with amines (figure 4.3).<sup>4</sup>

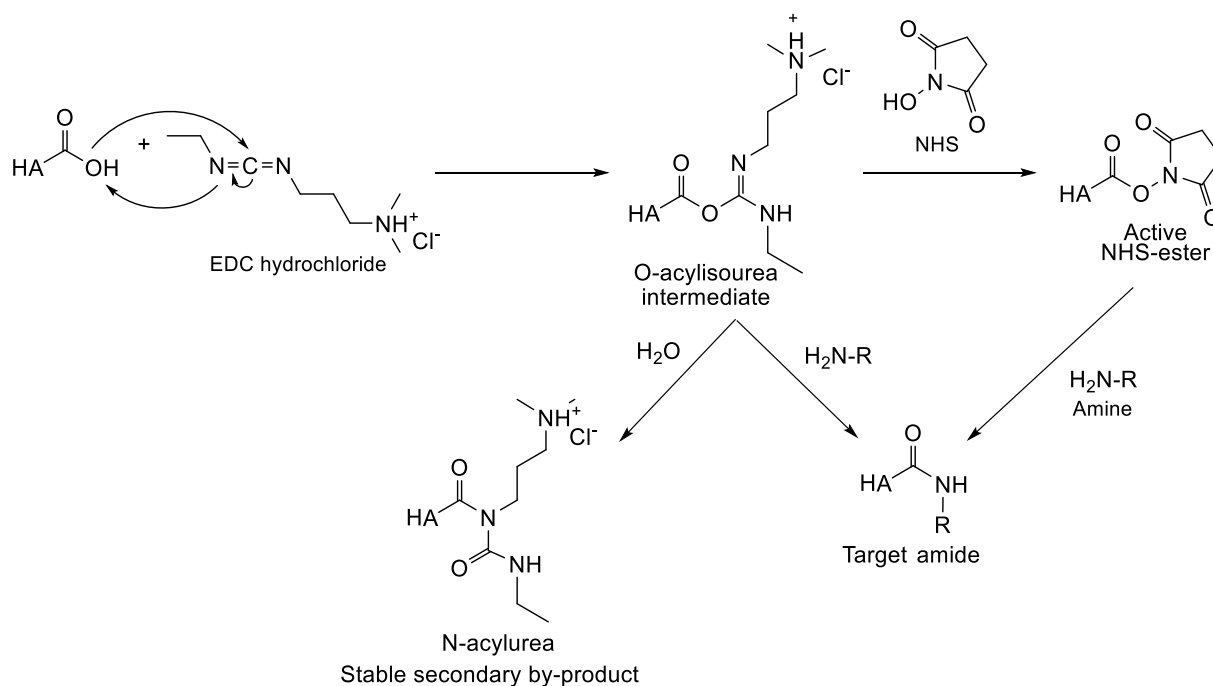


**Fig. 4.3:** General mechanism for the amidation of hyaluronic acid with EDC/NHS in water. The use of EDC as coupling agent can lead to the formation of the desired amide or to a N-acylurea as stable by-product.

Taurinated samples were deeply studied using NMR spectroscopy. In particular, functionalization of HA was controlled by comparing the D<sub>2</sub>O proton spectrum of native polymer with those of HA-Tau bioconjugates. <sup>1</sup>H NMR spectra in D<sub>2</sub>O of unmodified HA, taurine and sulfonated HA-Tau 6 are shown in figure 4.4.

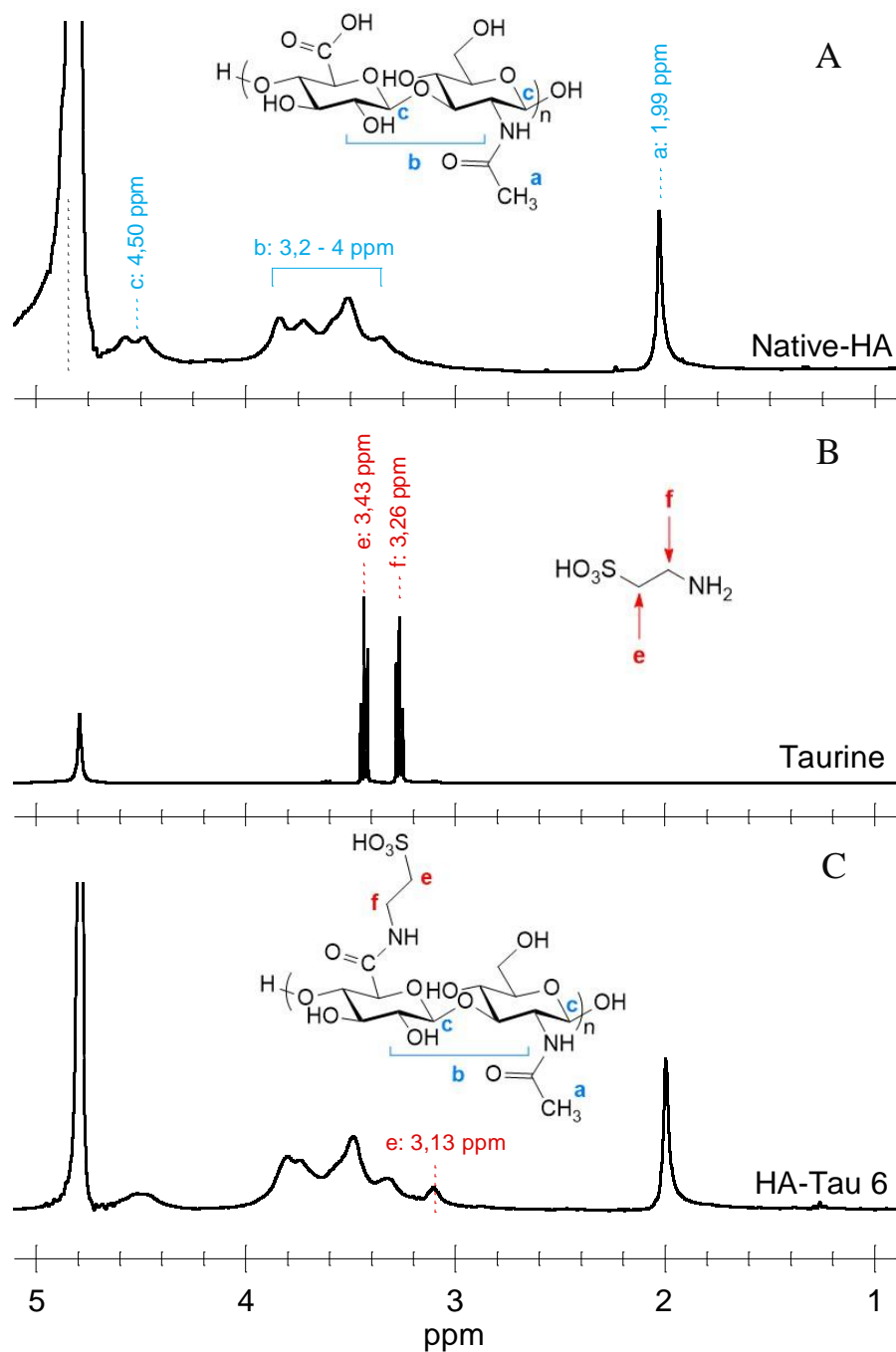


**Fig. 4.4:**  $^1\text{H}$  NMR spectra in  $\text{D}_2\text{O}$  of: native HA (A), taurine (B) and HA-Tau 6 derivative (C) and relative structures. Grafting of taurine is evidenced by the appearance of a peak at 3,31 ppm in spectrum C which is related to the methylene adjacent to the sulfonic group of tau.

The interpretation of HA proton spectrum (figure 4.4 A) is easy being it composed by three peculiar sets of peaks. The intense singlet at 1,99 ppm is associated to the methyl group in the N-acetylic function of glucosamine unit, while the broad signal between 3,2 - 4 ppm is related to the skeleton protons of disaccharide unit. Lastly, the two anomeric protons doublets are located respectively at 4,47 and 4,55 ppm. In taurine spectrum (figure 4.4 B), the two triplets at 3,26 and 3,43 ppm are related to the methylene groups adjacent to the aminic and sulfonic

functions, respectively. The signal of methylene linked to  $-\text{SO}_3\text{H}$  shifts to 3,1 ppm as results of taurine conjugation to hyaluronic acid, as can be seen from the comparison of HA and HA-Tau2 spectra (figure 4.4 C).<sup>5,6</sup> Signal of the  $\text{CH}_2$  adjacent to  $\text{NH}_2$  in the HA-Tau conjugate cannot be detected since it is hidden by saccharide protons (peak at 3,4 ppm).

Percentage degree of substitution (DS %) was calculated comparing the area of  $\text{OCH}_3$  peak at 1,99 ppm (3 protons) with that associated to the methylene group of taurine at 3,1 ppm in the HA-Tau derivative ( $\text{A}(\text{CH}_2)$ , 2 protons for complete amidation), using equation:

$$DS = \frac{3}{2} * \frac{A(\text{CH}_2)}{A(\text{CH}_3)} * 100$$

Equation 4.1

Calculated DS % for all HA-Tau samples obtained by EDC coupling are summarized in table 4.3. Samples are sorted with respect to the reaction pH.

**Table 4.3:** List of characteristics and functionalization values calculated from <sup>1</sup>H NMR spectra of HA-Tau derivatives obtained using EDC/NHS. t<sub>R</sub> = reaction time, DS % = degree of substitution.

pH	Sample, EDC:Tau, t <sub>R</sub>	DS (%)
<b>4</b> MES buffer	HA-Tau 1, 1:6, 1d	33
	HA-Tau 2, 3:6, 1d	37,5
	HA-Tau 3, 6:6, 1d	66
<b>5,5</b> Acidified water with HCl 0,1 M	HA-Tau 4, 1:1, 1d	-
	HA-Tau 4a, 1:1, 5d	< 2
	HA-Tau 5, 1:3, 1d	-
	HA-Tau 6, 1:6, 1d	33
	HA-Tau 6a, 1:6, 5d	51
	HA-Tau 7, 3:6, 1d	30
	HA-Tau 8, 3:6*, 1d	33
	HA-Tau 9, 1:12, 1d	18
	HA-Tau 10, 3:12, 1d	31,5
	HA-Tau 10a, 3:12, 5d	30
<b>6,5</b> Distilled water	HA-Tau 11, 3:6, 1d	30
	HA-Tau 11a, 3:6, 5d	51
<b>7,4</b> PBS buffer	HA-Tau 12, 1:6, 1d	-
	HA-Tau 13, 3:6, 1d	-

\* EDC:NHS:Tau=3:6:6

First attempts to sulfonate hyaluronic acid were conducted with equimolar reactants at pH 5,5 on the assumption that EDC coupling is more efficient in an acidic environment. NMR analysis of samples HA-Tau 4 and HA-Tau 4a revealed no amidation in one-day reaction and very low functionalization, almost undetectable from proton spectrum, for the five-days reaction (spectra not shown).

DS % improvement was achieved increasing the amount of taurine <sup>7</sup> and maintaining EDC and NHS equimolar to hyaluronic acid R.U. (EDC:Tau = 1:6), both for MES buffer and acidified water. In particular, samples HA-Tau 1 and HA-Tau 6 showed a DS % slightly higher than 30% after 24 hours. On the other hand, when the same reaction was carried out in PBS (HA-Tau 12), no taurine peaks were detected in the proton spectrum (figure 4.5).

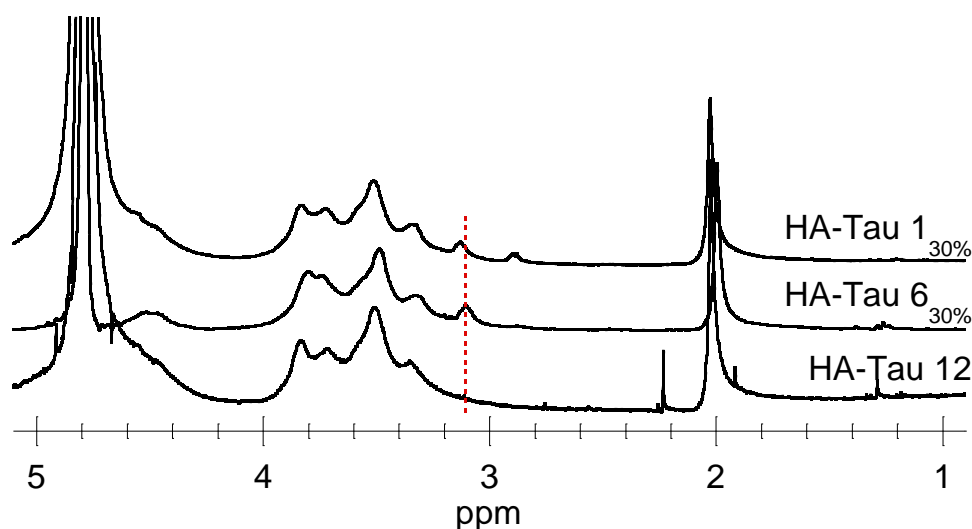


Fig. 4.5:  $^1\text{H}$  NMR spectra of sample HA-Tau 1, HA-Tau 6 and HA-Tau 12.

Almost the same functionalization was obtained when EDC was triplicate (EDC:Tau = 3:6) in MES, acidified and distilled water for the one-day coupling (HA-Tau 2, HA-Tau 7 and HA-Tau 11). The 2-(N-morpholino) ethanesulfonic acid buffer led to the highest DS % (37%). Again, amidation efficiency resulted to be low when conducted in PBS, as well as for HA-Tau 13, confirming the importance of an acidic medium for the amidation yield when a water-soluble carbodiimide is employed. Spectra are shown below in figure 4.6.

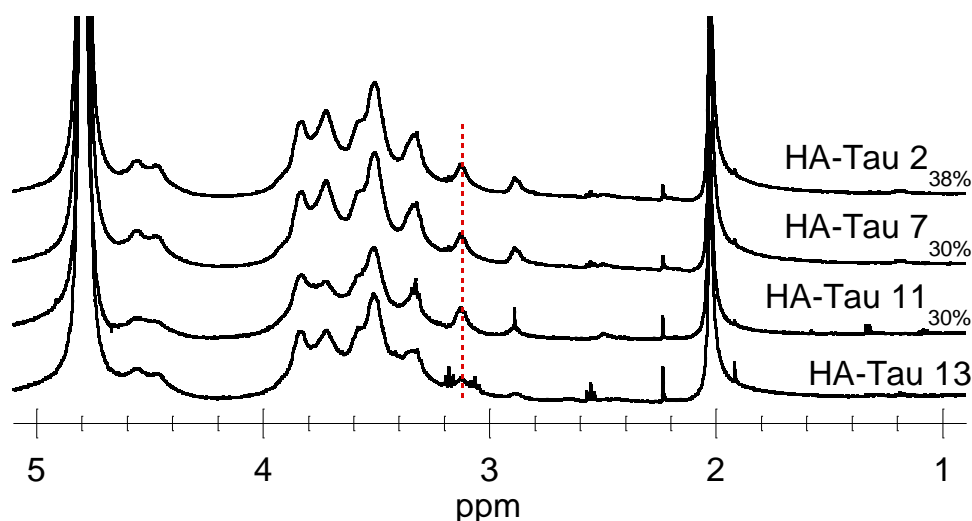


Fig. 4.6:  $^1\text{H}$  NMR spectra of sample HA-Tau 2, HA-Tau 7, HA-Tau 11 and HA-Tau 13.

Since the addition of NHS should favor the formation of an active ester, thus promoting the aminolysis reaction, NHS amount was increased. Nevertheless, no effect on functionalization degree was evidenced in acidic medium and a similar DS for HA-Tau 8 and HA-Tau 7 was observed (DS = 30%, spectra not shown).

The increase of EDC for sample HA-Tau 3 (EDC:Tau=6:6) in MES buffer caused a significant increase in amidation degree, that changes from 30% for HA-Tau 2 (EDC:Tau=3:6) to 66% (figure 4.7). However, purity of samples worsen, probably due to the formation of by-products covalently bonded to hyaluronic acid backbone (see figure 4.3 for EDC coupling mechanism.).

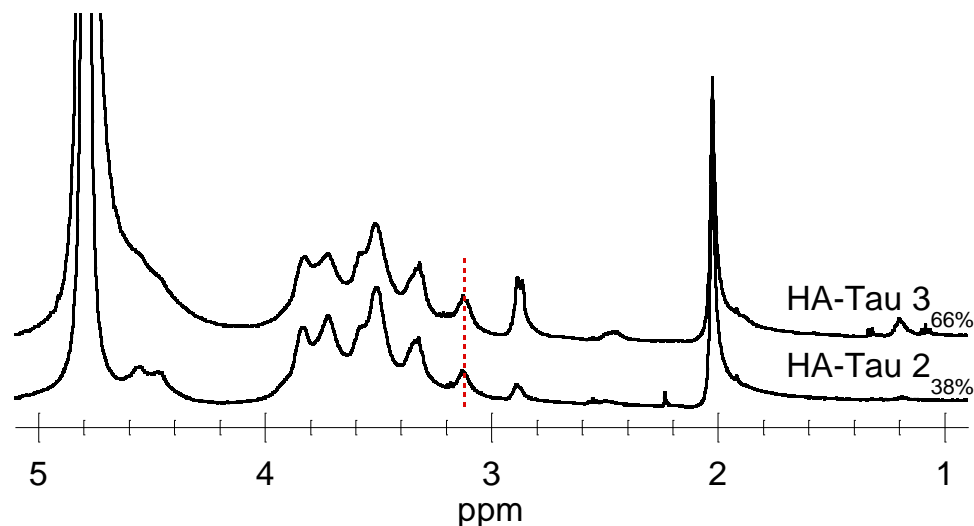
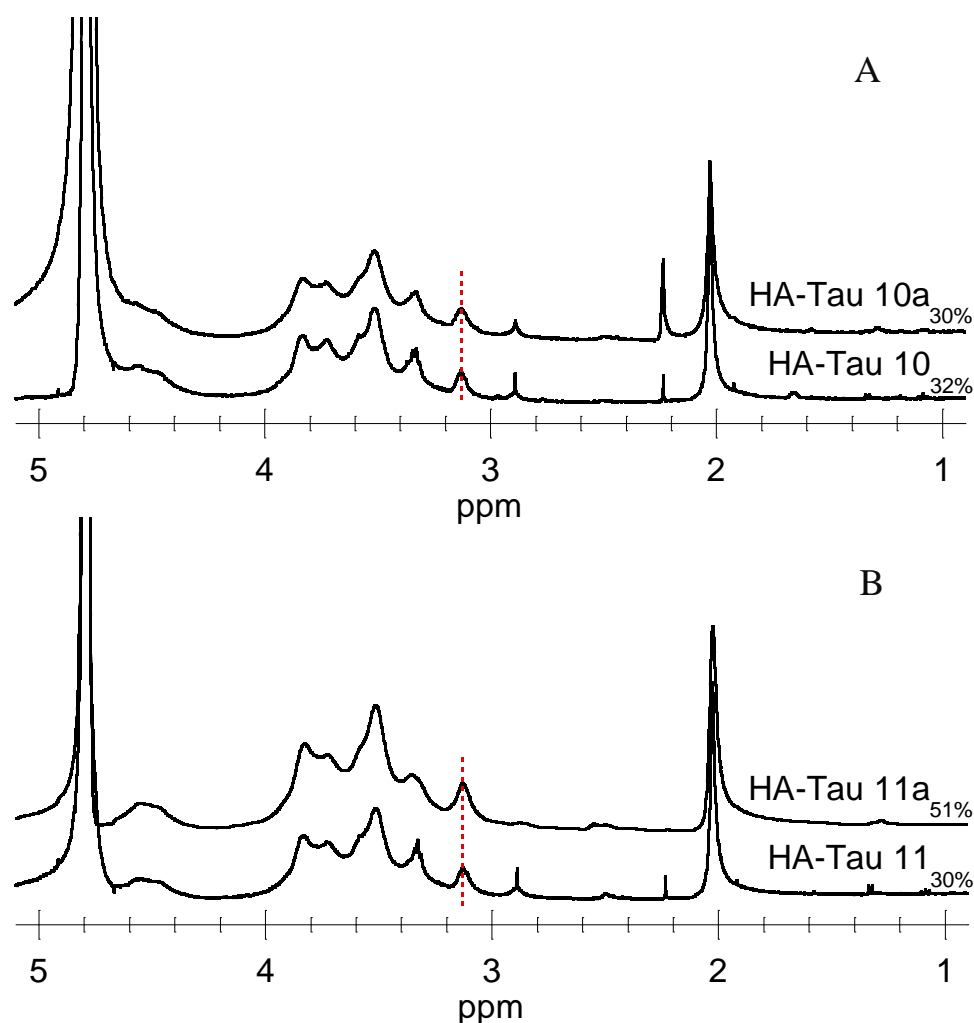


Fig. 4.7:  $^1\text{H}$  NMR spectra of sample HA-Tau 3 and HA-Tau 2.

Similarly to HA-Tau 1 and HA-Tau 2 in MES, no relevant modification in functionalization was detected in acidified water when molar ratio of EDC:Tau was moved from 1:6 to 3:6 as observed for HA-Tau 6 and HA-Tau 7 samples. However, at the same pH, the strong excess of taurine caused a lowering in substitution degree (EDC:Tau moves from 1:6 to 1:12 for HA-Tau 6 and HA-Tau 9, respectively), while a DS of 30 % remains unaltered when EDC:Tau ratio is 3:6 or 3:12 for HA-Tau 7 and HA-Tau 10. Same condition of sample HA-Tau 7 were adopted for amidation in distilled water (HA-Tau 8) but no change in DS % can be observed since functionalization remains at 30% (spectra not shown).

Lastly, we studied the effect of reaction time ( $t_R$ ) on the degree of substitution for samples prepared in acidified and distilled water. In particular, HA-Tau 10 (EDC:Tau=3:12) in acidified water and HA-Tau 11 (EDC:Tau=3:6) in distilled water were compared to the corresponding five-days reactions (figure 4.8 A for samples 10 and 10a; B for samples 11 and 11a). For the first couple HA-Tau 10 - HA-Tau 10a DS % is almost unaltered, meanwhile a prominent increase in functionalization was observed for HA-Tau 11 - 11a, obtained in slightly acidic conditions (yields varies from 30 to 51%).



**Fig. 4.8:** <sup>1</sup>H NMR spectra of sample HA-Tau 1o and HA-Tau 10a (A); sample HA-Tau 11 and HA-Tau 11a (B).

In conclusion, the highest substitution degree was achieved in MES buffer for sample HA-Tau 3 although reaction required a great amount of coupling agent. HA-Tau 11a led to a similar taurine functionalization with low reactants and longer reaction time. For samples prepared in acidified water, changes in molar ratio of coupling agent and amine as well as the increase of reaction time didn't affect amidation degree that settled at around 30%.

#### 4.2.2 Coupling with DMTMM: mechanism and NMR analysis

In order to improve hyaluronic acid amidation with taurine, we chose to test DMTMM as coupling agent, which is used in the field of peptide synthesis. It is particularly suitable for the amidation of hydrophilic substrates due to its water solubility. DMTMM resulted to be water resistant, differently to EDC, not showing degradation in water at room temperature, with 100% recovery after 3 h.<sup>8</sup> Activation of HA starts with an aromatic substitution on DMTMM to form an active s-triazine intermediate ester that is reactive toward nucleophilic

attack of an amine, or nucleophiles in general (figure 4.9). N-methylmorpholinium (NMM) and 4,6,-dimethoxy-1,3,5-triazin-2-ol are released in the first and in the second step respectively. Furthermore, Matteo D’Este and coworkers <sup>2</sup> evidenced that if DMTMM and hyaluronic acid are reacted in a “blank reaction”, i.e. in absence of the amine, no stable by-products are formed and the s-triazine intermediate ester does not leave residues. The coupling reactive has been used for the synthesis of both hyaluronic acid ester <sup>9</sup> and amide <sup>10</sup> derivatives in water.

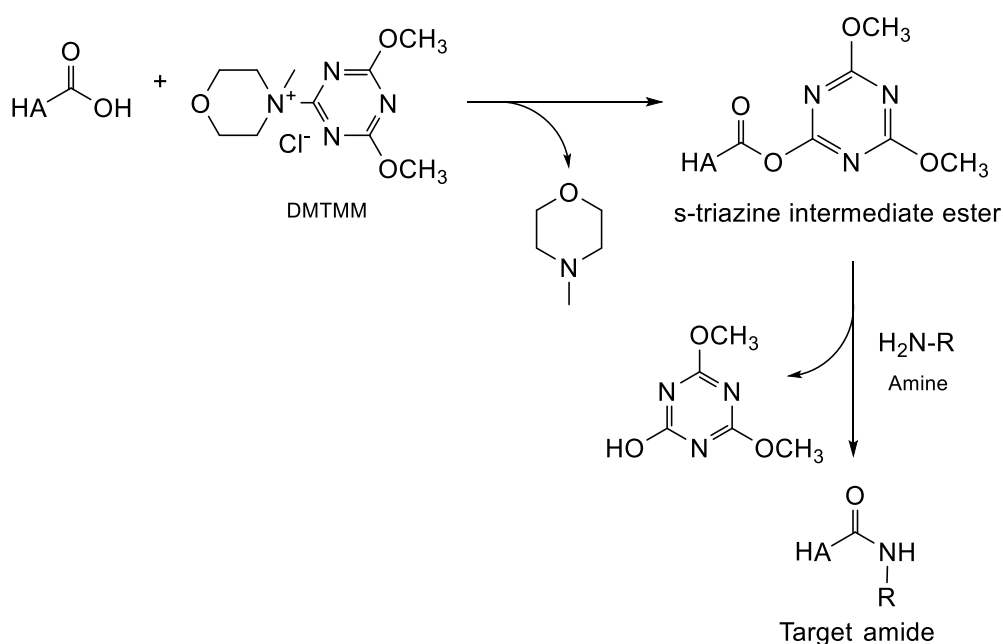


**Fig. 4.9:** Overall representation of DMTMM coupling for hyaluronic acid in water.

We replicated some conditions adopted in the reaction with EDC, comparing yields and purity of samples with those obtained with DMTMM. Reaction conditions and sample code are reported in table 4.4. The degree of substitution values obtained in the presence of DMTMM or EDC are also compared.

**Table 4.4:** List of characteristics and functionalization values calculated from  $^1\text{H}$  NMR spectra of HA-Tau derivatives obtained using DMTMM. Sample functionalization is compared to that calculated for EDC couplings.  $t_{\text{R}}$  = reaction time, DS % = degree of substitution.

pH	Sample, DMTMM:Tau, $t_{\text{R}}$	DMTMM DS (%)	EDC DS(%)
5,5 Acidified water with HCl 0,1 M	HA-Tau 14a, 1:1, 5d	-	-
	HA-Tau 15a, 1:6, 5d	70	51
	HA-Tau 16a, 3:12, 5d	100	30
6,5 Distilled water	HA-Tau 17a, 3:6, 5d	100	51

DMTMM samples show a significant increase in degree of amidation compared with the carbodiimide one, both in acidified or distilled water. Similarly to HA-Tau 4a, when DMTMM is used in stoichiometric amount, very low functionalization is obtained (HA-Tau 14a). However, amidation degree attests at 70% for HA-Tau 15a when 6-fold molar excess of taurine are reacted and DMTMM was stoichiometric to hyaluronic acid (the correspondent EDC sample resulted in an amidation degree of 50 %). Complete amidation of hyaluronic acid has been achieved for HA-Tau 16a and HA-Tau 17a, with reactants ratio of 3:12 and 3:6 respectively. The pH seemed not to influence reaction, in contrast to what occurred for the corresponding EDC samples HA-Tau 10a and HA-Tau 11a, even with different taurine ratio (spectra in figure 4.10). Besides considerations about functionalization degree, HA-Tau 15a and HA-Tau 17a resulted to be highly pure, as evidenced from their proton spectra, and no unreacted DMTMM or ester by-products remained.

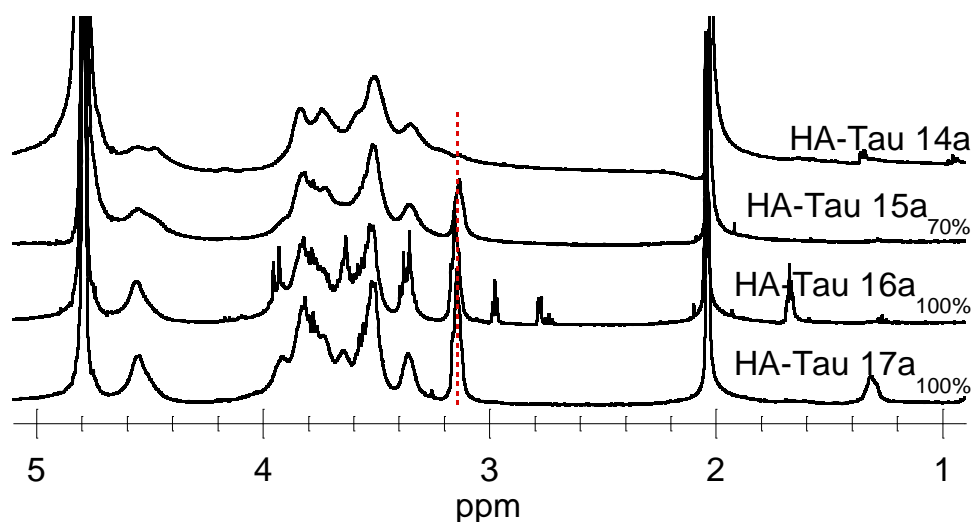


**Fig. 4.10:**  $^1\text{H}$  NMR spectra of sample HA-Tau 14a, HA-Tau 15a, HA-Tau 16a and HA-Tau 17a.

### 4.2.3 Infrared and thermal characterization of HA-Tau derivatives

Further characterization studies were carried out on selected samples with a degree of sulfonation varying from < 2% up to 100%. In the acronyms, the sample DS % is indicated in the subscript. Proton spectra of selected samples, along with that of native hyaluronic acid, are collected in figure 4.11.

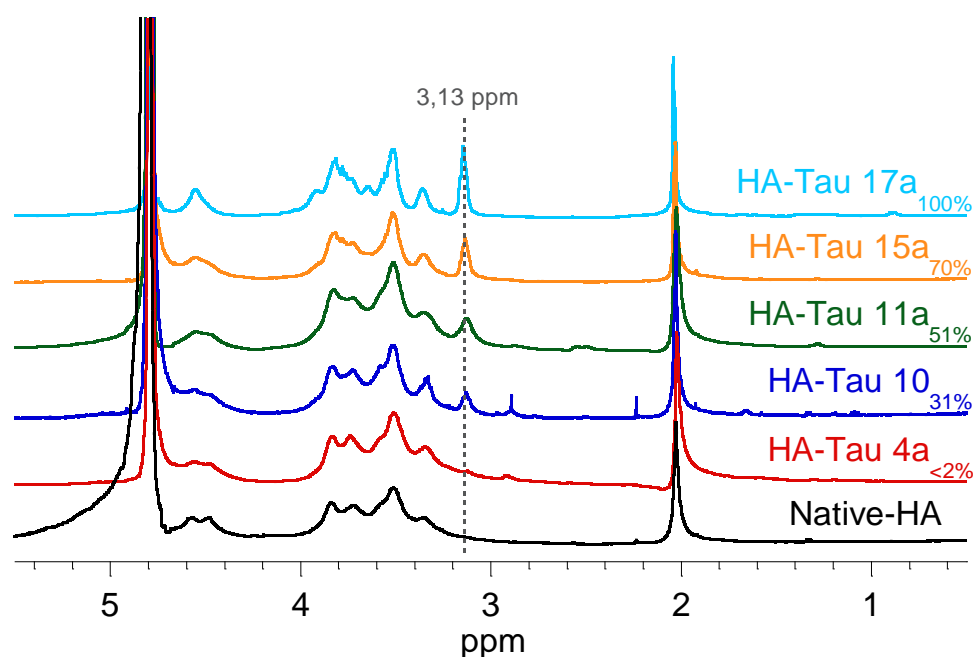


**Fig. 4.11:**  $^1\text{H}$  NMR spectra of native HA and some HA-Tau derivatives with increasing degree of substitution (from <2% up to 100%). Samples illustrated are those chosen for the physico-chemical characterization.

Amidation was studied using FTIR spectroscopy. Figure 4.12 shows FTIR spectra of pristine hyaluronic acid (Native-HA in black), HA-Tau 4a<2%, HA-Tau 10<sub>31%</sub>, HA-Tau 11a<sub>51%</sub>, HA-Tau 15a<sub>70%</sub> and HA-Tau 17a<sub>100%</sub>. As a consequence of amidation, the main differences can be seen in the region of carboxylic and amidic stretching between 1800 and 1500  $\text{cm}^{-1}$  and about 1200  $\text{cm}^{-1}$ . The absorption centered at 1605  $\text{cm}^{-1}$  is attributed to the stretching of  $\text{COO}^-$  while the shoulder at 1650 and band at 1560  $\text{cm}^{-1}$  are related to stretching of amide I and II of hyaluronic acid. After taurine amidation,  $\text{COO}^-$  band decreases and amide bands became predominant. Furthermore, a new band at 1205  $\text{cm}^{-1}$ , assigned to the asymmetrical stretching of  $\text{R-SO}_3^-$ ,<sup>11</sup> appears in samples with a functionalization higher than 30% (from HA-Tau 10 to HA-Tau 17a). Symmetrical stretching of  $\text{R-SO}_3^-$  group is not visible because it is hidden by the intense peak at 1035  $\text{cm}^{-1}$ , related to the stretching of C-OH groups of HA.

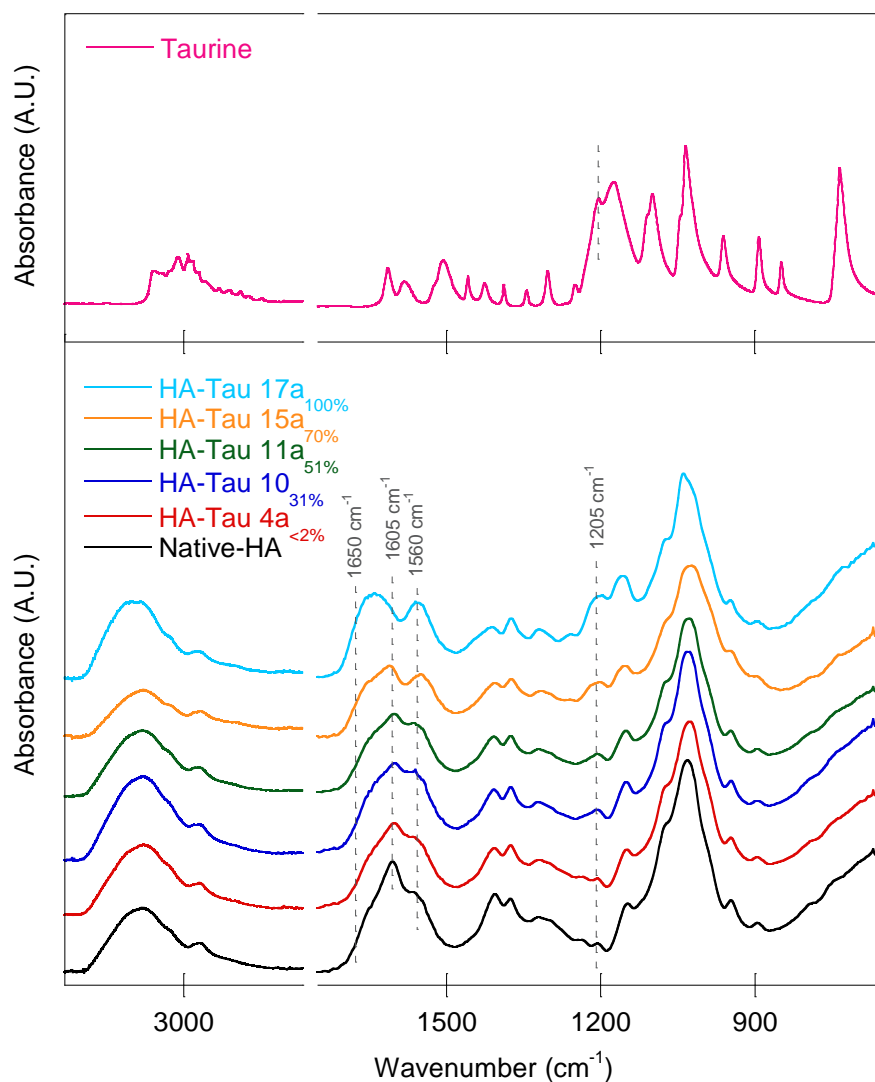


**Fig. 4.12:** FTIR spectra of selected samples compared to that of native HA (black). The formation of new amide bond by the linkage of taurine causes the decrease of COO<sup>-</sup> band at 1650 cm<sup>-1</sup> and the increase of amidic absorption bands at 1605 and 1560 cm<sup>-1</sup> and the SO<sub>3</sub>H band at 1205 cm<sup>-1</sup>.

Semi-quantitative analysis was performed on the FTIR spectra of hyaluronic acid conjugates acidified below the pK<sub>a</sub> of COOH (pK<sub>a</sub> = 3-4). Selected dried samples were solubilized in a solution of HCl 0.1 M, dried and, then, the spectra were recorded. Comparison of the different acidified spectra is shown in figure 4.13. The stretching of carboxylic group appears at 1726 cm<sup>-1</sup>, as result of protonation of COO<sup>-</sup>, while the bands of amide I-II stretching remain centered at 1650 and 1560 cm<sup>-1</sup>. Carboxylic absorption can be still observed for HA-Tau 17a, albeit functionalization calculated from NMR resulted to be equal to 100%. This could be related to an overrating of DS % caused by a base line distortions or to a partial hydrolysis of amidic bonds in the HA-Tau derivatives after dissolution in acidic media. Lastly, it is

interesting to note that the stretching of  $\text{SO}_3\text{H}$  at  $1205\text{ cm}^{-1}$  is increased and sharpened for taurinated samples.

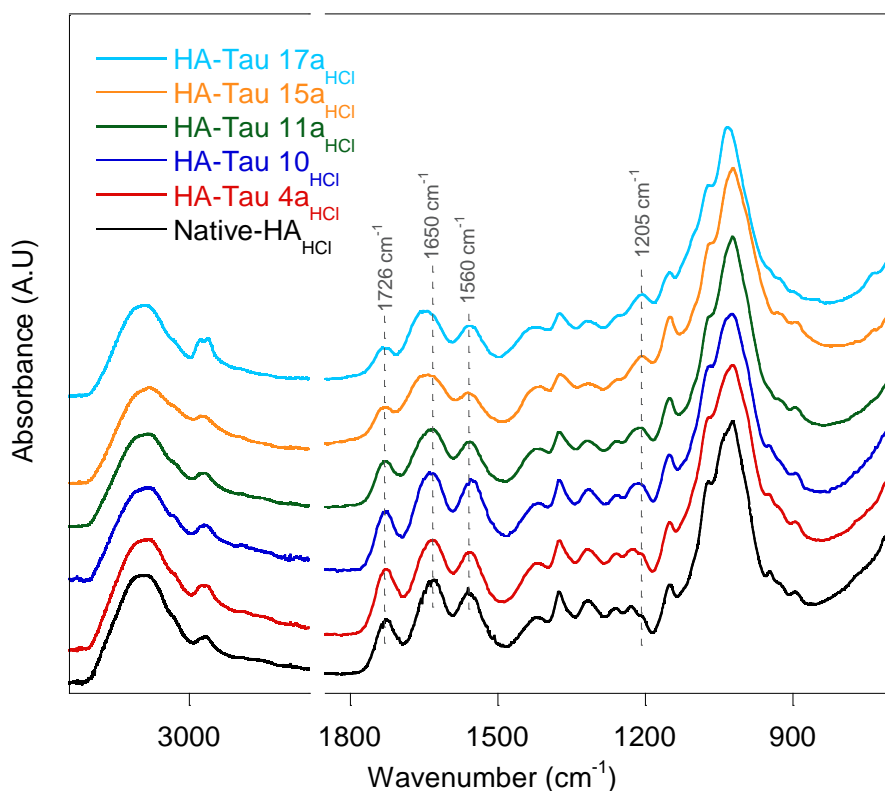


**Fig. 4.13:** FTIR spectra of selected acidified HA-Tau samples compare to that of native HA (black). Taurine linkage leads to the lowering of COOH band at  $1726\text{ cm}^{-1}$ .

Whereas taurine grafting on HA leads to the formation of new amide bonds and thus, to the consumption of  $\text{COO}^-$ , it is reasonable to estimate degree of amidation from ratio between carbonylic groups in the form of amides respect to the total amount of carbonyls (both in amidic or carboxylic state). At this regard, areas of amidic carbonyls ( $1650$  and  $1560\text{ cm}^{-1}$  for Amide I-II) and COOH carbonyls (band at  $1726\text{ cm}^{-1}$ ) were measured and the ratios between amidic/total carbonyls were calculated ( $R^{\text{Am/Tot}}$ ). Areas were measured choosing a base line suitable for all the samples in the region between  $1780$  and  $1480\text{ cm}^{-1}$ . The ratio of each sample as function of correspondent NMR substitution degree is shown in figure 4.14.

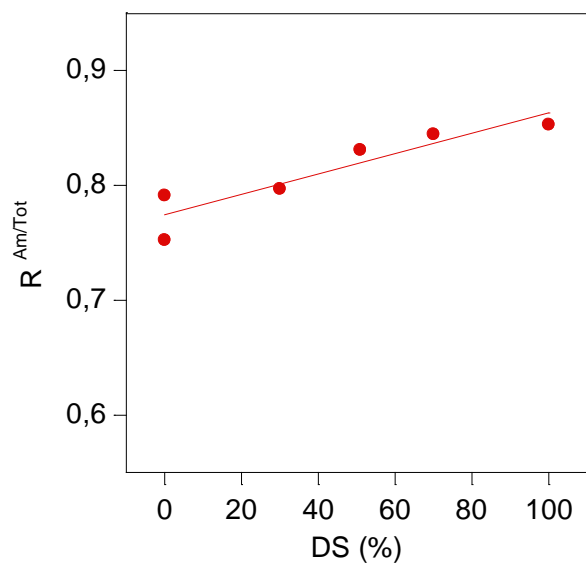


**Fig. 4.14:** Dependence of Amide/(Carboxylic + Amide) areas ratio ( $R^{Am/Tot}$ ) as function of DS % calculated from  $^1H$  NMR for the selected samples.  $R^{Am/Tot}$  increases linearly with DS %.

As expected,  $R^{Am/Tot}$  increases linearly with degree of substitution as result of new amides formation on hyaluronic acid skeleton, demonstrating how the conversion of carbonyl moieties into amides can be easily valuated using a non-destructive analysis such as infrared spectroscopy.

Sulfonation of hyaluronic acid can influence polysaccharide thermal properties like decomposition temperature and, in general, thermal stability of the material. TGA experiments were carried out on pristine HA and taurinated samples and thermogravimetric curves were compared (figure 4.15 A). All samples were heated between 30 and 500 °C in order to reach complete decomposition of materials with a heating rate of 10 °C/min. Weight loss percentage in correspondence of the end of decomposition process ( $WL_{300\text{ }^\circ\text{C}}$ ) has been calculated from thermogravimetric curves, while degradation temperatures at maximum rate of degradation ( $T_d^{\text{MAX}}$ ) have been measured from the temperature derivative of weight loss, in correspondence of the minima (figure 4.15 B).

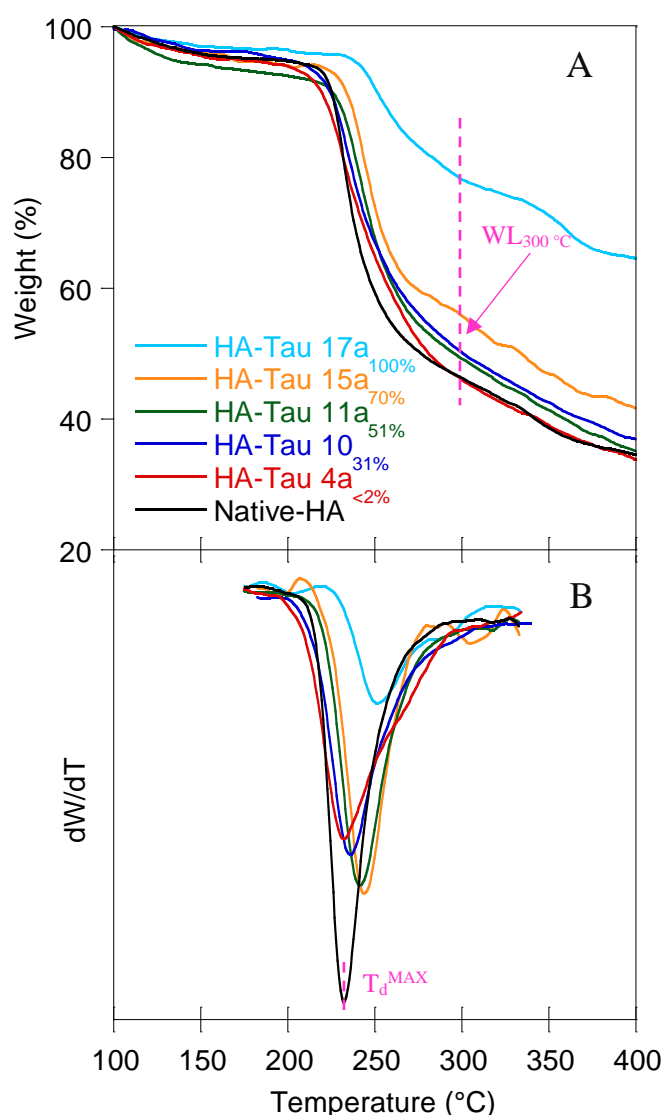


**Fig. 4.15:** Thermogravimetric curves of HA-Tau conjugates: weight loss as function of temperature (A), derivative curves as function of temperature (B).  $WL_{300\text{ }^\circ\text{C}}$  = Weight loss percentage at 300 °C,  $T_d^{\text{MAX}}$  = degradation temperatures at maximum rate of degradation.

All samples are characterized by an initial decrease in weight between 100 – 150 °C that can be attributed to the loss of strongly bonded water (10% for HA, 15 and 20% for HA-TAU 15a<sub>70%</sub> and HA-TAU 17a<sub>100%</sub>, respectively). Then, around 200 °C, the massive weight variation is related to decomposition of material that continues up to about 300 °C.  $T_d^{MAX}$ , together with the weight loss, reveals that taurine grafting lead to a thermal stabilization of hyaluronic acid (figure 4.16 **A** and **B**, respectively). In fact, TGA curves shift along the temperature axis with sulfonation degree resulting in the rise of  $T_d^{MAX}$ . In addition, the amount of material which decompose till 300 °C diminishes by increasing the taurine grafting yield. This effect is stronger for samples with DS > 70 % (HA-Tau 15a<sub>70%</sub> and HA-Tau 17a<sub>100%</sub>).

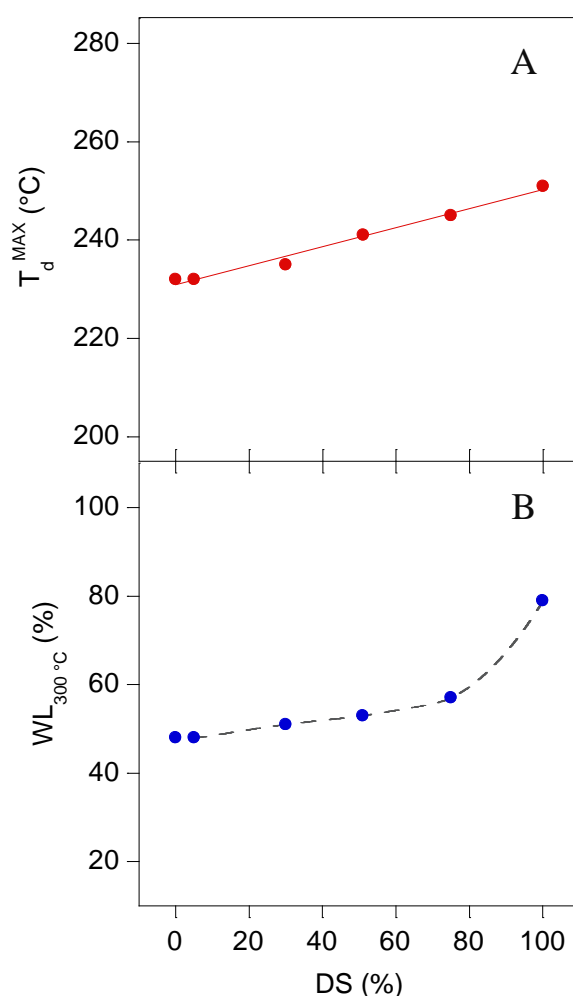


**Fig. 4.16:** Thermogravimetric evaluation of HA-Tau derivatives. **A)** Degradation temperature calculated at maximum rate of decomposition; **B)** Weight loss at 300 °C as function of temperature for native hyaluronic acid and taurinated derivatives. The dashed line is a guide for the eye.

#### 4.2.4 Cytotoxicity of samples

The *in vitro* toxicity studies were performed on human primary chondrocytes (HPCs) by incubating the cells with HA and HA-Tau derivatives, such as the HA-Tau 17a<sub>100%</sub>, HA-Tau11a<sub>51%</sub> and HATau10<sub>31%</sub> (results in figure 4.17). Three different concentrations were evaluated in order to obtain solution with suitable viscosity for cells analyses. In particular, cells were treated with 0,3 – 0,1 – 0,03 and 0,015 % polymeric solutions for 48 h.

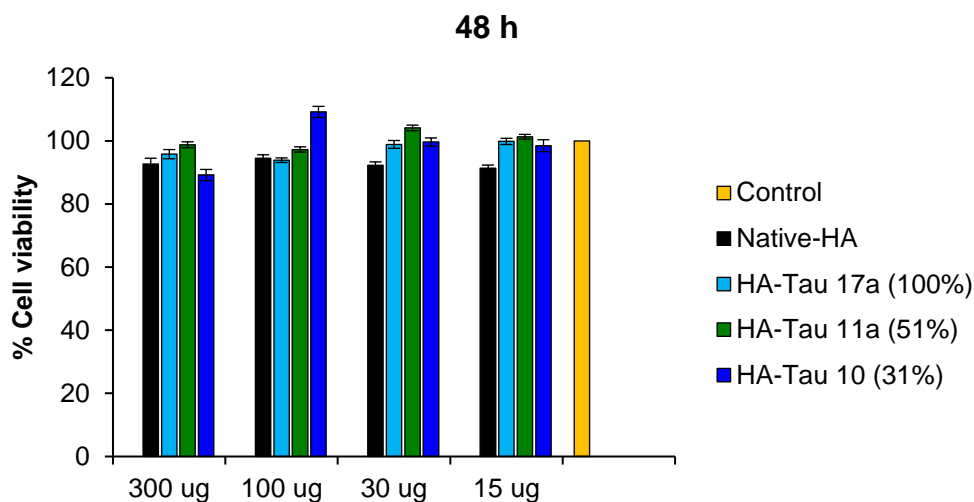


**Fig. 4.17:** Cells viability results of MTS assay after 48 h on chondrocytes. The cells were treated with pristine HA and few HA-Tau derivatives for 48 h at three different concentration (0,3 – 0,1 – 0,03 and 0,015 %). Values reported are means of at least three experiments  $\pm$  SD.

No toxic effect of all HA derivatives was evidenced after 48 h treatment and cells resulted to be perfectly viable for each concentration used. Each HA-Tau conjugate showed cell viability value higher than 90 % and, thus, similar to that obtained for untreated cells (control). In conclusion, HA-Tau derivatives showed no hazardous effect on chondrocytes maintaining a cytocompatibility equal to that of unmodified hyaluronic acid in the explored conditions.

### 4.3 Conclusion

Sulfonation of hyaluronic acid in water was successfully accomplished by means of 2-aminoethanesulfonic acid (taurine) amidation. Grafting of taurine onto carboxylate moiety of HA was operated comparing the reactivity of two type of water soluble coupling reagents, 1-Ethyl-3-(3-dimethylaminopropyl)carbodiimide hydrochloride (EDC HCl) and the 4-(4,6-dimethoxy-1,3,5-triazin-2-yl)-4-methyl-morpholinium chloride (DMTMM), and reaction conditions by varying pH and molar ratios of reactants involved. Efficiency of coupling was evaluated after 1 or 5 days reaction. In the case of the carbodiimide, HA-Tau derivatives with 50% of functionalization as maximum were obtained, as revealed by  $^1\text{H}$  NMR analysis. The reaction showed to be pH dependent and better results have been obtained from the amidation in slightly acidic environment. The same conditions used in EDC reaction were studied in the DMTMM coupling experiments. It was found that a totally sulfonated material was synthesized independently from pH. A semi-quantitative characterization of HA-Tau derivatives was carried out using infrared spectroscopy, correlating the intensity of amidic and carboxylic absorption bands. Thermogravimetric analysis showed that the thermal stability of sulfonated materials at high temperature results to be increased respect to that of unmodified HA. Lastly, HA-Tau derivatives showed to be completely safe when in contact with human primary chondrocytes (HPCs).

Respect to other reported methods, the use of taurine as sulfonating agent revealed to be a green, easy and tunable method for the modification of sodium hyaluronan, with different degree of amidation, without the exposure of HA to drastic conditions or organic solvents. The introduction of a  $-\text{SO}_3\text{H}$  function in the disaccharide repeating unit could have several consequences on the physico chemical behavior of HA and could represent a valid procedure for the synthesis of new hyaluronan system with enhanced enzyme resistance and improved blood-compatibility.

## 4.4 References

- (1) Kuo, J. W., Swann, D. A., & Prestwich, G. D. (1991). Chemical modification of hyaluronic acid by carbodiimides. *Bioconjugate chemistry*, 2(4), 232-241.
- (2) D'Este, M., Eglin, D., & Alini, M. (2014). A systematic analysis of DMTMM vs EDC/NHS for ligation of amines to hyaluronan in water. *Carbohydrate polymers*, 108, 239-246.
- (3) Schanté, C. E., Zuber, G., Herlin, C., & Vandamme, T. F. (2011). Chemical modifications of hyaluronic acid for the synthesis of derivatives for a broad range of biomedical applications. *Carbohydrate polymers*, 85(3), 469-489.
- (4) Young, J. J., Cheng, K. M., Tsou, T. L., Liu, H. W., & Wang, H. J. (2004). Preparation of cross-linked hyaluronic acid film using 2-chloro-1-methylpyridinium iodide or water-soluble 1-ethyl-(3, 3-dimethylaminopropyl) carbodiimide. *Journal of Biomaterials Science, Polymer Edition*, 15(6), 767-780.
- (5) Joung, Y. K., Sengoku, Y., Ooya, T., Park, K. D., & Yui, N. (2005). Anticoagulant supramolecular-structured polymers: Synthesis and anticoagulant activity of taurine-conjugated carboxyethylester-polyrotaxanes. *Science and Technology of Advanced Materials*, 6(5), 484.
- (6) Matsusaki, M., Serizawa, T., Kishida, A., Endo, T., & Akashi, M. (2002). Novel functional biodegradable polymer: synthesis and anticoagulant activity of poly ( $\gamma$ -glutamic acid) sulfonate ( $\gamma$ -PGA-sulfonate). *Bioconjugate chemistry*, 13(1), 23-28.
- (7) Totaro, K. A., Liao, X., Bhattacharya, K., Finneman, J. I., Sperry, J. B., Massa, M. A., ... & Pentelute, B. L. (2016). Systematic investigation of EDC/sNHS-mediated bioconjugation reactions for carboxylated peptide substrates. *Bioconjugate chemistry*, 27(4), 994-1004.
- (8) Kunishima, M., Kawachi, C., Monta, J., Terao, K., Iwasaki, F., & Tani, S. (1999). 4-(4, 6-dimethoxy-1, 3, 5-triazin-2-yl)-4-methyl-morpholinium chloride: an efficient condensing agent leading to the formation of amides and esters. *Tetrahedron*, 55(46), 13159-13170.

- (9) Choi, Y. R., Kim, H. J., Ahn, G. Y., Lee, M. J., Park, J. R., Jun, D. R., ... & Choi, S. W. (2018). Fabrication of dihydroxyflavone-conjugated hyaluronic acid nanogels for targeted antitumoral effect. *Colloids and Surfaces B: Biointerfaces*, 171, 690-697.
- (10) Loebel, C., D'Este, M., Alini, M., Zenobi-Wong, M., & Eglin, D. (2015). Precise tailoring of tyramine-based hyaluronan hydrogel properties using DMTMM conjugation. *Carbohydrate polymers*, 115, 325-333.
- (11) Hausman, R., Digman, B., Escobar, I. C., Coleman, M., & Chung, T. S. (2010). Functionalization of polybenzimidazole membranes to impart negative charge and hydrophilicity. *Journal of membrane science*, 363(1-2), 195-203.

## **5. SULFONATION OF HYALURONIC ACID: PREPARATION OF HA-BASED SULFONATED HYDROGEL**

Hyaluronic acid hydrogels were prepared using 1,4-Butanediol diglycidyl ether (BDDE), the crosslinker agent used in the majority of the market-leading HA fillers. Its stability, biodegradability, and long safety record spanning more than 15 years are what make it the industry standard, ahead of other crosslinkers such as divinyl sulfone and 2,7,8-diepoxyoctane. An important aspect to take into account is that BDDE has a significantly lower toxicity than other ether-bond crosslinking chemistry based agents (e.g., divinyl sulfone), is biodegradable, and has been well studied.<sup>1</sup> The use of crosslinked-HA is fundamental for the preparation of cosmetic fillers or viscosupplementation injections because the enzymatic resistivity of the polymer is largely strengthened. Furthermore, a mechanical properties of hyaluronic acid could be empowered by increasing crosslinker amount, thus preparing tunable 3D manufactures suitable for cells growth.

The reaction with BDDE is based on the epoxide ring opening by the hydroxylate groups of hyaluronic acid to form ether bonds, that are more stable than ester or amid bonds, and, therefore, more appropriate for long-term applications. Generally, high pH is required for the reaction because OH functions are enough nucleophilic towards the epoxide opening only when deprotonated ( $\text{pH} > 10$ ). Primary HA hydroxylic position is the main group involved in the crosslinking due to its higher reactivity respect to the other hydroxylates and carboxylate group in the polysaccharide repeat unit. Considering the alkaline environment, hydroxylate reacts preferably with the less hindered primary position of epoxide ring. The scheme for the overall reaction is reported in figure 5.1 (primary OH are represented in the deprotonated form, implying the alkaline environment).

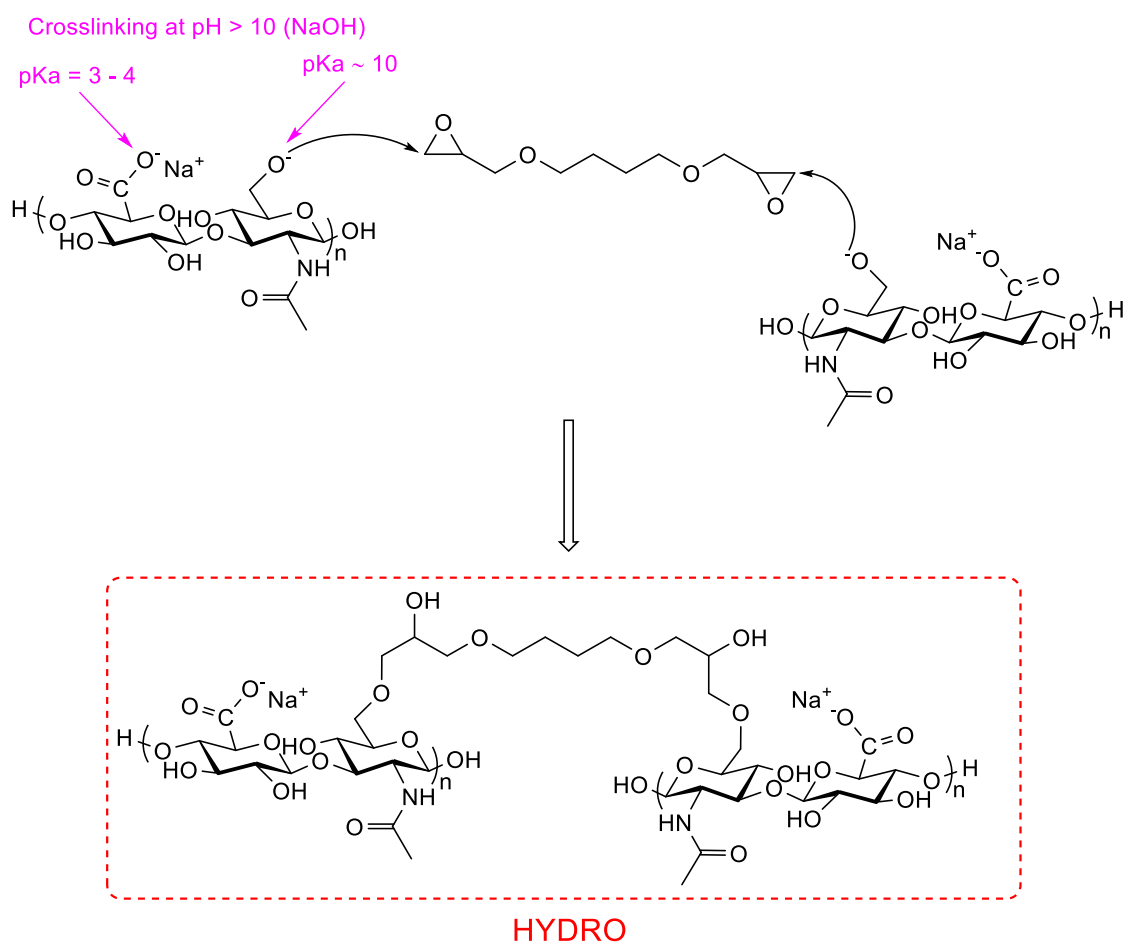


**Fig. 5.1:** Crosslinking mechanism at the base of hyaluronic acid/1,4-Butanediol diglycidyl ether reaction for the preparation of HYDRO samples in an alkaline medium. At high pH, the ring opening epoxide is at the expense of hydroxylate groups.

The unreacted BDDE could be removed by rinsing the hydrogel with distilled water. According to the industry standard for cosmetic surgery fillers (injected gels), the residual quantity of crosslinking agents should be no more than 2  $\mu\text{g/g}$  in crosslinked sodium hyaluronate gel.<sup>2</sup> BDDE in dermal filler is maintained at trace amount mostly because of its the mutagenic potential ascribable to the reactive nature of the epoxide groups.<sup>1</sup> Nevertheless, no carcinogenic effect of unreacted BDDE has been demonstrated yet.<sup>3</sup> Different by-products of HA-BDDE gel can be formed in the crosslinking reaction (figure 5.2). In fact, the diepoxy can react completely, linking two hyaluronan chains (fig. 5.2 **A**), or can be mono-linked, when only one epoxy reacts with HA (fig. 5.2 **B**), can be transformed in non-linked diol form, if epoxydic rings react with water as nucleophile (fig. 5.2 **C**) or can be present in the unreacted form (fig. 5.2 **D**). The quality and toughness of the resulting hydrogels will depend upon the ability of the crosslinker to connect simultaneously two polymeric chains thus forming fully

interlinked networks.<sup>4</sup> HA-BDDE degradation products have not demonstrated any cytotoxicity and epoxide compounds are hydrolyzed into simple diols.<sup>5</sup>

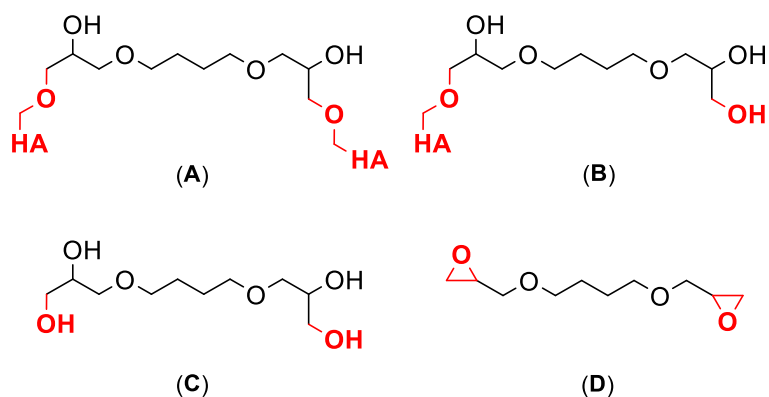


**Fig. 5.2:** Possible derivatives of BDDE as result of HA crosslinking in alkaline environment: fully-linked (A), mono-linked (B), non-linked tetraol derivative (C) and unreacted BDDE (D).

Hydrogels sulfonation was carried out using Taurine (Tau) and N,N-bis(2-hydroxyethyl)-2-aminoethanesulfonic acid (Bes) in a one-pot crosslinking procedure, as shown in figure 5.3 (crosslinking A and crosslinking B, respectively). The nucleophile groups of sulfonated agents, such as  $\text{NH}_2$  for Tau and OH for Bes, are able to react with the epoxy rings of the crosslinker together with the primary hydroxylic group of hyaluronic acid to form stable carbon-nitrogen or carbon-oxygen bond respectively. In this way, Tau and Bes could be inserted in the saccharide network, leading to the synthesis of the sulfonated hydrogels HYDROTau and HYDROBes.

Likewise hyaluronic acid, alkaline conditions are suitable for Tau and Bes grafting being aminic and hydroxylic moieties both deprotonated at high pH and, hence, more reactive towards epoxide ring opening.

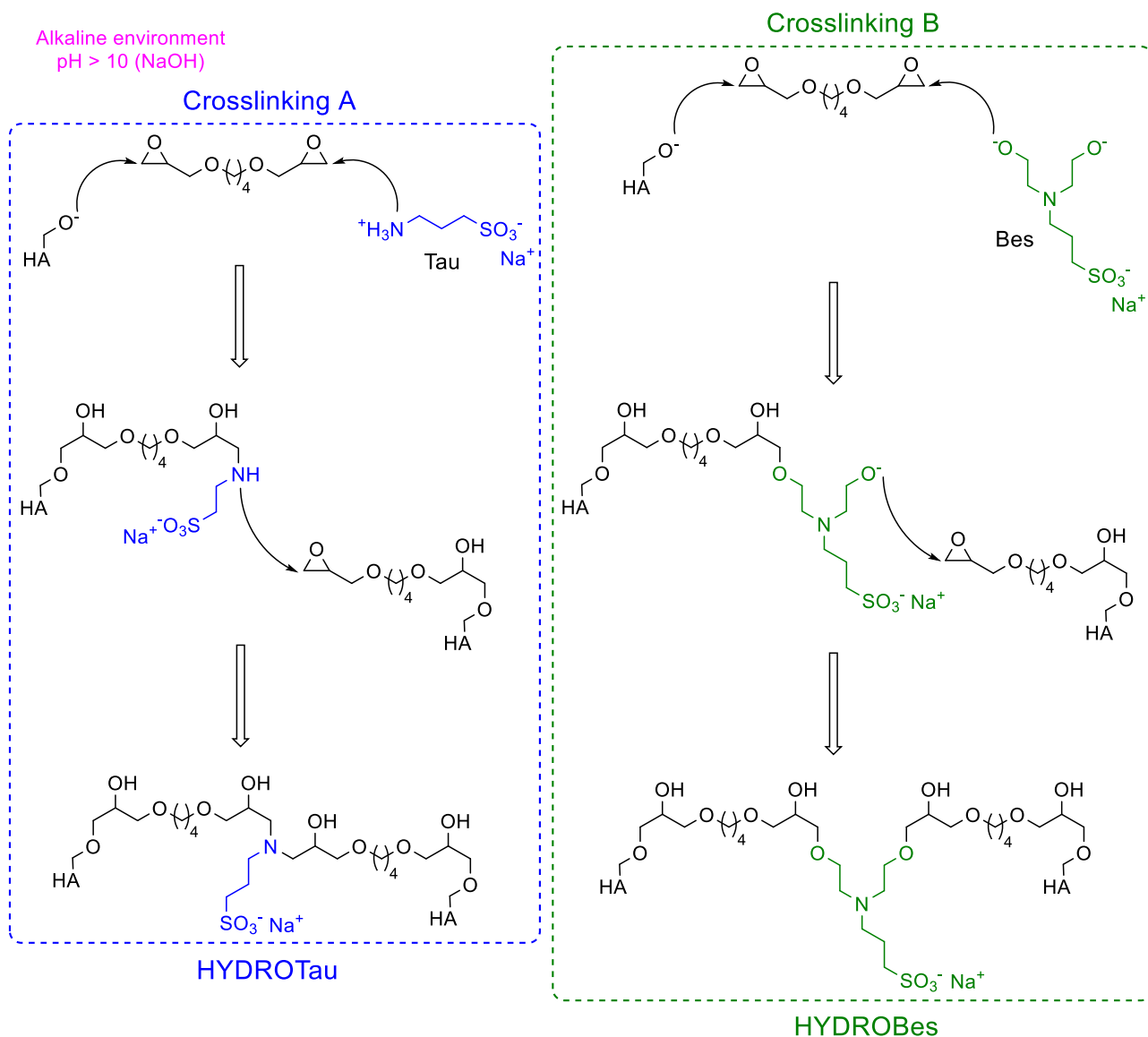


**Fig. 5.3:** Crosslinking mechanism at the base of hyaluronic acid/1,4-Butanediol diglycidyl ether reaction in the presence of Tau and Bes for the preparation of HYDROTau and HYDROBes samples. The sulfonating agents are able to react with the diepoxy simultaneously with HA, forming a sulfonated 3D network.

The primary amine of taurine attacks one epoxydic ring of BDDE, already linked to HA, forming a secondary amine which in turn reacts with another terminal epoxide chain (crosslinking A, blue dashed box). Similarly, epoxide chains can undergo nucleophilic attack by the hydroxylate groups of N,N-bis(2-hydroxyethyl)-2-aminoethanesulfonic acid leading to the formation of ether bonds (crosslinking pathway B, green dashed box). The equivalents of sulfonation agents, crosslinker and HA should be properly adjusted to permit a simultaneous sulfonation/gelation, without consumption of crosslinker at the expense of hyaluronic acid.

## 5.1 Materials and methods

Hyaluronic acid with MW = 1200 – 1500 kDa was purchased from Flower tales (Milan, Italy). Taurine, N,N-bis(2-hydroxyethyl)-2-aminoethanesulfonic acid, 1,4-Butanediol diglycidyl ether, sodium hydroxide and phosphate-buffered saline were bought from Sigma Aldrich (Milan, Italy). All reactants were used without any further purification.

### 5.1.1 General procedure for hyaluronic acid coupling

Hydrogels were prepared starting from 10 % solutions (wt/v) of hyaluronic acid in NaOH 0,25 M. Complete dissolution of HA in the alkaline medium required at least three hours of stirring at room temperature. For the sulfonated hydrogels, specific amount of Tau or Bes were added to the HA basic solution and the mixtures were stirred for additional two hours to obtain clear and homogeneous solution. Then, the crosslinking agent was added and solutions were mixed vigorously for 10 minutes further, till transparent solutions were obtained. Viscous mixtures were slowly injected into Teflon molds (internal diameter 0,6 or 0,8 cm) with a syringe and the pre-hydrogels were sonicated for 30 minutes at 40 °C to homogenize the mixtures and to remove possible air bubbles. Crosslinking was conducted at room temperature for 24, 72 or 96 h (figure 5.4).

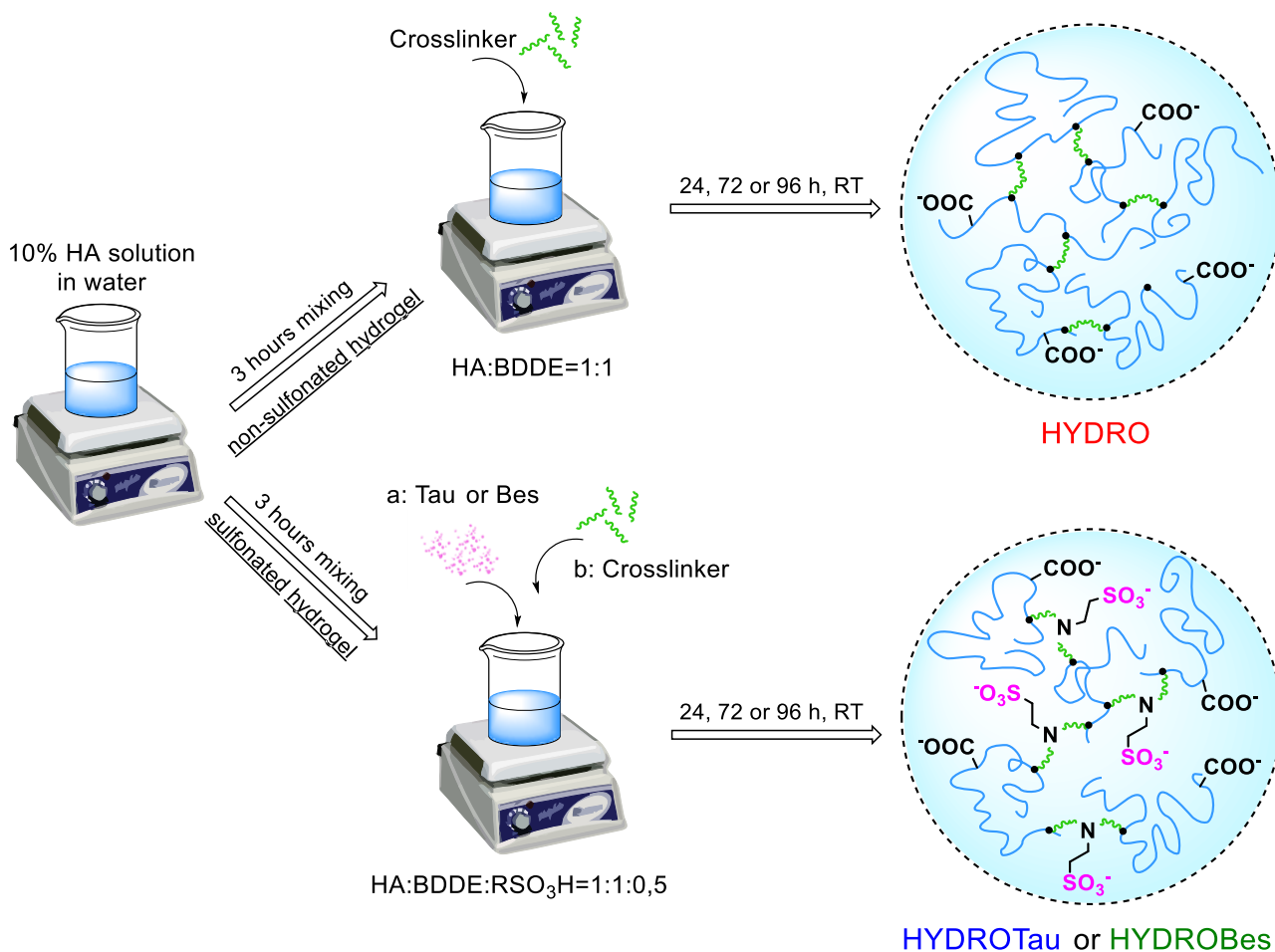


**Fig. 5.4:** Schematic representation of HA hydrogels preparation with and without sulfonation agent. HYDROTau and HYDROBes hydrogels are enriched in polar sulfonic groups.

Later, water insoluble hydrogels were soaked in distilled water and washed out for 3 days to neutralize hydrogels and to remove unreacted molecules, such as residual crosslinker. Hydrogels were cut in regular disks with suitable height depending on the characterization and freeze-dried. Table 5.1 summarizes sample name, molar ratio of reactants and crosslinking time.

**Table 5.1:** Acronyms and properties of hydrogels. Type, reactants molar ratio,  $t_{\text{CROS}}$  = crosslinking time, sample name.

Hydrogel	HA:BDDE	Tau	Bes	$t_{\text{CROS}}$ (hours)	Sample
<b>HYDRO</b> (HA/BDDE)	1:1	-	-	24	HYDRO 24 h
				72	HYDRO 72 h
				96	HYDRO 96 h
<b>HYDROTau</b> (HA/BDDE/Tau)	1:1	0,5	-	24	HYDROTau 24 h
				72	HYDROTau 72 h
				96	HYDROTau 96 h
<b>HYDROBes</b> (HA/BDDE/Bes)	1:1	-	0,5	24	HYDROBes 24 h
				72	HYDROBes 72 h
				96	HYDROBes 96 h

HYDRO 72 h sample before (height 3 mm, diameter 2 cm, left) and after (right) freeze-drying is shown in figure 5.5 below.



**Fig. 5.5:** Illustration of a HYDRO samples before (left) and after (right) freeze-drying process.

### 5.1.2 Infrared spectroscopy (FTIR)

FTIR spectroscopy was used to characterize crosslinked and sulfonated hydrogels. The spectra were acquired in attenuated total reflection mode (ATR) using a Nicolet 6700 (Thermo Fisher Scientific, Waltham, MA, USA) equipped with a Golden Gate single reflection diamond ATR accessory. All spectra were recorded with 200 scans/spectrum and at 4 cm<sup>-1</sup> resolution.

### 5.1.3 Swelling studies

Water uptake properties of hydrogels were studied following the equilibrium swelling ratio SR (g/g) in distilled water and PBS 0,01 M by means of gravimetric measurements. Two types of swelling measurements were carried out, the indirect and the direct swelling. For the indirect swelling analysis (SR<sub>ind</sub>) dry specimens were weighed, merged in distilled water, or in PBS, at 37 °C, and then weighed again in the equilibrium swollen state (swollen weight, W<sub>s</sub><sup>H<sub>2</sub>O</sup> or W<sub>s</sub><sup>PBS</sup>) after 48 h. For the direct swelling ratio (SR<sub>dir</sub>) in water, weight was measured on freshly prepared hydrogels before (wet weight, W<sub>w</sub><sup>H<sub>2</sub>O</sup>) and after lyophilization (dry weight, W<sub>d</sub><sup>H<sub>2</sub>O</sup>). For measurements in phosphate buffered saline, wet hydrogels were soaked in PBS for 24 h to let the hydrogels absorb completely the buffered medium. Again, they were weighed in the wet state (W<sub>w</sub><sup>PBS</sup>) and after lyophilization (W<sub>d</sub><sup>PBS</sup>). The swelling ratios SR in both media were calculated as follows:

$$SR_{ind} = \frac{W_s}{W_d} \qquad SR_{dir} = \frac{W_w}{W_d}$$

Equation 5.1

Swelling measurements were made in triplicate and final values were reported as means ± standard deviations. Direct and indirect swelling analysis were carried out consecutively on the same set of samples.

### 5.1.4 Thermal analysis

Differential scanning calorimetry (DSC) was used to evaluate the state of water in the swollen hydrogels. In fact, the ΔH of melting of water in the hydrogel at around 0 °C can be used to estimate the water content of the samples.<sup>6</sup> The analysis was conducted on 3 - 5 mg of

hydrogels, accurately cut, weighted and sealed in aluminum pans, using a Mettler Toledo DSC822 instrument. Specimens were cooled to -30 °C with a cooling rate of 5 °C/min and then heated up to 25 °C at 5 °C/min. The comparison of  $\Delta H_m$  of water to the melting endothermic heat of fusion (-334 J/g) for pure water can be used to define the amount of water bonded in the hydrogel. In particular, when an hydrogel is swollen, three types of water can be defined:

1. Bound water ( $W_b$ ) or non-freezing water: it is the water interacting with swollen material polar groups through strong hydrogen bonds and it is characterized by restricted mobility. It represents the internal hydration shell in the network. This water does not melt.
2. Secondary bound freezing water ( $W_{fb}$ ): water molecules that have weaker interactions with the polymer (secondary or tertiary hydration shell) or because confined in nanocavity.<sup>7</sup> This freezing water has the melting point at  $T < 0$  °C.
3. Free water ( $W_f$ ) or bulk water: it is characterized by high degree of mobility because it is not bonded to the material. The free freezing water melts at 0 °C.

The amount of  $W_b$  percentage can be calculated as follow:

$$W_b (\%) = W_t - (W_{fb} + W_f)$$

Equation 5.2

The total water  $W_t$  fraction, evaluated by gravimetric measurements, is also described as the equilibrium water content (EWC) by Huglin and coauthors<sup>8</sup> and it can be calculated through the indirect swelling ratio as:

$$W_t = EWC = \frac{SR_{ind} - 1}{SR_{ind}}$$

Equation 5.3

The fraction of freezing water, expressed as the sum of secondary bounded and free water, is calculated as the ratio of the experimental endothermic peak area of water-swollen hydrogel ( $\Delta H_w$ ) to heat of fusion of pure water ( $\Delta H_w^0 = -334$  J/g). Thus equation 5.2 can be expressed as:

$$W_b (\%) = EWC - \left( \frac{\Delta H_W}{\Delta H_W^0} \right) * 100$$

Equation 5.4

### 5.1.5 Mechanical measurements

Uniaxial compression measurements on the hydrogels before the lyophilization were conducted at RT using an INSTRON 4502 instrument (Instron Inc., Norwood, Ma, USA). The samples, cut in parallelepiped shape (base dimensions (9x6) mm<sup>2</sup>, height of 6 mm), were placed between the two Instron flat plates and compressed with a constant deformation rate of 5 mm/min using a 2 N load cell. Compression moduli (CM) and stresses at a fixed deformation ( $\sigma_\varepsilon$ ) were calculated from stress-strain curves obtained by plotting nominal stress  $\sigma_n$  as function of the deformation  $\varepsilon$ . In particular, CM was calculated from the slope of the linear zone in the stress-strain curve in the range  $0 < \varepsilon < 0,2$  while the stress at constant deformation was calculated at  $\varepsilon=0,2$ . The results are reported as average values  $\pm$  standard deviations on at least three parallel experiments conducted on different specimens.

### 5.1.6 Bulk structure analyses (SEM)

Bulk of hydrogels were studied by field emission scanning electron microscopy (FESEM, AURIGA Carl Zeiss AG, Oberkochen, Germany). Lyophilized hydrogels were cut with a blade, placed on SEM stab and sputtered with gold before the analysis. The longitudinal and the cross-section surfaces of the hydrogels were observed. The free software ImageJ (<https://imagej.nih.gov/ij>) was used to analyze images and to define pores dimension.

### 5.1.7 *In vitro* degradation

Degradation in buffer and in enzymatic solution was investigated for non-sulfonated and sulfonated hydrogels. In particular, the weight loss of hydrogels under the influence of lysozyme in PBS was monitored. Freshly prepared hydrogels were merged in PBS 0,01 M for 24 h at 37 °C in order to achieve the complete absorption of solution into the hydrogel. Then, the specimens were removed from PBS, accurately wiped and weighted (initial weight,  $W_i$ ) and placed in a fresh solution of PBS containing lysozyme (1,5  $\mu$ g/ml) and incubated at 37 °C. The concentration of lysozyme was chosen corresponding to the concentration in human

serum.<sup>9</sup> After 1, 3, 7 or 15 days, the swollen samples were removed from the lysozyme solution, wiped and weighted (weight at specific time,  $W_t$ ). The weight loss (WL %) was determined as follow:

$$WL (\%) = \frac{W_i - W_t}{W_i} * 100\%$$

Equation 5.5

Each experiment was repeated three times and the weight loss was expressed as means  $\pm$  standard deviations.

## 5.2 Results

Crosslinking and sulfonation of hyaluronic acid was achieved by means of a one pot procedure. In preliminary studies, high content of crosslinker was used (HA:BDDE=1:4-8-16) but hydrogels resulted to be stiff. In addition, samples didn't resist to lyophilization/swelling/re-lyophilization cycle, leading to an unusable material (figure 5.6). Then, stoichiometric amount of crosslinker was used, whereas one diepoxy molecule is able to link two repeating unit of hyaluronic acid. The same molar ratio between HA and crosslinker was maintained for sulfonated hydrogels. In this case, Tau and Bes were added in order to introduce on average one  $\text{SO}_3^-$  group every two repeating unit of hyaluronic acid (HA:BDDE: $\text{SO}_3^-$  agent=1:1:0,5). In fact, an excess of sulfonating agent could provoke the consumption of crosslinker at the expense the crosslinking reaction with HA, affecting the formation of a stabile polymeric network, especially in the case of a strong nucleophile such as taurine.



**Fig. 5.6:** HYDRO with high crosslinker content: first freeze-drying (left), swollen state (middle) and second freeze-drying (right).

Another aspect to consider, is the high viscosity of the hyaluronan solutions that underwent crosslinking, related to the high molecular weight of the polysaccharide and to the large volume occupied by each chain (MW = 1200 – 1500 kDa).<sup>10</sup> Crosslinking was carried out in NaOH 0,25 M because intramolecular hydrogen bonds in HA molecules are easily disrupted at high pH values<sup>11</sup> and polymeric chains are more flexible. The alkaline environment enhances the molecular mobility and, thus, the reaction with the crosslinker. Preliminary analysis were made in order to optimize the concentration of the starting HA solutions with equimolar crosslinker, unaltered sodium hydroxide molarity and no sulfonating agent. No gel formation was visible for the 5% wt/v solutions after 24, 72 or 96 hours, probably because the low initial viscosity. Furthermore, when HA is dissolved in alkaline media, hydrolytic degradation of polymer takes place, viscosity dramatically decreases and gelation process is

prevented.<sup>12</sup> For this reason, the initial concentration has to be adjusted in order to overcome molecular weight fragmentation, but keeping a suitable solution viscosity which ensures the crosslinking. 8% wt/v solutions led to the formation of soft gels after 24 h, thus concentration was enhanced and the hydrogels were prepared from a 10% wt/v solutions of hyaluronan in sodium hydroxide 0,25 M (crosslinking time 24, 72 and 96 h). Solutions revealed to be especially sensible to viscosity change in the presence of sulfonating agents. In particular, the addition of a certain amount of Tau or Bes led to the abrupt raise of viscosity, as a consequence of ionic strength increase, and a proper stirring of the solution was limited (this phenomenon was particularly evident with Bes considering that the molecule has three negative charged groups when dissolved at  $\text{pH} > 10$ ). Thus, mixable blends were obtained only using a ratio between HA and the sulfonating agent equal to 1:0,5.

### 5.2.1 FTIR analysis

ATR spectra were recorded on dried samples in order to point out differences caused by the reaction of HA with the crosslinker and sulfonated molecules (figure 5.7). Only the spectra recorded for the 24 h crosslinked hydrogels are shown, since no other distinctive differences could be observed after 72 or 96 hours.

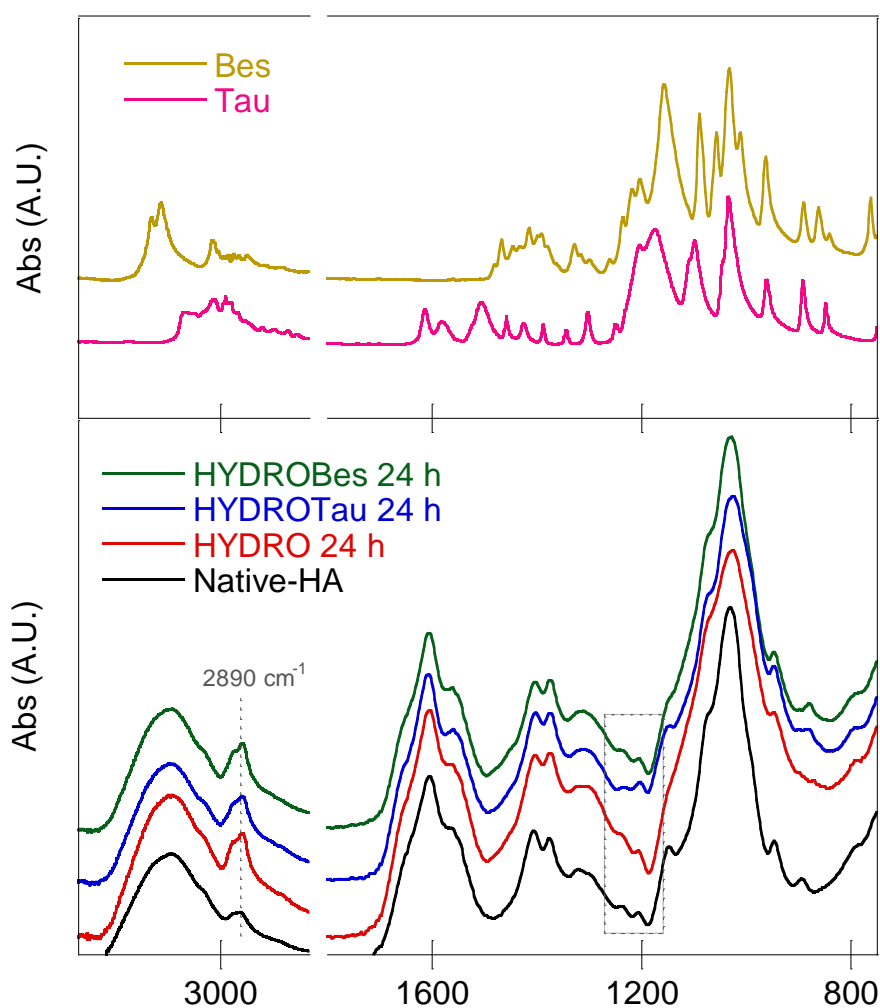


**Fig. 5.7:** FTIR spectra of HYDRO (red), HYDROTau (blue) and HYDROBes (green) after 24 of crosslinking in the region between 3800 – 790 cm<sup>-1</sup>. Spectra are compared to that of pristine hyaluronic acid (black, lower panel), Tau (pink) and Bes (yellow) in the upper box.

Unfortunately, no significant differences can be detected in the spectra before and after crosslinking with BDDE, being the FTIR spectra of hydrogels similar to that of water-soluble hyaluronic acid. This result is in agreement with the fact that the bonds formed during reaction of HA with the diepoxy are similar to that already existing in the saccharide unit, as also found by Anna Strom<sup>13</sup> and Kenji Tornihata<sup>14</sup> with similar diepoxides. Respect to pristine HA, the networks shows a slight increase of aliphatic stretching at 2890 cm<sup>-1</sup> related to the increase of

methylene groups as result of the presence of BDDE. In addition, the absence of an ester peak at  $1730\text{ cm}^{-1}$  confirms that hydrogel formation at  $\text{pH}>10$  occurred via epoxide ring opening promoted by the alcoholic moieties and not by carboxylate groups.<sup>15</sup>

A small but reproducible change in HYDROTau and HYDROBes 24 h spectra can be seen in the region between  $1240$  and  $1200\text{ cm}^{-1}$ . Reasonably, this could be attributed to the stretching of  $\text{SO}_3^-$  groups of sulfonated agents covalently bonded to the hyaluronate network.<sup>16</sup> As for BDDE, no other spectroscopic evidences could be observed in the spectra of sulfonated networks, taking into account the similarity of bonds involved.

## 5.2.2 Swelling studies

Indirect and direct swelling ratios in water and phosphate buffered saline are displayed in figure 5.8 while the ratio between  $SR_{ind}$  and  $SR_{dir}$ , indicative of the re-swelling capability, is reported in table 5.2.

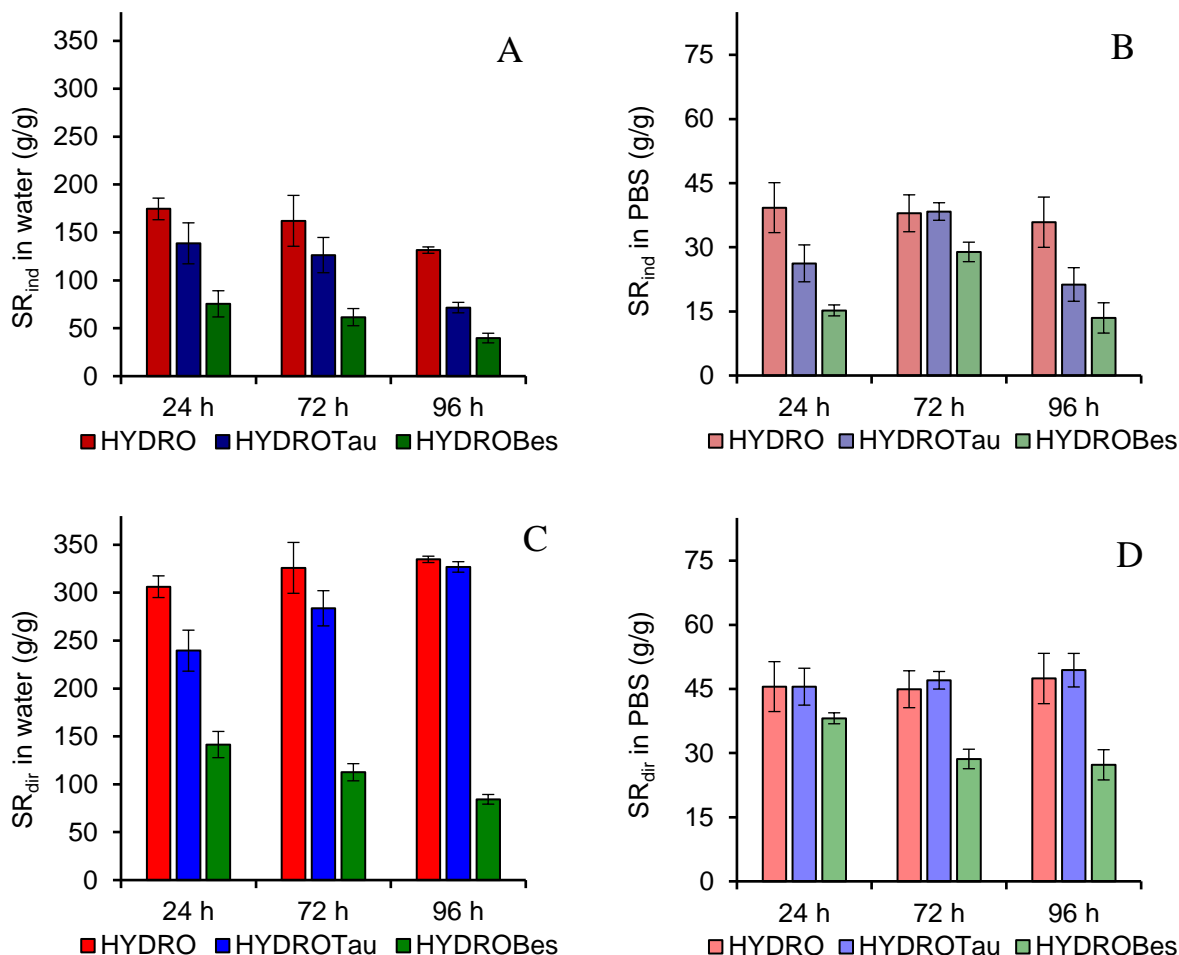


**Fig. 5.8:** Indirect swelling ratio values (swollen weight/dried weight) in distilled water (A) and in PBS (0,01 M isotonic solution, B) of the swollen hydrogels after 48 h; direct swelling ratio values (wet material weight/dried material weight) in distilled water (C) and in PBS (0,01 M isotonic solution, D) of the “as-prepared” hydrogels. All measurements were performed at 37 °C.

**Table 5.2:** Ratios between indirect swelling ( $SR_{ind}$ ) and direct swelling ( $SR_{dir}$ ) calculated in water and in PBS for HYDRO, HYDROTau and HYDROBes. Ratios are related to the capability of the hydrogels to re-hydrate after freeze-drying.

Sample		$SR_{ind}/SR_{dir}$ in H <sub>2</sub> O	$SR_{ind}/SR_{dir}$ in PBS
<b>HYDRO</b>	24 h	0,57	0,86
	72 h	0,50	0,84
	96 h	0,39	0,76
<b>HYDROTau</b>	24 h	0,58	0,58
	72 h	0,45	0,82
	96 h	0,22	0,43
<b>HYDROBes</b>	24 h	0,53	0,40
	72 h	0,55	1,01
	96 h	0,47	0,49

Water swelling is a complex phenomenon that depends on the crosslinking degree and polymer network composition. In fact, the introduction of polar SO<sub>3</sub>H groups by Tau and Bes can favor the interaction with water but, on the other hand, could influence the crosslinking efficiency of BDDE. For instance, the presence of BDDE dangling branches bearing a sulfonate molecule increase the polymer hydrophilicity and does not act as crosslink. Then, a direct interpretation of the swelling degree values obtained as a function of reactants and reaction time is a complex task. However, some general consideration on the results reported in figure 5.8 can be done.

All the hydrogels showed high water uptake increasing their dried weight 50 - 180 folds when swollen in distilled water. As expected, in PBS the water uptake is lower and the gels reach a maximum weight 50 times higher than that of dry samples. HYDRO sample seems to reach the maximum crosslinking density just in the first reaction time, not showing a significant variation in the swelling degrees.

The direct water swelling data show that by increasing the reaction time only the HYDROBes sample decreases the water uptake significantly, presumably because of the increasing crosslink density. The same trend can be observed in the indirect experiments in water and in direct tests in PBS. Then, HYDROBes is the sample with the higher crosslinking density. This finding will be confirmed by mechanical tests, as shown later. As far as the HYDROTau

sample, the swelling increases with the reaction time. In this case, it may be presumed that the BDDE reacts mainly with one Tau molecule which, because of steric hindrance, does not form the crosslink with another epoxy group.

As far as the re-swelling capacity, the differences between direct and indirect results show that the re-swelling is partially reversible. Specifically, it can be deduced that during the cooling in liquid nitrogen and lyophilization the polymeric chains rearrange in a stable network that is not reversibly hydrated. This phenomenon is the reason why a hysteresis in the swelling process occurs. The re-swelling process in water is not reversible for the hydrogels, since  $SR_{ind}/SR_{dir}$  is always  $< 1$ , while in PBS the hydrogels reach a swollen weight close to that measured before lyophilization ( $W_w^{PBS}$ ).

However, it is important to consider that re-swelling is fast for all samples, evidencing the great affinity of the network with water. Each hydrogel reaches a weight close to  $W_s$  within few minutes and for this reason it has been impossible to follow the kinetic of swelling with gravimetric measurements.

### 5.2.3 Thermal and mechanical characterization

Differential scanning calorimetry (DSC) was used to evaluate the type of water in the hydrogels before and after sulfonation. The mobility of water molecules in swollen hydrophilic polymers is tightly related to the interactions they establish with the host matrix and to their geometrical confinement. In general, in relation to the water thermal behavior, the water state in hydrated materials may be divided into three categories: non-freezing water ( $W_b$ ), freezing bound water ( $W_{fb}$ ) and free water ( $W_f$ )<sup>17,18</sup>

Thermograms for HYDRO 72 h, HYDROTau 72 h and HYDROBes 72 h in the region between -10 - 10 °C are showed in figure 5.9. All swollen hydrogels are characterized by an endothermic transition which is related to the melting of water contained in the sample. The onset temperature of the transition  $T_m^{On}$  is below 0 °C ( $T_m^{On} \sim -4$  °C) as a result of the interactions that are established between water and the polymeric material.

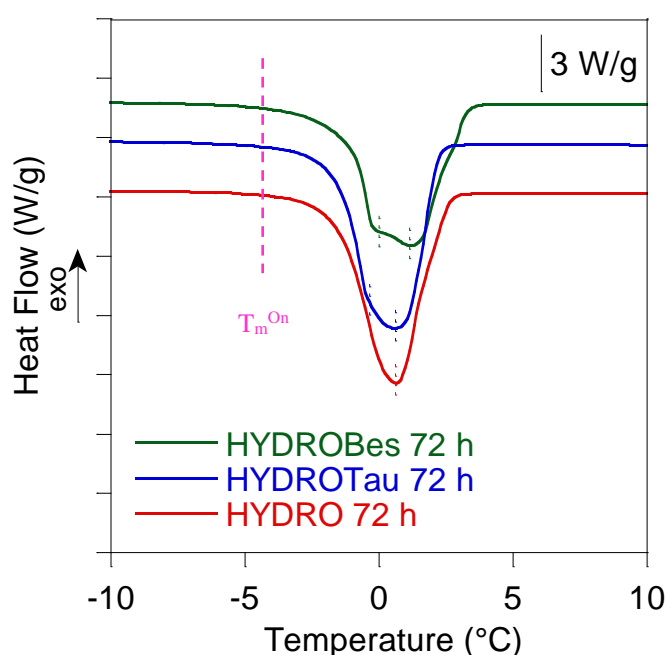


**Fig. 5.9:** DSC thermograms between -10 and 10 °C of samples HYDRO, HYDROTau and HYDROBes crosslinked for 72 h and swollen at 37 °C for 24 h. The endothermic peaks at about 0 °C are related to the melting of secondary bound water ( $W_{fb}$ ) and the free water ( $W_f$ ).

The water melting peaks are located in the temperature range between 0 and 1,4 °C (dashed line). The DSC traces evidence a complex transition, likely because of the presence of two type of water in the hydrogels, the freezing bound water and the free water. Because of the large peak superimposition, it has not been possible to separate the two fractions. However,

HYDROBes sample clearly shows a peak shoulder at low temperature, indicative of a higher freezing bound water content. The freezing water, intended as the sum of the freezing bound and free water, was evaluated from the ratio between the endothermic peak area for swollen samples to endothermic peak of fusion of pure water ( $\Delta H_m^0 = -334 \text{ J/g}$ ). The bound water, that is strongly bonded to the material and doesn't participate to the melting, was calculated as the difference between the total and the freezing water (table 5.3).

**Table 5.3:** Thermal properties, swelling values and water content of swollen HYDRO 72 h, HYDROTau 72 h and HYDROBes 72 h.  $W_b$  is the fraction of bound water calculated for each sample by means of differential scanning calorimetry (DSC).

Sample	SR <sub>ind</sub>	EWC (%)	Q <sub>endo</sub> (J/g)	W <sub>fb</sub> +W <sub>f</sub>	W <sub>b</sub> (%)
<b>HYDRO 72 h</b>	186	99	-291	87	12
<b>HYDROTau 72 h</b>	102	99	-288	86	13
<b>HYDROBes 72 h</b>	50	98	-270	81	18

HYDRO 72 h and HYDROTau 72 h show analogous values for EWC, as well as similar free water fraction. HYDROBes 72 h, instead, is characterized by the lowest equilibrium water content. Both EWC and the free water resulted to be lower for the hydrogel with the highest crosslink density, i.e. HYDROBes, indicating a more compact structure of network. Moreover, the bound water is significantly higher than that of the other two samples. At this regard, it could be assumed that the presence of N,N-bis(2-hydroxyethyl)-2-aminoethanesulfonic acid during gelation reflected in the formation of more tight network.

The stress-strain curves for samples HYDRO, HYDROTau and HYDROBes at 24, 72 and 96 hours are reported in figure 5.10 while calculated CM and  $\sigma_\varepsilon$  are showed in figure 5.11.

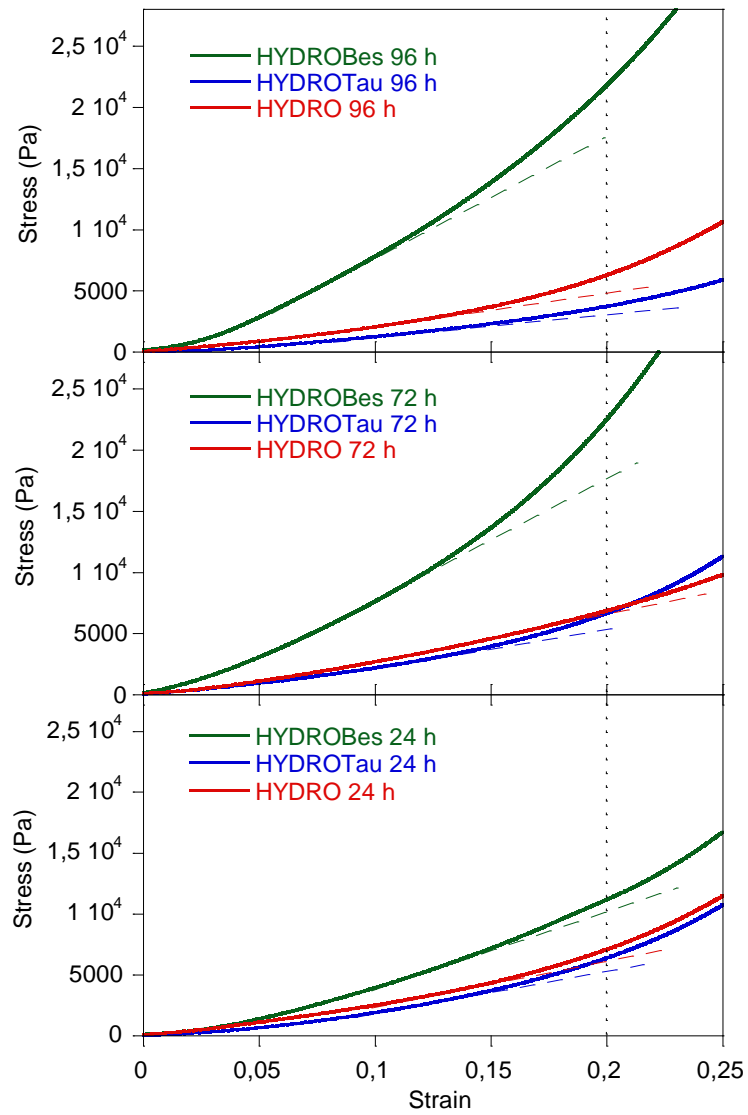


**Fig. 5.10:** Stress-strain curves for HYDRO (red), HYDROTau (blue) and HYDROBes (green) at different crosslinking times in the region between  $0 < \varepsilon < 0,2$ . Dashed lines represent the linear region of the stress-strain curve used to measure samples CM.

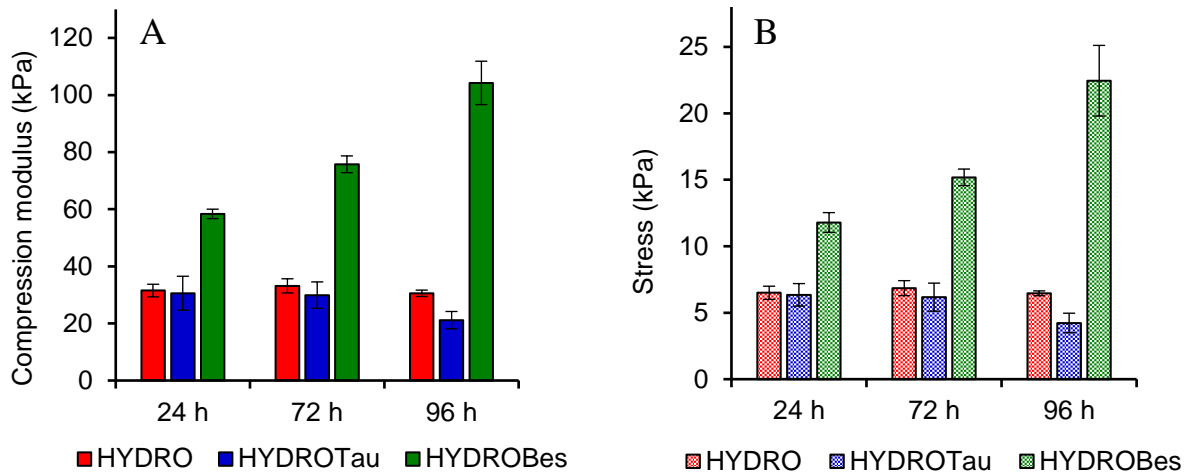


**Fig. 5.11:** Mechanical properties of hydrogels: compression modulus (A) and stress at a fixed strain (B) for all synthesized samples.

In general, the compression experiments show that the stress increases constantly in all the explored strain range, without inflection. This result evidences that the gels are stable and that their structure do not undergo embrittlement or rupture in all the explored strain range.

The mechanical responses pointed out peculiar differences between the hydrogels. In fact, HYDROBes samples exhibit the highest CM and  $\sigma_\epsilon$  and the values increase with crosslinking time. The CM range between 60 and 110 kPa while nominal stress at  $\epsilon = 0,2$  varies from 12 kPa to 22 kPa. Crosslinking time affects positively the mechanical properties enhancing hydrogel performances. In contrast, HYDRO and HYDROTau had a similar mechanical behavior with similar CM and  $\sigma_\epsilon$  for the three crosslinking times and values are close to 33 kPa and 6 kPa, respectively.

The comparison of the mechanical properties and the data about water swelling shows good agreement between compression modulus and the samples equilibrium water content ( $EWC_{dir}$ ) as shown in figure 5.12. In fact, the Bes-sulfonated hydrogel has the lowest water uptake, hence evidencing a robust and compenetrated structure with reasonable highest crosslinking density.

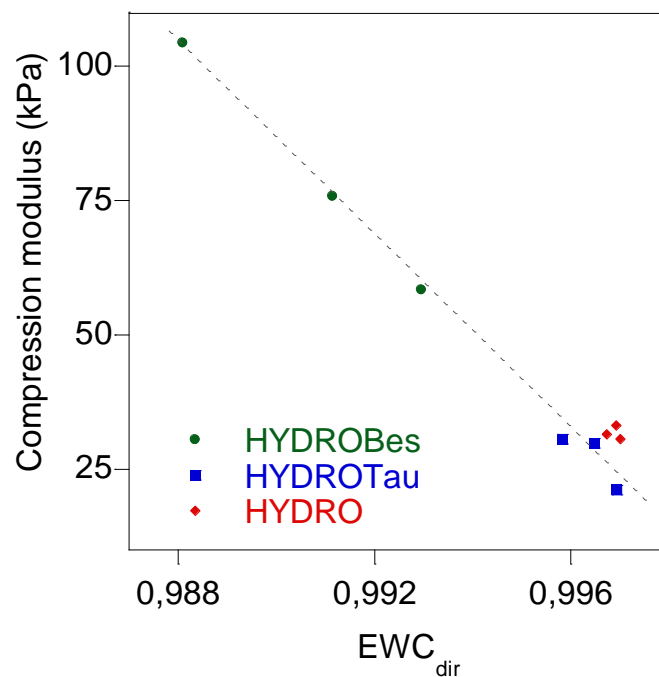


**Fig. 5.12:** Compression modulus for hydrogels at 24, 72 and 96 h of crosslinking as function of equilibrium water swelling (for direct swelling measurements). The elastic modulus shows a linear trend with the swelling, depending upon the type/presence of sulfonating agent.

Differently from the other samples, both CM and  $\sigma_\epsilon$  of HYDROBes increase as a function of the reaction time, together with equilibrium water content. On the other hand, taurine addition resulted in the synthesis of hydrogels with similar mechanical response to those obtain using only sodium hyaluronan but enriched in polar sulfonic groups (figure 5.7).

## 5.2.4 Bulk structure analyses

Internal morphology of the hydrogels was investigated by scanning electron microscope (SEM). At first, samples were quenched in liquid nitrogen and rapidly cut, but the hydrogel structure collapsed immediately when exposed to air at room temperature. Thus, slices were accurately cut from lyophilized hydrogels with a blade soon after lyophilization, taking care not to damage the internal structure. Different regions of the sample were observed by SEM in order to evaluate any possible morphological heterogeneity. The analysis showed no differences, for instance, between the sample outer and inner regions. SEM images of un-sulfonated and sulfonated hydrogel after 72 hours of crosslinking are displayed in figure 5.13 and the pore dimension ranges are reported in table 5.4.

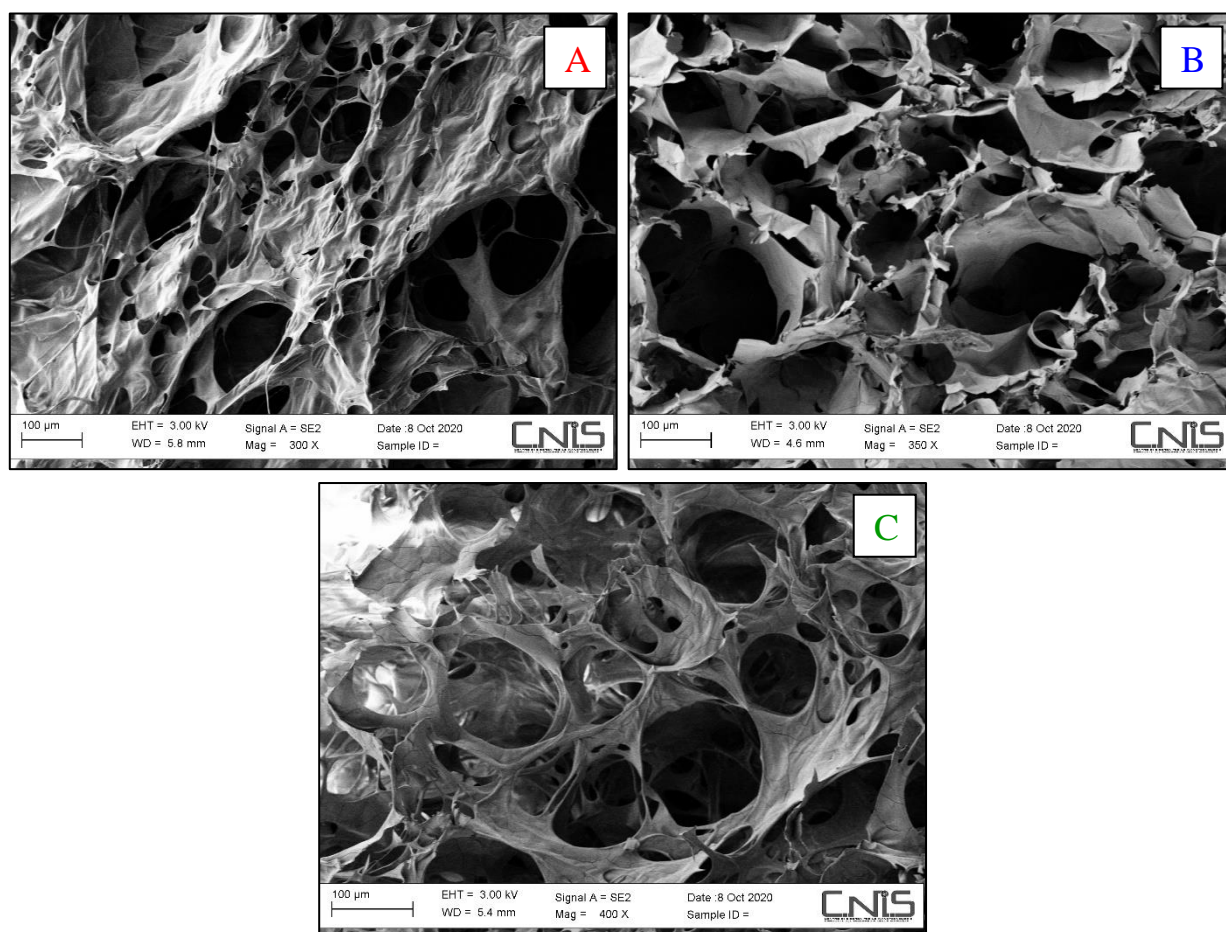


**Fig. 5.13:** Scanning Electron Microscopy (SEM) micrographs of HYDRO 72 h (A), HYDROTau 72 h (B) and HYDROBes 72 h (C).

**Table 5.4:** Pores size measured for sulfonated and non-sulfonated hydrogels after 72 hours of crosslinking (Red: HYDRO; Blue: HYDROTau; Green: HYDROBes).

Sample	Pore size ( $\mu\text{m}$ )
<b>HYDRO 72 h</b>	60-180
<b>HYDROTau 72 h</b>	70-150
<b>HYDROBes 72 h</b>	40-110

A porous structure with interconnected open pores was obtained after lyophilization for of all the hydrogels. HYDRO sample shows pore dimension heterogeneity and some closed continuous structures. The shape of pores becomes more regular in sulfonated hydrogels and the dispersion of dimensions decreases.

Both non sulfonated and sulfonated hydrogels are characterized by an adequate structure for tissue engineering, in terms of pores dimension and interconnection, considering that pores between 70–130  $\mu\text{m}$  are necessary for the regeneration of soft tissues (larger pores are needed for the engineering of hard tissues).<sup>19,20,21</sup> However, the HYDROBes sample shows the most homogeneous porous structure, characterized by large interconnection and pore regular dimension.

### 5.2.5 In vitro degradation

Biodegradability is an important feature of hyaluronic acid considering that the half-life of HA in body is very low and, thus, chemical modification of HA provides tools for its application as a biomaterial in medicine.<sup>22</sup> Some *in vitro* studies demonstrated that enzymatic resistance can be improved crosslinking sodium hyaluronate and that sulfated hyaluronic acid hydrogels showed high resistance towards hyaluronidase, chondroitinase.<sup>23</sup> Furthermore, modified hyaluronic acid showed less susceptibility towards enzymatic degradation when treated with lysozyme.<sup>24</sup> The enzyme, which is widely diffused in body fluids, is known to be responsible for the cleaving of linkages in polysaccharides.<sup>25</sup> At this regard, the enzymatic degradation of non-sulfonated and sulfonated hydrogels was tested in lysozyme (1,5  $\mu\text{g/ml}$ ) at 37 °C. Percentage of mass loss under the action of lysozyme in PBS buffer for HYDRO, HYDROTau and HYDROBes is shown in figure 5.14.

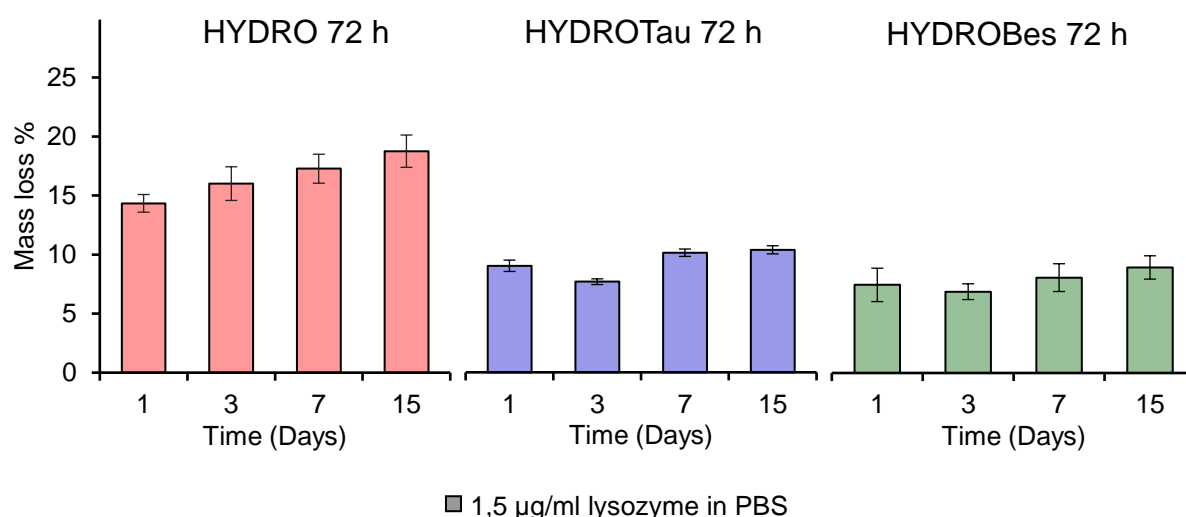


**Fig. 5.14:** Weight loss percentage measured for HYDRO 72 h (red), HYDROTau 72 h (blue) and HYDROBes 72 h (green) as a consequence of lysozyme in PBS degradation effect. Samples weights were measured after 1, 3, 7 and 15 days of degradation at 37 °C. The enzyme solution was replaced with that freshly prepared after every measurement.

As expected, all hydrogels undergo weight decrease within 15 days in PBS containing lysozyme. Mass loss resulted to be large for HYDRO 72 h under the enzyme effect. In fact, after 15 days, the non-sulfonated sample loss about 20 %  $\pm$  3 of the starting weight while the weight loss after sulfonation is much less, close to 10 %  $\pm$  2. No marked differences can be observed between HYDROTau 72 and HYDROBes 72 h at each time point. Lysozyme seems to accelerate degradation process in hydrogels but the enzyme effect is less hard on hydrogels containing SO<sub>3</sub>H groups after two weeks. The *in vitro* degradation of hydrogels can be

associated with many factors such as the chemical structure, formulation, morphology, and crosslinking density.<sup>26</sup> The obtained results, seems to be influenced not only by sample crosslinking density, as deduced from swelling experiments. The presence of the grafted sulfonic group increases the HA resistance to enzymatic degradation, as observed in other researches.<sup>23</sup>

### 5.3 Conclusion

A one-pot procedure for sulfonation and cross-linking of hyaluronic acid to give hydrogels has been presented. BDDE was used as crosslinker agent and the use of Tau and Bes allowed the preparation of HA-based hydrogels containing  $-SO_3H$  moieties. Concentration of solutions and molar ratio of reactants were optimized in order to synthesize non soluble HA-hydrogels, with (HYDRO Tau and HYDRO Bes) or without (HYDRO) sulfonating agents, in a one-pot sulfonation/crosslinking procedure based on the simultaneous ring opening epoxide at the expense of Tau/Bes and HA in an alkaline medium. Three crosslinking times were evaluated and synthesis was carried out at room temperature. The new formation of the networks was strongly influenced by the crosslinking time, showing a water uptake capability that varies with the presence and/or type of sulfonating agent. HYDRO Bes resulted to have the more compact structure, as shown by water swelling experiments, reasonably because the high crosslinking density obtained. As a consequence, mechanical characterization showed that the crosslinking of sodium hyaluronan in the presence of Bes brought about an increase of the compression modulus of the hydrogel. In general, an improvement of mechanical performances of the materials with crosslinking time was observed. A highly porous interconnected structures were obtained for all the synthesized supports, with pores dimension and shape influenced by Tau and Bes addition. Finally, sulfonated hydrogels showed a higher resistance towards lysozyme enzymatic degradation within 15 days respect to that of sodium hyaluronate, making it possible to prospect their use for long-lasting applications. The HA-based hydrogels endowed with polar sulfonic groups showed to have interesting key characteristics for cells growth. Sulfonic groups, in fact, could promote the interaction with biomolecules, such as collagen, favoring chondrocytes attachment. Furthermore, the presence of  $-SO_3H$  groups could provide the hydrogels with anti-clotting properties thus expanding their application in the biomedical area. The one pot procedure revealed to be an efficient methodology for the preparation of promising sulfonated HA-based materials that can be used in the field of tissue engineering.

## 5.4 References

- (1) De Boulle, K., Glogau, R., Kono, T., Nathan, M., Tezel, A., Roca-Martinez, J. X., ... & Stroumpoulis, D. (2013). A review of the metabolism of 1, 4-Butanediol Diglycidyl ether–crosslinked hyaluronic acid dermal fillers. *Dermatologic Surgery*, 39(12), 1758-1766.
- (2) Zhang, J., Ma, X., Fan, D., Zhu, C., Deng, J., Hui, J., & Ma, P. (2014). Synthesis and characterization of hyaluronic acid/human-like collagen hydrogels. *Materials Science and Engineering: C*, 43, 547-554.
- (3) Ciba-Geigy Corp. A cutaneous carcinogenicity study with mice on the diglycidyl ether of 1,4-butanediol. 1987.
- (4) Kenne, L., Gohil, S., Nilsson, E. M., Karlsson, A., Ericsson, D., Kenne, A. H., & Nord, L. I. (2013). Modification and cross-linking parameters in hyaluronic acid hydrogels—definitions and analytical methods. *Carbohydrate polymers*, 91(1), 410-418.
- (5) Nishi, C., Nakajima, N., & Ikada, Y. (1995). In vitro evaluation of cytotoxicity of diepoxy compounds used for biomaterial modification. *Journal of biomedical materials research*, 29(7), 829-834.
- (6) Collins, M. N., & Birkinshaw, C. (2007). Comparison of the effectiveness of four different crosslinking agents with hyaluronic acid hydrogel films for tissue-culture applications. *Journal of Applied Polymer Science*, 104(5), 3183-3191.
- (7) Faroongsarng, D., & Sukonrat, P. (2008). Thermal behavior of water in the selected starch- and cellulose-based polymeric hydrogels. *International journal of pharmaceutics*, 352(1-2), 152-158.
- (8) Huglin, M. B., Liu, Y., & Velada, J. (1997). Thermoreversible swelling behaviour of hydrogels based on N-isopropylacrylamide with acidic comonomers. *Polymer*, 38(23), 5785-5791.
- (9) Zhou, Z. H., He, S. L., Huang, T. L., Liu, L. H., Liu, Q. Q., Zhao, Y. M., ... & Cao, D. F. (2013). Degradation behaviour and biological properties of gelatin/hyaluronic acid composite scaffolds. *Materials Research Innovations*, 17(6), 420-424.

- (10) Cowman, M. K., Schmidt, T. A., Raghavan, P., & Stecco, A. (2015). Viscoelastic properties of hyaluronan in physiological conditions. *F1000Research*, 4.
- (11) M. Gatej, M. Popa, Rinaudo, Role of the pH on hyaluronan behavior in aqueous solution, *Biomacromolecules* 6 (2005) 61–67
- (12) Tavsanlı, B., & Okay, O. (2016). Preparation and fracture process of high strength hyaluronic acid hydrogels cross-linked by ethylene glycol diglycidyl ether. *Reactive and Functional Polymers*, 109, 42-51.
- (13) Ström, A., Larsson, A., & Okay, O. (2015). Preparation and physical properties of hyaluronic acid-based cryogels. *Journal of Applied Polymer Science*, 132(29).
- (14) Tomihata, K., & Ikada, Y. (1997). Preparation of cross-linked hyaluronic acid films of low water content. *Biomaterials*, 18(3), 189-195.
- (15) Schanté, C. E., Zuber, G., Herlin, C., & Vandamme, T. F. (2011). Chemical modifications of hyaluronic acid for the synthesis of derivatives for a broad range of biomedical applications. *Carbohydrate polymers*, 85(3), 469-489.
- (16) Hausman, R., Digman, B., Escobar, I. C., Coleman, M., & Chung, T. S. (2010). Functionalization of polybenzimidazole membranes to impart negative charge and hydrophilicity. *Journal of membrane science*, 363(1-2), 195-203.
- (17) Hatakeyama, H., & Hatakeyama, T. (1998). Interaction between water and hydrophilic polymers. *Thermochimica acta*, 308(1-2), 3-22.
- (18) Li, W., Xue, F., & Cheng, R. (2005). States of water in partially swollen poly (vinyl alcohol) hydrogels. *Polymer*, 46(25), 12026-12031.
- (19) Hwang, H. D., Cho, H. J., Balakrishnan, P., Chung, C. W., Yoon, I. S., Oh, Y. K., ... & Kim, D. D. (2012). Cross-linked hyaluronic acid-based flexible cell delivery system: application for chondrogenic differentiation. *Colloids and Surfaces B: Biointerfaces*, 91, 106-113.
- (20) Murphy, C. M., Haugh, M. G., & O'brien, F. J. (2010). The effect of mean pore size on cell attachment, proliferation and migration in collagen–glycosaminoglycan scaffolds for bone tissue engineering. *Biomaterials*, 31(3), 461-466.

- (21) Yoon, I. S., Chung, C. W., Sung, J. H., Cho, H. J., Kim, J. S., Shim, W. S., ... & Kim, D. D. (2011). Proliferation and chondrogenic differentiation of human adipose-derived mesenchymal stem cells in porous hyaluronic acid scaffold. *Journal of Bioscience and Bioengineering*, 112(4), 402-408.
- (22) Hahn, S. K., Park, J. K., Tomimatsu, T., & Shimoboji, T. (2007). Synthesis and degradation test of hyaluronic acid hydrogels. *International journal of biological macromolecules*, 40(4), 374-380.
- (23) Abatangelo, G., Barbucci, R., Brun, P., & Lamponi, S. (1997). Biocompatibility and enzymatic degradation studies on sulphated hyaluronic acid derivatives. *Biomaterials*, 18(21), 1411-1415.
- (24) Laffleur, F., Netsomboon, K., Erman, L., & Partenhauser, A. (2019). Evaluation of modified hyaluronic acid in terms of rheology, enzymatic degradation and mucoadhesion. *International journal of biological macromolecules*, 123, 1204-1210.
- (25) Islam, N., Wang, H., Maqbool, F., & Ferro, V. (2019). In vitro enzymatic digestibility of glutaraldehyde-crosslinked chitosan nanoparticles in lysozyme solution and their applicability in pulmonary drug delivery. *Molecules*, 24(7), 1271.
- (26) Li, X., Fan, D., Zhu, C., & Ma, X. (2014). Effects of self-assembled fibers on the synthesis, characteristics and biomedical applications of CCAG hydrogels. *Journal of Materials Chemistry B*, 2(9), 1234-1249.

## 6. GENERAL CONCLUSION

In the work of thesis, several aspects of hyaluronic acid chemical modification have been explored. In particular, the polysaccharide has been functionalized with NAPA, an amino acidic derivative of D-glucosamine and N-Acetyl-L-phenylalanine with chondroprotective properties, by means of esterification of the glucuronic unit. Preliminary biological studies on human primary chondrocytes (HPCs) has also been presented. The procedure discussed so far represents an innovative and fascinating method for the linkage of a glucosamine derivative to hyaluronic acid that could be useful also in the case of other GlcN-based products. The new HA bioconjugates could gain high relevance as injectable treatments against osteoarthritic disorders. An insight on racemization mechanism that occurs for N-acetylated amino acid was also conducted.

In addition, hyaluronic acid was subjected to sulfonation in water. Two sulfonating agents, such as Tau and Bes, were reacted in order to synthesized soluble HA-SO<sub>3</sub>H derivatives and 3D hydrogels enriched in polar sulfonic groups. In the first case, taurine was amidated onto hyaluronic acid skeleton comparing systematically the coupling efficiency of two water soluble coupling reagents. A physico-chemical characterization was also reported. In the second study, hyaluronic acid hydrogels were prepared using BDDE as crosslinker in the presence of Tau and Bes. Sulfonated networks were analyzed and materials demonstrated to have tunable properties depending upon reaction conditions and presence of sulfonic moieties. Due to the partial suspension of the PhD activity for Covid-19 emergency, biological tests on HA derivatives are in a preliminary stage. For this reason, no cellular evaluation on hydrogels has been presented in the thesis.

## List of Abbreviations

### Chapter 2

THF: tetrahydrofuran

DMF: N,N-Dimethylformamide

DCM: dichloromethane

MeOH: methanol

EtOH: ethanol

DMSO: dimethyl sulfoxide

HA: hyaluronic acid

D,L-NAPA: 2-(N-Acetyl)-D,L-phenylalanyl-amido-2-deoxy-D-glucose

D-Glu HCl: D-glucosamine hydrochloride

N-Ac-L-Phe: N-Acetyl-L-phenylalanine

N-Ac-D-Phe: N-Acetyl-D-phenylalanine

EDC HCl: 1-Ethyl-3-(3-dimethylaminopropyl)carbodiimide hydrochloride

NHS: N-Hydroxysuccinimide

IBCF: isobutyl chloroformate

TEA: triethylamine

TMSCl: chlorotrimethylsilane

TBTU: O-(Benzotriazol-1-yl)-N,N,N',N'-tetramethyluronium tetrafluoroborate

DIPEA: N,N-Diisopropylethylamine

DCC: N,N'-Dicyclohexylcarbodiimide

DMAP: N,N-Dimethylpyridin-4-amine

NMM: N-Methyl morpholine

HOBt: 1-Hydroxybenzotriazole

N-Cbz-L-Phe: N-(Carbobenzyloxy)-L-phenylalanine

T3P: 1-Propanephosphonic anhydride

TBA-OH: tetrabutylammonium hydroxide

HA-TBA: tetrabutylammonium hyaluronate

## Chapter 4 and 5

Tau: 2-aminoethanesulfonic acid (Taurine)

HA-Tau: hyaluronic acid amidated with Tau

DMTMM: 4-(4,6-Dimethoxy-1,3,5-triazin-2-yl)-4-methylmorpholinium chloride

PBS: phosphate buffered saline

MES: 2-(N-morpholino)ethanesulfonic acid

BDDE: 1,4-Butanediol diglycidyl ether

Bes: N,N-bis(2-hydroxyethyl)-2-aminoethanesulfonic acid

HYDRO: HA-based hydrogel

HYDROTau: HA-based hydrogel with Tau

HYDROBes: HA-based hydrogel with Bes